

A thesis for the Degree of Ph.D. in Engineering

**Molecular Dynamics Study of the  
Vibrational Spectra of Clathrate Hydrates**

January 2015

Graduate School of Science and Technology  
Keio University

**Masaki Hiratsuka**

©2014  
Masaki Hiratsuka  
All Rights Reserved

*To my parents, Takashi and Kyoko Hiratsuka*

# Acknowledgment

I would like to express my deepest gratitude to my supervisor, Professor Kenji Yasuoka, for his continuous support and encouragement during my graduate school years. I would like to thank him in particular for suggesting me to work on this subject, continuous encouragement and his kind advice at times when they were necessary. His guidance has been the most important factor for my thesis.

I wish to sincerely thank the members of my examining committee: Professor Jun Yamauchi, Professor Koji Fukagata, Professor Ryo Ohmura for lending their time, and interest and insight. I am highly motivated by the discussion on the research and also other things in life. I would like to thank Professor Yasuhiko Mori and Professor Kuniyasu Ogawa for valuable discussion during the weekly seminars. I am also extremely grateful to Professor Amadeu K. Sum and Professor Saman Alavi for constructive discussion from the early stage of my study. I also gratitude to Professor Tom Woo for supports and discussion during my three month stay in Ottawa. I would like to thank to Dr. Yoshio Kondo, and Mr. Yuuki Fujita in NGK insulators, LTD. for the continuous and valuable discussion.

I would also like to thank my friends and colleagues for their contributions and support. I am grateful to Dr. Takuma Akimoto, Dr. Daisuke Takaiwa, Dr. Hideo Doi, Dr. Paul Brumby, Dr. Noriyoshi Arai, Dr. Donguk Suh, Dr. Toshihiro Kaneko, and Dr. Ryuji Sakamaki for helpful discussion for my studies. Of course, I wish to thank Dr. Kazuaki Z. Takahashi, Mr. Taizo Shibuya, and Dr. Sanehiro Muromachi, Yagaura members, for helpful discussion. I wish to thank the former and the current students in the lab, especially for the members who study clathrate hydrates, molecular vibrations, and *ab initio* calculations for interesting discussion.

I acknowledge the support by the Fellowships of the Japan Society of the Promotion of Science for Japanese Junior Scientists and Global COE Program.

Finally, I would like to thank my parents. I am grateful for their encouragement and unending support.

# Abstract

Clathrate hydrates are crystalline inclusion compounds consisting of hydrogen-bonded water molecules forming cages enclosing guest molecules. Vibrational spectra of guest molecules provide information of the clathrate hydrates such as the cage occupancy and the structure of clathrate hydrates. In this study, molecular dynamics (MD) simulations were employed to calculate the vibrational spectra of guest molecules and to analyze the mechanism of the frequency changes.

Firstly, the vibrational spectra of structure I (sI) methane hydrates were computed by *ab initio* MD simulations because the origins of the vibrational peaks in the system were well determined in the previous experimental observations. The calculated vibrational frequencies of methane molecules in clathrate hydrates well agreed with the experimental observations. Secondly, the vibrational spectra of structure H clathrate hydrates were calculated. As a result, the origins of the spectra peaks of stretching vibrations in methane molecules that were not clearly reported in the previous experiments were determined. Thirdly, the vibrational spectra of sI deuterated methane hydrates were calculated. The deuteration of the water molecules in clathrate hydrates was commonly used in experimental observation of the spectra. The results indicated that the vibrational frequencies of intramolecular vibrations of guest methane molecules were changed due to the motion of the deuterated water molecules in the host framework. Finally, the vibrational spectra of C<sub>5</sub>H<sub>12</sub>O molecules in structure II and H clathrate hydrates were calculated by MD simulations. The results showed the formation of guest-host hydrogen bonding in both structures and the large frequency shift of the O-H group of the alcohols are due to hydrogen bonding. The guest-host hydrogen bonding played an important role in the determination of the structure of clathrate hydrates.

These results of MD simulations for clathrate hydrates showed new insights into the effect of guest-host interactions on the vibrational spectra, structure, and stability of clathrate hydrates.

# Contents

|                 |   |    |
|-----------------|---|----|
| Acknowledgement |   | i  |
| Abstract        |   | ii |
| Chapter 1       | Introduction  | 1  |
| 1.1             | Clathrate hydrates . . . . .  | 1  |
| 1.2             | Vibrational spectra of clathrate hydrates . . . . .                       | 2  |
| 1.3             | Thesis objective and outline . . . . .                                    | 4  |
| Chapter 2       | Computational methods   | 6  |
| 2.1             | Methodology of classical molecular dynamics simulation . . . . .          | 6  |
| 2.1.1           | Numerical integration method of Newton's equation of motion . . . . .     | 6  |
| 2.1.2           | Intermolecular interaction in classical MD . . . . .                      | 7  |
| 2.1.3           | Coulombic interactions . . . . .  | 7  |
| 2.1.4           | Periodic boundary condition . . . . .                                     | 9  |
| 2.2             | Density functional theory . . . . .                                       | 10 |
| 2.2.1           | Born-Oppenheimer approximation . . . . .                                  | 10 |
| 2.2.2           | Hohenberg-Kohn theorems . . . . .   | 11 |
| 2.2.3           | Kohn-Sham equation . . . . .  | 12 |
| 2.2.4           | Local density approximation, Generalized gradient approximation . . . . . | 13 |
| 2.3             | Car-Parrinello molecular dynamics simulation . . . . .                    | 14 |
| Chapter 3       | Structure I methane hydrate   | 16 |
| 3.1             | Introduction . . . . .  | 16 |
| 3.2             | Computational details . . . . .   | 18 |
| 3.2.1           | Calculation of autocorrelation functions . . . . .                        | 20 |

---

|           |   |    |
|-----------|---|----|
| 3.3       | Results and Discussions . . . . .                                       | 22 |
| 3.3.1     | Autocorrelation function of methane molecules . . . . .                 | 22 |
| 3.3.2     | Vibrational spectra . . . . .   | 26 |
| 3.3.3     | Distribution of guest molecule in the cages . . . . .                   | 34 |
| 3.4       | Conclusions . . . . .   | 36 |
| Chapter 4 | Structure H methane hydrate   | 37 |
| 4.1       | Introduction . . . . .  | 37 |
| 4.2       | Computational method . . . . .  | 38 |
| 4.3       | Results and Discussions . . . . .                                       | 39 |
| 4.3.1     | Vibrational spectra . . . . .   | 39 |
| 4.4       | Conclusions . . . . .   | 51 |
| Chapter 5 | Structure I deuterated methane hydrate                                  | 52 |
| 5.1       | Introduction . . . . .  | 52 |
| 5.2       | Computational method . . . . .  | 53 |
| 5.3       | Results and Discussions . . . . .                                       | 54 |
| 5.3.1     | Vibrational spectra . . . . .   | 54 |
| 5.4       | Conclusions . . . . .   | 65 |
| Chapter 6 | Structure II and Structure H amyl-alcohol hydrate                       | 66 |
| 6.1       | Introduction . . . . .  | 66 |
| 6.2       | Computational method . . . . .  | 68 |
| 6.2.1     | <i>ab initio</i> MD simulations . . . . .                               | 68 |
| 6.2.2     | Classical MD simulation . . . . .                                       | 69 |
| 6.3       | Results and Discussions . . . . .                                       | 69 |
| 6.3.1     | Effect of charges in hydrate cages . . . . .                            | 69 |
| 6.3.2     | Probability of guest-host hydrogen bonding . . . . .                    | 72 |
| 6.3.3     | Vibrational spectra . . . . .   | 74 |
| 6.3.4     | Radial distribution function . . . . .                                  | 77 |
| 6.3.5     | Rotation of guest molecules . . . . .                                   | 80 |
| 6.3.6     | Guest-guest hydrogen bonding . . . . .                                  | 84 |
| 6.3.7     | Displacement of water molecule by the O–H group of<br>alcohol . . . . . | 85 |
| 6.4       | Conclusions . . . . .   | 86 |

|           |             |    |
|-----------|-------------|----|
| Chapter 7 | Conclusions | 88 |
|-----------|-------------|----|

|            |  |    |
|------------|--|----|
| References |  | 91 |
|------------|--|----|

# List of Figures

|      |   |    |
|------|---|----|
| 1.1  | Three common structures of clathrate hydrates and cages . . . . .   | 2  |
| 3.1  | Vibrational modes of methane molecule . . . . .   | 17 |
| 3.2  | The five types of calculated autocorrelation functions . . . . .  | 20 |
| 3.3  | Autocorrelation function from velocity of hydrogen atoms in methane molecules . . . . .   | 23 |
| 3.4  | Autocorrelation function from velocity of carbon atoms in methane molecules . . . . .   | 23 |
| 3.5  | Autocorrelation function from C–H bond length in methane molecules  | 24 |
| 3.6  | Autocorrelation function from H–C–H angle in methane molecules  | 24 |
| 3.7  | Autocorrelation function from C–H vector in methane molecules .   | 25 |
| 3.8  | Autocorrelation function from center of mass of methane molecules   | 25 |
| 3.9  | Vibrational spectra of stretching vibrations of sI methane hydrates   | 27 |
| 3.10 | Dependence of the vibrational frequency of C-H symmetric stretching vibrations on averaged time . . . . .                             | 29 |
| 3.11 | Dependence of the frequency differences of C-H symmetric stretching vibrations between cages on averaged time . . . . .               | 30 |
| 3.12 | Dependence of the vibrational frequency of C-H symmetric stretching vibrations on the length of the autocorrelation functions . . . . | 30 |
| 3.13 | Vibrational spectra of bending and rocking vibrations of sI methane hydrates . . . . .  | 32 |
| 3.14 | Vibrational spectra of rotation and translation motions of sI methane hydrates . . . . .  | 33 |
| 3.15 | Distribution of methane and water molecules from the center of each cages . . . . .   | 35 |
| 4.1  | Vibrational spectra of stretching vibrational modes in sH hydrate .   | 41 |
| 4.2  | Vibrational spectra for bending and rocking modes in sH hydrate .   | 44 |

---

|     |  |    |
|-----|--|----|
| 4.3 | Vibrational spectra for the molecular rotation and translation of methane molecules in sH hydrate . . . . .  | 46 |
| 4.4 | Image of the $5^{12}$ and $4^35^66^3$ cages . . . . .  | 47 |
| 4.5 | Distribution of methane and water molecules from the center of each cage type in sH hydrates . . . . .   | 49 |
| 4.6 | Distributions of distance for methane and water molecules in the computation for each cage type . . . . .  | 50 |
| 5.1 | Vibrational spectra of $\text{CH}_4$ and $\text{H}_2\text{O}$ molecules . . . . .  | 56 |
| 5.2 | Vibrational spectra of $\text{CH}_4$ and $\text{D}_2\text{O}$ molecules . . . . .  | 56 |
| 5.3 | Vibrational spectra of $\text{CD}_4$ and $\text{H}_2\text{O}$ molecules . . . . .  | 57 |
| 5.4 | Dependence of the vibrational frequency of C-H symmetric stretching vibrations in $\text{H}_2\text{O}$ and $\text{D}_2\text{O}$ lattice on averaged time . . . . .       | 59 |
| 5.5 | Radial distribution functions between H or D atoms in methane and $\text{H}_2\text{O}$ or $\text{D}_2\text{O}$ molecules . . . . .                                       | 60 |
| 5.6 | Dependence of the averaged guest-host distance on averaged time . . . . .  | 61 |
| 5.7 | Low frequency vibrational spectra of the hydrogen atoms in $\text{CH}_4$ molecules in the $\text{H}_2\text{O}$ and $\text{D}_2\text{O}$ lattice of sI hydrates . . . . . | 64 |
| 6.1 | Snapshots of the $5^{12}6^4$ cages in sII and $5^{12}6^8$ cage in sH clathrate hydrates from the <i>ab initio</i> MD simulations. . . . .                                | 73 |
| 6.2 | Vibrational spectra of 3-methyl-1-butanol in the sII hydrate and 2-methyl-2-butanol in the sH hydrate . . . . .  | 76 |
| 6.3 | Radial distribution function from <i>ab initio</i> MD . . . . .  | 78 |
| 6.4 | Radial distribution function from classical MD . . . . .   | 79 |
| 6.5 | Decay of the $M_2$ autocorrelation functions with time . . . . .   | 82 |
| 6.6 | Decay of the $S_{\text{HB}}$ with time . . . . .   | 83 |
| 6.7 | Snapshot of the guest-guest hydrogen bond between 3-methyl-1-butanol molecules in sII hydrate . . . . .  | 84 |
| 6.8 | Vibrational spectrum and snapshot of a 3-methyl-1-butanol molecule that replaces a water molecule . . . . .  | 85 |

# List of Tables

|     |  |    |
|-----|--|----|
| 1.1 | Characteristics of common crystalline structures of clathrate hydrates   | 1  |
| 3.1 | Frequencies of stretching vibrational modes of sI methane hydrate  | 28 |
| 3.2 | Frequencies of isolated methane molecules  | 29 |
| 4.1 | Comparison of the stretching vibrational frequencies and average C–H bond lengths.   | 42 |
| 5.1 | Frequencies of the calculated C-H and C-D stretching vibrations in H <sub>2</sub> O and D <sub>2</sub> O lattices of sI hydrates   | 58 |
| 5.2 | Averaged guest-host distances  | 60 |
| 5.3 | Frequencies of the bending, rocking and overtones the bending vibrations for CH <sub>4</sub> and CD <sub>4</sub> in H <sub>2</sub> O and D <sub>2</sub> O lattice of sI hydrates | 62 |
| 6.1 | Coulomb potential energies for a point charge placed at center of the each cage for sI hydrates  | 70 |
| 6.2 | Coulomb potential energies for a point charge placed at center of the each cage for sII hydrates   | 71 |
| 6.3 | Coulomb potential energies for a point charge placed at center of the each cage for sH hydrates  | 71 |
| 6.4 | Averaged probability of hydrogen bond.   | 74 |
| 6.5 | Fitted relaxation time   | 82 |

# Chapter 1

## Introduction

### 1.1 Clathrate hydrates

Clathrate hydrates are crystalline inclusion compounds consisting of hydrogen bonded water molecules forming cages (host) enclosing small molecules (guests) [1]. Typically hydrophobic guest molecules, such as methane, ethane and carbon dioxide are enclosed in the cages. Structure of clathrate hydrates are usually stabilized by guest-host non-covalent interactions under low temperature and high pressure conditions.

First discovery of clathrate hydrates was documented in 19th century by Sir Humphrey Davy [2] on chlorine hydrate. The first corroboration of clathrate hydrate was archived by Faraday [3]. In the early stage, the study of clathrate hydrates were motivated by the physical interest. However, after the discovery of the effect of clathrate hydrates on the pipeline plugging, the study of the clathrate hydrates are very important in the field of flow assurance [4]. Recently, wider industrial applications of clathrate hydrates are considered. Huge amounts of natural gas hydrates are reported in the ocean floor and considered as potential resources of future fossil-fuels [5].

There are three typical structures of clathrate hydrates, structure I (sI), struc-

Table 1.1 Characteristics of common crystalline structures of clathrate hydrates

|              | Structure I |             | Structure II |             | Structure H |             |             |
|--------------|-------------|-------------|--------------|-------------|-------------|-------------|-------------|
| Structure    | Cubic       |             | Cubic        |             | Hexagonal   |             |             |
| $N$ of water | 46          |             | 136          |             | 34          |             |             |
| Cage types   | $5^{12}$    | $5^{12}6^2$ | $5^{12}$     | $5^{12}6^4$ | $5^{12}$    | $4^35^66^3$ | $5^{12}6^8$ |
| $N$ of cages | 2           | 6           | 16           | 8           | 3           | 2           | 1           |
| Cage radius  | $\sim 0.50$ | $\sim 0.58$ | $\sim 0.50$  | $\sim 0.66$ | $\sim 0.50$ | $\sim 0.53$ | $\sim 0.86$ |

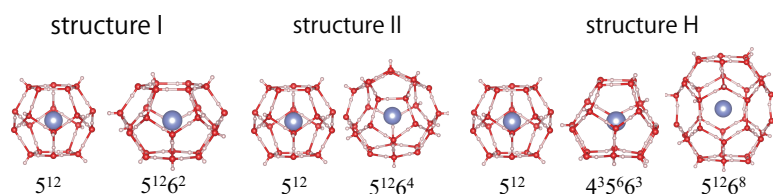


Fig.1.1 Three common structures of clathrate hydrates and cages

ture II (sI), and structure H (sH). Structure of the clathrate hydrates are composed of several types of hydrate cage as shown in Table 1.1. Structure I clathrate hydrate is a cubic crystal structure composed of two dodecahedron ( $5^{12}$ ) and six tetrakaidecahedron ( $5^{12}6^2$ ) cages, which are formed from the hydrogen bonding of water molecules as shown in Figure 1.1 [1]. A unit cell of the sI clathrate hydrates is composed of 46 water molecules. sII unit cell is composed of 136 water molecules and consists of sixteen  $5^{12}$  cages and eight hexakaidecahedron ( $5^{12}6^4$ ) cages. Unit cell of structure H is composed of three  $5^{12}$  cages, two dodecahedron ( $4^35^66^3$ ) cages, and one micosahedron ( $5^{12}6^8$ ) cage with 34 water molecules. The structure of the cages and host lattice are stabilized by suitably sized guest molecules. Therefore the crystal structure of the simple methane hydrate is sI and the methane molecules are included in  $5^{12}$  and  $5^{12}6^2$  cages. When a large molecule guest substance such as 2,2-dimethylbutane coexists with methane, sH hydrate is formed. Methane molecules occupy  $5^{12}$  and  $4^35^66^3$  cages, and large molecule guest substances (LMGSs) occupy the  $5^{12}6^8$  cages.

## 1.2 Vibrational spectra of clathrate hydrates

For application of the clathrate hydrates, understanding of types of guest molecules in the cages, occupancy, and thermal stability is important. The vibrational spectra of guest molecules in clathrate hydrates are experimentally observed from Raman and IR spectroscopy, which are often used to characterize the hydrate phase. Molecular vibrations of guest molecules in clathrate compounds differ from those in the bulk phase. Since the changes in the molecular vibrations reflect the molecular environment and dynamics of guest molecules, we can obtain physical insight of the interactions by observing the molecular vibrations of the guests in hydrates: the formation and/or existence of clathrate hydrates in a system, the occupancy of the cages, and the guest-host interactions and dynamics in the cages, etc.

However, a clear account of the molecular mechanism for the changes in the vibrational spectra is still missing. Direct molecular simulations of the guest molecules in the hydrate cages offer one possible way to carefully study the molecular interactions in the hydrate structure. To understand the vibrational spectra, it is necessary to analyze the molecular interactions of guest and host molecules and the resulting vibrational modes, such as bending, rocking, and stretching. Although several classical molecular dynamics (MD) simulations [6–8] succeeded to show the frequency shift of methane molecules in the clathrate hydrates, for an accurate computation of the molecular vibrations, a quantum chemical description of the chemical bonding in the molecules must be considered, thus avoiding the “empirical” parameterization of forcefields used in classical MD simulations. To fulfill this need, *ab initio* molecular dynamics simulations are required and most suitable for this purpose.

*Ab initio* MD calculations were previously performed to observe the vibrations of guest and host molecules forming clathrate hydrates [9, 10]. Ikeda and Terakura analyzed vibrational spectra to identify the phase transition from a deuterated clathrate hydrate to filled ice at high pressure [9]. The first *ab initio* MD study focusing on the details of the C–H vibrational frequencies of methane in sI methane hydrate was performed by Tse [10]. That *ab initio* MD simulation for sI methane hydrate using Spanish Initiative for Electronic Simulations with Thousands of Atoms (SIESTA) [11] showed that the C–H symmetric and asymmetric stretching vibrational frequencies in the large cages were lower than those in the small cages. The SIESTA method employs a localized atomic basis set in conjunction with the pseudo-potential approximation. Those results were revealing but suffered from large fluctuations in the calculated spectra, which was partially due to the short simulation time ( $\sim 6$  ps). Another limitation of that study was that the autocorrelation function of the velocity of the hydrogen atoms was exclusively considered. In the present study, to improve the calculation of the vibrational spectra in clathrate hydrates, we analyze different types of autocorrelation functions that are suitable to separate the vibrational spectra, such as the bond length, the angle, and the directions that are explained in the next chapter.

Although many guest substances are known to form hydrates, methane hydrate still represent the most important system, as they are central to energy and environmental related issues, such as a potential future energy resource and geo-hazard for seafloor stability caused by gas hydrates dissociation [5].

In this thesis, the following three methane hydrate systems were studied to understand the effect of enclathration on the vibrational frequency of guest molecules in clathrate hydrates. First, vibrational spectra of the sI methane hydrate were calculated by *ab initio* MD simulation. The vibrational frequencies of sI methane hydrates are well determined by the previous experimental observation. This calculation were used to confirm the effects of using several types of autocorrelation functions to separate the vibrational modes as the first step of this thesis. Second, the vibrational frequencies of methane molecules in sH clathrate hydrate that are still unclear in experimental observation were calculated. Third, the effect of the deuteration of water molecules in clathrate hydrate on vibrational spectra of guest molecules were revealed by the calculations. At last, vibrational spectra of hydrophilic guest molecules in clathrate hydrates were calculated. Usually clathrate hydrates are stabilized by suitably sized and hydrophobic guest molecules. Hydrophilic molecules like methanol, ethanol, and ammonia that form hydrogen bonds with water were historically applied as thermodynamic inhibitors of hydrate formation [12, 13]. However, recent experimental observation reported the formation of clathrate hydrates with these hydrophilic guest molecules without inhibition [14–20]. The effect of the guest-host hydrogen bonding on structure and stability of clathrate hydrates are still unclear. In the clathrate hydrates containing alcohol molecules, guest-host hydrogen bonding are indicated by experimental and theoretical studies. Especially for amyl-alcohol ( $C_5H_{12}OH$ ) molecules, the effect of guest-host hydrogen bonding of the vibrational spectra are reported. To reveal the mechanism of the enclathration of alcohol molecules and effect of vibrational spectra, the dynamics of alcohol molecules in clathrate hydrates are calculated by molecular dynamics study.

### 1.3 Thesis objective and outline

The objective of this thesis is to improve the calculation of vibrational spectra of each mode using *ab initio* molecular dynamics simulation and analyze the mechanism of the vibrational changes of clathrate hydrates, in particular, sI, sH methane hydrates, sI deuterated methane hydrate, and sII and sH alcohol clathrate hydrates.

In chapter 2, the computational methodology of classical and *ab initio* molecular dynamics simulations are introduced. In chapter 3, the vibrational spectra of structure I methane hydrates are calculated by *ab initio* molecular dynamics simulation. The frequency shift of the vibrational modes of methane molecules in sI clathrate

---

hydrate are discussed. In chapter 4, the vibrational spectra of structure H methane hydrates are calculated by *ab initio* molecular dynamics simulation. The differences of the vibrational spectra between sI and sH clathrate hydrates are explained. In chapter 5, the vibrational spectra of the deuterated methane hydrates are calculated by *ab initio* molecular dynamics simulation. The effect of the dynamics of host lattice on the intramolecular vibration of guest molecules are discussed. In chapter 6, the vibrational spectra of alcohol O-H bonds were calculated by *ab initio* and classical MD simulations are performed on the sII 3-methyl-1-butanol clathrate hydrate and sH 2-methyl-2-butanol clathrate hydrate. The effect of the guest-host hydrogen bonding on the structure of the clathrate hydrates and vibrational spectra are discussed. In chapter 7, the conclusions from this thesis and future direction are discussed.

## Chapter 2

# Computational methods

In this chapter, the basic theories of the classical and *ab initio* MD simulations used in this research are introduced.

## 2.1 Methodology of classical molecular dynamics simulation

### 2.1.1 Numerical integration method of Newton's equation of motion

In molecular dynamics simulations, the trajectories of atoms and molecules are calculated by numerically solving of Newton's equation of motion, i.e.,

$$m \frac{d^2 \mathbf{r}}{dt^2} = \mathbf{F}, \quad (2.1)$$

where  $m$  is the mass of the molecule,  $\mathbf{r}$  is the position of particle,  $\mathbf{F}$  is the force on the molecule, and  $N$  is total number of particles.

The Verlet integration algorithm [21] is a frequently used algorithm in molecular dynamics simulation because of its greater stability. This algorithm also satisfy the physical feature, time-reversibility and symplectic form. The equation of the Verlet algorithm is derived from the Taylor expansions of the position  $\mathbf{r}$  at time  $t$ . The time integration of the position  $\mathbf{r}(t)$  and velocity  $\mathbf{v}(t)$  of particle are expressed by

$$\mathbf{r}(t + \Delta t) = 2\mathbf{r}(t) - \mathbf{r}(t - \Delta t) + \frac{\mathbf{F}(t)}{m} \Delta t^2 + \mathcal{O}(\Delta t^4), \quad (2.2)$$

$$\mathbf{v}(t) = \frac{\mathbf{r}(t + \Delta t) - \mathbf{r}(t - \Delta t)}{2\Delta t} + \mathcal{O}(\Delta t^3), \quad (2.3)$$

where  $\Delta t$  is a time step.

However, the original Verlet algorithm is inconvenient to use because of the time in the equation of the position and velocity,  $\mathbf{r}(t + \Delta t)$  and  $\mathbf{v}(t)$ . To calculate the velocity and position at the same time instant, the Velocity Verlet algorithm [22],

i.e.,

$$\mathbf{r}(t + \Delta t) = \mathbf{r}(t) + \mathbf{v}(t)\Delta t + \frac{\mathbf{F}(t)}{2m}\Delta t^2 + \mathcal{O}(\Delta t^4), \quad (2.4)$$

$$\mathbf{v}(t + \Delta t) = \mathbf{v}(t) + \mathbf{v}(t)\Delta t + \frac{\mathbf{F}(t) + \mathbf{F}(t + \Delta t)}{2m}\Delta t^2 + \mathcal{O}(\Delta t^2), \quad (2.5)$$

is more commonly used.

### 2.1.2 Intermolecular interaction in classical MD

In molecular dynamics simulation using atomistic models, intermolecular and intramolecular interactions are frequently considered. The intermolecular interaction which stems from the electrostatic interaction between molecules is modeled using the Lennard-Jones potential [23], the dispersion and repulsion forces, and the Coulombic potential. The potential between particle  $i$  and  $j$  is expressed by

$$U_{ij}(r) = 4\varepsilon \left[ \left( \frac{\sigma}{r_{ij}} \right)^{12} - \left( \frac{\sigma}{r_{ij}} \right)^6 \right] + \frac{q_i q_j}{4\pi\varepsilon_0 r_{ij}}, \quad (2.6)$$

where  $\varepsilon$  is the depth of the potential,  $\sigma$  is the finite distance at which the interparticle potential is zero,  $r_{ij}$  is the distance between particle  $i$  and  $j$ ,  $q$  is charge at the particle, and  $\varepsilon_0$  is the vacuum permittivity.

The parameters  $\varepsilon$  and  $\sigma$  in the Lennard-Jones potential, are defined for each molecules. To calculate the Lennard-Jones interaction between different species, the Lorentz-Berthelot rule are employed as

$$\sigma_{ab} = \frac{\sigma_{aa} + \sigma_{bb}}{2}, \quad (2.7)$$

$$\varepsilon_{ab} = \sqrt{\varepsilon_{aa}\varepsilon_{bb}}. \quad (2.8)$$

### 2.1.3 Coulombic interactions

The electrostatic potential between charged particles  $i$  and  $j$  are expressed by the Coulombic potential, i.e.,

$$U_e(r_{ij}) = \frac{1}{4\pi\varepsilon_0} \frac{Q_i Q_j}{r_{ij}}, \quad (2.9)$$

where,  $Q$  is the charge of the particle and  $r_{ij}$  is the distance between particle  $i$  and  $j$ . The decay of this potential is slower than the Lennard-Jones potential ( $r^6$ ), so the cutoff method used in that case cause large error in calculation. Therefore Ewald

method are suggested as accurate computational method for coulombic interaction in periodic boundary condition.

### Ewald method

In the Ewald method, the interaction between particles are separated into the real space and reciprocal space functions. The potential energy of the Coulombic interaction in the Ewald method is

$$U_{\text{Ewald}} = U_{\text{Ewald}}^{\text{real}} + U_{\text{Ewald}}^{\text{recip}} + U_{\text{Ewald}}^{\text{self}} + U_{\text{Ewald}}^{\text{intra}}, \quad (2.10)$$

$$U_{\text{Ewald}}^{\text{real}} = \frac{1}{2} \sum_i^N \sum_j^N \frac{Q_i Q_j}{4\pi\epsilon_0} \frac{\text{erfc}(\alpha r_{ij})}{r_{ij}}, \quad (2.11)$$

$$U_{\text{Ewald}}^{\text{recip}} = \frac{1}{4\pi\epsilon_0} \frac{1}{2\pi V} \sum_{\mathbf{m} \neq 0} \frac{\exp(-\pi - 2\mathbf{m}^2/\alpha^2)}{m^2} \quad (2.12)$$

$$\left[ \left( \sum_i^N Q_i \cos(2\pi \mathbf{m} \cdot \mathbf{r}_i) \right)^2 + \left( \sum_i^N Q_i \sin(2\pi \mathbf{m} \cdot \mathbf{r}_i) \right)^2 \right], \quad (2.13)$$

$$U_{\text{Ewald}}^{\text{self}} = -\frac{1}{4\pi\epsilon_0} \frac{\alpha}{\sqrt{\pi}} \sum_i^N Q_i^2, \quad (2.14)$$

$$U_{\text{Ewald}}^{\text{intra}} = \sum_k^M \sum_{i,j \in k} -\frac{Q_i Q_j}{4\pi\epsilon_0} \frac{\text{erf}(\alpha r_{ij})}{r_{ij}}. \quad (2.15)$$

Similarly, the Coulombic force between charged particles are

$$F_i = F_i^{\text{real}} + F_i^{\text{recip}}, \quad (2.16)$$

$$F_i^{\text{real}} = \sum_{j \neq i}^N \frac{Q_i Q_j}{4\pi\epsilon_0} \left\{ \frac{\text{erfc}(\alpha r_{ij})}{r_{ij}} + \frac{2\alpha}{\sqrt{\pi}} \exp(-\alpha^2 r_{ij}^2) \right\} \frac{r_{ij}}{r_{ij}^2}, \quad (2.17)$$

$$F_i^{\text{recip}} = \frac{Q_i}{4\pi\epsilon_0} \frac{2}{V} \sum_{\mathbf{m} \neq 0} \frac{\exp(-\pi^2 \mathbf{m}^2/\alpha^2)}{m^2} \mathbf{m} \quad (2.18)$$

$$\left[ \sin(2\pi \mathbf{m} \cdot \mathbf{r}_i) \sum_j^N Q_j \cos(2\pi \mathbf{m} \cdot \mathbf{r}_j) - \cos(2\pi \mathbf{m} \cdot \mathbf{r}_i) \sum_j^N Q_j \sin(2\pi \mathbf{m} \cdot \mathbf{r}_j) \right].$$

### 2.1.4 Periodic boundary condition

There are several boundary conditions used in molecular simulations. The most common boundary conditions are free boundary condition and periodic boundary condition. The free boundary condition is mainly used in the calculations for the isolated molecular systems and the periodic boundary condition is suitable for the bulk phase systems.

## 2.2 Density functional theory

In this chapter, *ab initio* molecular dynamics using density functional theory is introduced. To perform the calculations based on quantum mechanics, solving the Schrödinger equation is one of direct methods. However, it is impossible to obtain the analytic solution of Schrödinger equation for many-body system is impossible. So there are many types of approximation to solve the actual problems for quantum mechanics. Density functional theory (DFT) is one of the quantum mechanical modeling methods widely used in computational physics and chemistry. In density functional theory, the properties of many-electron system can be determined by functionals of electron density.

### 2.2.1 Born-Oppenheimer approximation

At first, Born-Oppenheimer approximation is introduced which is used to separate the motions of nuclei and electrons in atoms. For the system composed of  $N$  electrons and  $N_a$  nuclei, the Schrödinger equation of the total system is given by

$$\hat{H}_{\text{tot}}\Psi_{\text{tot}}(\mathbf{r}, \mathbf{R}) = E_{\text{tot}}\Psi_{\text{tot}}(\mathbf{r}, \mathbf{R}), \quad (2.19)$$

where  $\Psi_{\text{tot}}(\mathbf{r}, \mathbf{R})$  is the wave function of the total system,  $\mathbf{r} = \mathbf{r}_1, \dots, \mathbf{r}_N$  is coordinates of electrons including spin, and  $\mathbf{R} = \mathbf{R}_1, \dots, \mathbf{R}_{N_a}$  indicates coordinates of nucleus.  $E_{\text{tot}}$  is the total energy.  $\hat{H}_{\text{tot}}$  is Hamiltonian operator of the total system given by

$$\begin{aligned} \hat{H}_{\text{tot}} &= -\sum_i \frac{1}{2} \nabla_i^2 - \sum_I \frac{1}{2M_I} \nabla_I^2 + \frac{1}{2} \sum_{i \neq j} \frac{1}{|\mathbf{r}_i - \mathbf{r}_j|} - \sum_{i,I} \frac{Z_I}{|\mathbf{r}_i - \mathbf{R}_I|} + \frac{1}{2} \sum_{I \neq J} \frac{Z_I Z_J}{|\mathbf{R}_I - \mathbf{R}_J|} \\ &= \hat{T}_e + \hat{T}_n + \hat{V}_{ee} + \hat{V}_{ne} + \hat{V}_{nn}, \end{aligned} \quad (2.20)$$

where, the subscript  $i, j$  indicate the serial of electrons and  $I, J$  are for nucleus.  $M$  and  $Z$  are mass and charge of nucleus, respectively. Hartree atomic unit ( $\hbar = m_e = e = a_0 = 1$ ) is used. The first and second term indicates the kinetic energy of electrons and nucleus, respectively and the following terms are for potential energy of electron-electron, electron-nuclei, nuclei-nuclei interactions. Even in the case of the most light atom, hydrogen atom, the mass of the nuclei is 1836 times greater than that of electron. The motion of nuclei is quite slower than that of electrons. Therefore, electrons would respond instantaneously to nuclear motion and always

occupy the ground state of the nuclear configuration. In this assumption, the motion of electrons and nuclear are separated. In this approximation, the eigenfunction that satisfies the equation (2.19) is assumed as follow.

$$\Psi_{\text{tot}}(\mathbf{r}, \mathbf{R}) = \Psi_{\text{el}}(\mathbf{r}, \mathbf{R})\Psi_{\text{nuc}}(\mathbf{R}). \quad (2.21)$$

The  $\Psi_{\text{el}}$  is eigenfunction of the electron part of the Hamiltonian  $\hat{H}_{\text{el}}$  in the equation (2.20),

$$\hat{H}_{\text{el}} = -\sum_i \frac{1}{2} \nabla_i^2 + \frac{1}{2} \sum_{i \neq j} \frac{1}{|\mathbf{r}_i - \mathbf{r}_j|} - \sum_{i,I} \frac{Z_I}{|\mathbf{r}_i - \mathbf{R}_I|}, \quad (2.22)$$

$$\hat{H}_{\text{el}}\Psi_{\text{el}}(\mathbf{r}, \mathbf{R}) = E_{\text{el}}(\mathbf{R})\Psi_{\text{el}}(\mathbf{r}, \mathbf{R}), \quad (2.23)$$

where the energy eigenvalue of the electrons  $E_{\text{el}}$  is depending on geometry of the nuclei. With this assumption, the equation (2.19) can be written as

$$\begin{aligned} \hat{H}_{\text{tot}}\Psi_{\text{tot}} = \Psi_{\text{el}} \left[ -\sum_I \frac{1}{2M_I} \nabla_I^2 + E_{\text{el}}(\mathbf{R}) + \frac{1}{2} \sum_{I \neq J} \frac{Z_I Z_J}{|\mathbf{R}_I - \mathbf{R}_J|} \right] \Psi_{\text{nuc}} \\ - \sum_I \frac{1}{2M_I} \{2\nabla_I \Psi_{\text{el}} \cdot \nabla_I \Psi_{\text{nuc}} + \Psi_{\text{nuc}} \nabla_I^2 \Psi_{\text{el}}\}. \end{aligned} \quad (2.24)$$

The second term of the equation (2.24) indicates the effect of the motion of nuclei on the state of the electrons. In the Born-Oppenheimer approximation, the motions of electrons and nuclei are separated and the equation can be written as

$$\left[ -\sum_I \frac{1}{2M_I} \nabla_I^2 + E_{\text{el}}(\mathbf{R}) + \frac{1}{2} \sum_{I \neq J} \frac{Z_I Z_J}{|\mathbf{R}_I - \mathbf{R}_J|} \right] \Psi_{\text{nuc}} = E\Psi_{\text{nuc}}. \quad (2.25)$$

In this approximation, nuclei of atom feels the energy of the electron as classical potential. On the other hand, the wave function of the electrons  $\Psi_{\text{el}}$  obey only on the position of nuclei. The electron energy of the ground state is a function of the position of the nuclei.

### 2.2.2 Hohenberg-Kohn theorems

In this section Hohenberg-Kohn theorems that legitimized the use of electron density  $\rho(\mathbf{r})$  to describe the electronic system is introduced. Hamiltonian of the electronic system in the external potential  $V_{\text{ext}}(\mathbf{r})$  is given by

$$\hat{H} = -\frac{1}{2} \sum_i \nabla_i^2 + \sum_i V_{\text{ext}}(\mathbf{r}_i) + \frac{1}{2} \sum_{i \neq j} \frac{1}{|\mathbf{r}_i - \mathbf{r}_j|}. \quad (2.26)$$

In this condition, Hohenberg and Kohn gave the following theorems [24].

1. The external potential  $v_{\text{ext}}(\mathbf{r})$  is determined, within a trivial additive constant, by the electron density  $\rho_0(\mathbf{r})$ .

The first theorem of Hohenberg-Kohn shows that the ground state density  $\rho_0(\mathbf{r})$  uniquely determines the external potential and thus all properties of the system, including the many-body wave function. Electron density of the ground state of the system  $\rho_0(\mathbf{r})$  uniquely determines the external potential  $V_{\text{ext}}(\mathbf{r})$  by the Hohenberg-Kohn theorem. The Hamiltonian (2.26) composed of the external potential  $V_{\text{ext}}$  give the wave function including excited states and ground state of the system  $\Psi_i(\mathbf{r})$  and  $\Psi_0(\mathbf{r})$ . The  $\rho_0(r)$  is given by the  $\Psi_0(\mathbf{r})$ .

The second theorem is the energy variational principle.

2. Energy of the electronic system as functional of density  $E_{\text{HK}}[\rho]$  can be defined for any external potential  $V_{\text{ext}}(\mathbf{r})$ . The ground energy state of the system is the state that have minimal of the functional. For a trial density  $\tilde{\rho}(r)$ , such that  $\tilde{\rho}(\mathbf{r}) \geq 0$  and  $\int \tilde{\rho}(\mathbf{r}) d\mathbf{r} = N$ ,

$$E_0 \leq E_{\text{HK}}[\tilde{\rho}]. \quad (2.27)$$

The energy functional  $E_{\text{HK}}[\rho]$  is

$$\begin{aligned} E_{\text{HK}}[\rho] &= T[\rho] + E_{\text{int}}[\rho] + \int d\mathbf{r} V_{\text{ext}}(\mathbf{r})\rho(\mathbf{r}) + E_{\text{II}} \\ &\equiv F_{\text{HK}} + \int d\mathbf{r} V_{\text{ext}}(\mathbf{r})\rho(\mathbf{r}) + E_{\text{II}}, \end{aligned} \quad (2.28)$$

where  $E_{\text{II}}$  is interactions among nuclei. Therefore, we can calculated the density and energy at the ground state of the system if we can derive the functional  $F_{\text{HK}}[\rho]$ .

### 2.2.3 Kohn-Sham equation

With the previous equation, the electron density and ground state energy can be derived by variational principle. However, the form of the accurate energy as functional of many-body electron density is not known. The energy of grand state in Hohenberg-Khon theorem (2.28) is written as follows in Kohn-Sham method, i.e.,

$$E_{\text{KS}} = T_s[\rho] + \int d\mathbf{r} V_{\text{ext}}(\mathbf{r})\rho(\mathbf{r}) + E_{\text{Hartree}}[\rho] + E_{\text{II}} + E_{\text{xc}}[\rho], \quad (2.29)$$

where  $T_s$  is kinetic energy of non-interacting particles written by

$$\begin{aligned} T_s &= -\frac{1}{2} \sum_{\sigma} \sum_i \langle \psi_i^{\sigma} | \nabla^2 | \psi_i^{\sigma} \rangle \\ &= \frac{1}{2} \sum_{\sigma} \sum_i \int d\mathbf{r} |\nabla \psi_i^{\sigma}(\mathbf{r})|^2. \end{aligned} \quad (2.30)$$

where  $\sigma$  is spin of electrons.  $H_{\text{KS}}$  is classical Coulombic interaction energy of electron density  $\rho(\mathbf{r})$  interacting itself,

$$E_{\text{Hartree}} = \frac{1}{2} \int d\mathbf{r} d\mathbf{r}' \frac{\rho(\mathbf{r})\rho(\mathbf{r}')}{|\mathbf{r} - \mathbf{r}'|}. \quad (2.31)$$

Here  $V_{\text{ext}}$  is external potential from nuclei and other interactions from out of the system. In this equation, effect of many-body interactions, such as exchange and correlation term is included in  $E_{\text{ex}}$ .

Kohn-Sham Schrödinger equation is derived by the variational principle, i.e.,

$$(H_{\text{KS}}^{\sigma} - \epsilon_i^{\sigma})\psi_i^{\sigma}(\mathbf{r}) = 0, \quad (2.32)$$

where  $\epsilon_i^{\sigma}$  is eigenvalue and  $H_{\text{KS}}^{\sigma}$  is effective Hamiltonian.

$$H_{\text{KS}}^{\sigma}(\mathbf{r}) = -\frac{1}{2}\nabla^2 + V_{\text{KS}}^{\sigma}(\mathbf{r}), \quad (2.33)$$

$$V_{\text{KS}}^{\sigma}(\mathbf{r}) = V_{\text{ext}}(\mathbf{r}) + V_{\text{Hartree}}(\mathbf{r}) + V_{\text{ex}}^{\sigma}(\mathbf{r}). \quad (2.34)$$

This equation is solved self-consistently.

### 2.2.4 Local density approximation, Generalized gradient approximation

To perform actual calculation in Kohn-Sham method, specific formula of the exchange-correlation term is required. However, the accurate form of the exchange-correlation is not known. Therefore there are several approximations to describe the exchange and correlation term in the potential. Local density approximation (LDA) is a class of approximation to the exchange-correlation energy functional. The distribution of the electron density is approximated by local elements of uniform electron densities. The  $E_{\text{ex}}$  is depending only on the local density  $\rho(\mathbf{r})$ ,

$$E_{\text{xc}}^{\text{LDA}} = \int \rho(\mathbf{r}) \epsilon_{\text{xc}}^{\text{LDA}}(\rho(\mathbf{r})) d\mathbf{r}. \quad (2.35)$$

Real systems are not homogeneous as LDA approximation and have varying density landscape around electrons. Generalized gradient approximation (GGA) is

more accurate XC functionals that consider both of local and semilocal information. The local density  $\rho(\mathbf{r})$  and its gradient of at a given point  $\nabla\rho(\mathbf{r})$  is

$$E_{\text{xc}}^{\text{GGA}} = \int F_{\text{xc}}(\rho(\mathbf{r}), \nabla\rho(\mathbf{r})) d\mathbf{r}. \quad (2.36)$$

There are several other extended functionals for more accurate calculations. For examples, Meta-GGA methods are the approximations of the exchange-correlation term that consider kinetic energy of the electron density ( $\nabla^2\rho$ ). The Hybrid functional methods introduce Hartree-Fock term.

## 2.3 Car-Parrinello molecular dynamics simulation

Car-Parrinello molecular dynamics is molecular dynamics simulation using Car-Parrinello method, a method of the *ab initio*, or first principles molecular dynamics simulation. In Born-Oppenheimer molecular dynamics, the time development of electron and nuclei are separated. So calculation of the ground state of electron is required in all of the MD steps. However, the time development of electron and nuclear are performed at same calculation without matrix diagonalization by the Car-Parrinello method. In the Car-Parrinello MD, the computational time is quite reduced compared to Born-Oppenheimer MD. The Car-Parrinello method is based density functional theory and introduces the electronic degrees of freedom as fictitious dynamical values, writing an extended Lagrangian  $\mathcal{L}_{\text{CP}}$  for the system.

$$\begin{aligned} \mathcal{L}_{\text{CP}} = & \frac{1}{2} \sum_I M_I \dot{\mathbf{R}}_I^2 + \sum_i^N \int \mu |\dot{\psi}_i(\mathbf{r})|^2 d\mathbf{r} \\ & - E_{\text{KS}}[\psi, \mathbf{R}] - \sum_{i,j} \Lambda_{ij} \left[ \int \psi_i^*(\mathbf{r}) \psi_j(\mathbf{r}) d\mathbf{r} - \delta_{ij} \right], \end{aligned} \quad (2.37)$$

where  $\mu$  is the fictitious mass of the orbital degrees of freedom and  $\Lambda$  is Lagrangian multiplier matrix to satisfy the orthonormality constraint. The Newtonian equations of motion are computed from the Euler-Lagrange equations,

$$\frac{d}{dt} \left( \frac{\delta \mathcal{L}_{\text{CP}}}{\delta \dot{\psi}_i^*(\mathbf{r})} \right) = \frac{\delta \mathcal{L}_{\text{CP}}}{\delta \psi_i^*(\mathbf{r})}, \quad (2.38)$$

$$\frac{d}{dt} \left( \frac{\partial \mathcal{L}_{\text{CP}}}{\partial \dot{\mathbf{R}}_I} \right) = \frac{\partial \mathcal{L}_{\text{CP}}}{\partial \mathbf{R}_I}. \quad (2.39)$$

Equation of motions of Kohn-Sham orbital and nuclear is

$$\mu \ddot{\psi}_i(\mathbf{r}) = -\frac{\delta E_{\text{KS}}[\psi, \mathbf{R}]}{\delta \psi_i^*(\mathbf{r})} + \sum_j \Lambda_{ij} \psi_j(\mathbf{r}), \quad (2.40)$$

$$M_I \ddot{\mathbf{R}}_I = -\frac{\partial E_{\text{KS}}[\psi, \mathbf{R}]}{\partial \mathbf{R}_I} + \sum_{ij} \Lambda_{ij} \frac{\partial}{\partial \mathbf{R}_I} \int \psi_i^*(\mathbf{r}) \psi_j(\mathbf{r}) d\mathbf{r}. \quad (2.41)$$

If the initial state of the electron is enough close to the ground state, we can calculate the trajectories of the nuclear by solving these equations, *ab initio* MD. In the Car-Parrinello MD, following Hamiltonian is conserved:

$$\mathcal{H}_{\text{CP}} = \frac{1}{2} \sum_I^{N_a} M_I \dot{\mathbf{R}}_I^2 + \sum_i^N \mu \int |\dot{\psi}_i(\mathbf{r})|^2 d\mathbf{r} + E_{\text{KS}}[\psi, \mathbf{R}]. \quad (2.42)$$

## Chapter 3

# Structure I methane hydrate

### 3.1 Introduction

Simple methane hydrate forms sI, a cubic crystal structure composed of two small ( $5^{12}$ ) and six large ( $5^{12}6^2$ ) cages, which are formed from the hydrogen bonding of water molecules [1]. It is now well known that the symmetric C–H stretching vibrational frequencies of methane molecules in the large cages ( $2905\text{ cm}^{-1}$ ) are lower than those in the small cages ( $2915\text{ cm}^{-1}$ ), relatively to that in the gaseous state ( $2917\text{ cm}^{-1}$ ) [25]. A semi-empirical “loose cage-tight cage model” [26] has been proposed to explain the experimentally observed shift in the vibrational frequency [27]. In this model, the higher frequency is ascribed to the steeper gradient of the cell potential in the small cages. The vibrational frequency shift ( $\nu$ ) in the model is obtained by treating the anharmonic term in the potential energy function as small perturbations to the harmonic potential of the free molecule, which can be described by a matrix of interactions. If the derivative of the potential in the matrix is negative (large distance, loose cage), the  $\nu$  is negative, and whereas for a positive derivative (small distance, tight cage), the  $\nu$  is positive. This loose cage-tight cage model predicts the trends of the vibrational frequencies for guests trapped in clathrate hydrate cages, with lower frequency of the stretching vibration for the guests in the larger cages.

There are nine vibrational modes (15 degrees of freedom 3 translations 3 rotations), which are classified into four kinds of vibrational types, such as three bending, two rocking, one symmetric stretching, and three asymmetric stretching vibrational types. Frequencies in gas phases are  $1306\text{ cm}^{-1}$ ,  $1534\text{ cm}^{-1}$ ,  $2917\text{ cm}^{-1}$ , and  $3019\text{ cm}^{-1}$ , respectively [28]. Figure 3.1 is images of the vibrational mode of methane molecule.

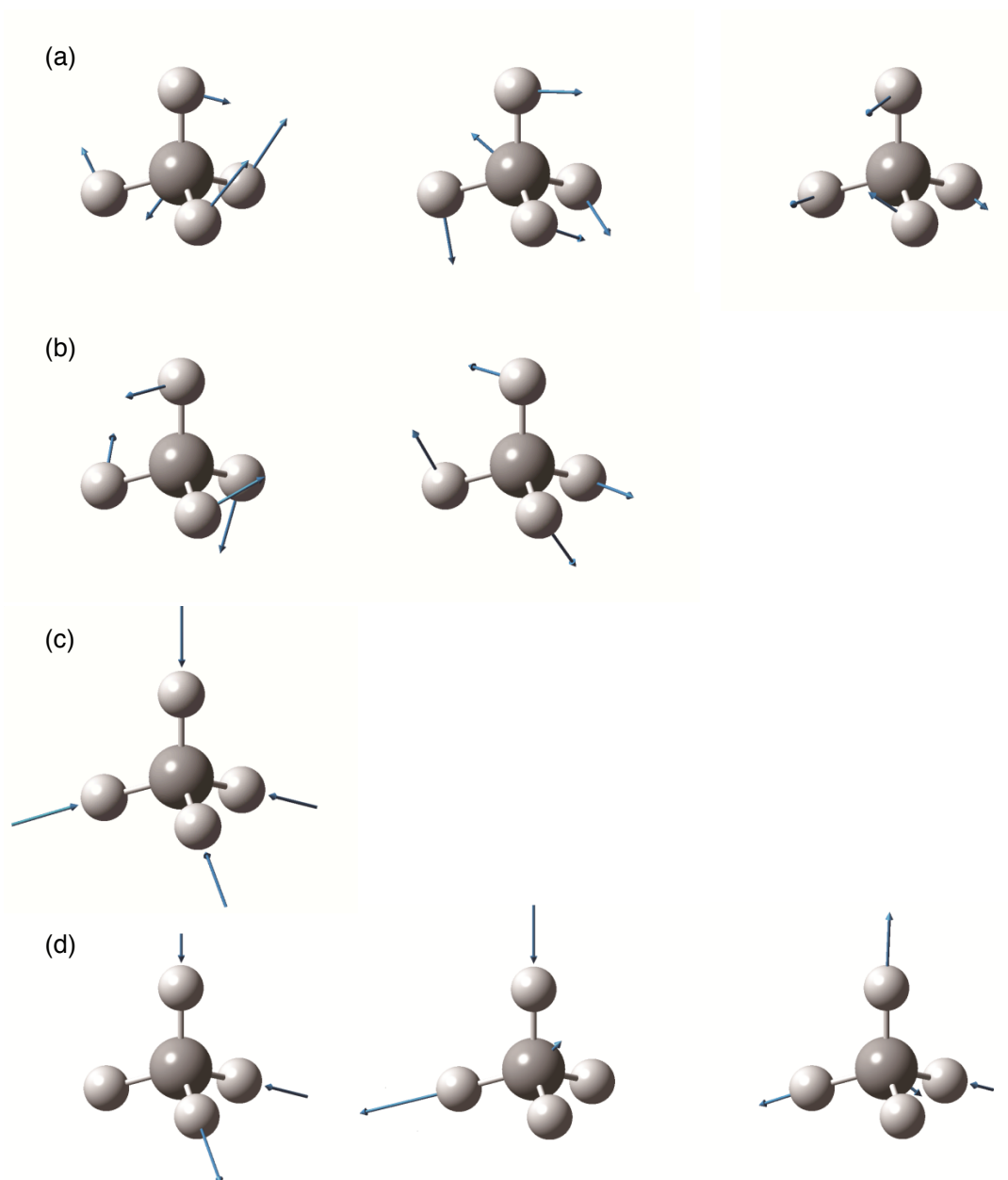


Fig.3.1 (a) bending mode: three degenerated motions, (b) rocking mode: two degenerated motions, (c) symmetric stretching: no degenerated motion, (d) asymmetric stretching: three degenerated motions. The vectors of the vibrational modes were calculated in harmonic approximation using Car-Parrinello MD.

In the present study, we analyze five different autocorrelation functions: velocity of hydrogen atoms, change in the C–H bond length, change in the H–C–H angle, change in the C–H vector direction, and center of mass velocity of the methane molecule. Figure 3.2 schematically illustrates the five modes of molecular motions for the autocorrelation functions considered. A systematical way to analyze the molecular vibrations is to perform a normal mode analysis for the 15 Cartesian coordinates of the methane molecule for the center of mass motion, molecular rotation, and intramolecular vibrations. The normal modes are extracted by separating out the modes of center of mass and rotation from all of the modes of molecular motions. Our approach with the autocorrelation functions for the vibrational spectra, it allows to approximately extract the normal modes by using suitable autocorrelation functions. The center of mass velocities that we used separate the molecular translation. The C–H vector direction includes molecular rotation and intramolecular vibration. These two modes are approximately separable since rotation and intramolecular vibration, bending and rocking, have rather different frequencies. The C–H bond length and H–C–H angle have information of intramolecular vibrations and approximately represent each intramolecular vibrations for bond stretching and angle vibrations, respectively. The velocities of hydrogen atoms include all many types of vibrations. Therefore, the velocity of hydrogen, C–H bond length, H–C–H angle, and C–H direction modes provide direct information of the intramolecular vibrations. The velocity of hydrogen, C–H direction, and center of mass provide information of molecular vibrations. These autocorrelation functions and computed vibrational spectra consider the vibrational modes of methane molecules, which are coupled and affected by the water molecules forming the cages. The identification of the symmetric, asymmetric stretching, rocking, and bending were performed by comparing observed frequencies with methane molecule in gas phase [28]. To treat the large number of atoms in a unit cell of structure I clathrate hydrate and calculate longer simulation time, the Car-Parrinello method [29] is employed for the *ab initio* MD simulation.

## 3.2 Computational details

The Car-Parrinello MD (CPMD) simulation was performed using the CPMD package [30] to provide the trajectories for calculation of the autocorrelation functions. Although it is known that there is a redshift in the dynamics of light atoms due to

the factious of the electron dynamics in the Car-Parrinello MD method, we employed this method because the redshift has little effect in the observed differences of the vibrational frequencies between cages. Our simulation was based on the DFT using the Perdew-Burke-Ernzerhof [31] for the approximation of the exchange-correlation terms, which is the same as in previous simulations [9, 10]. The valence-core interaction was described by the Troullier-Martines [32] and norm-conserving pseudopotential using the Kleinman-Bylander [33] separation scheme for carbon, hydrogen, and oxygen. The plane wave functions were used for the basis set with an energy cutoff of 80 Ry. The Brillouin zone of the supercell was sampled at the  $\Gamma$  point. The simulation system was a cubic unit cell of structure I clathrate hydrate. The unit cell was composed of 46 water molecules consisting of two  $5^{12}$  and six  $5^{12}6^2$  cages, each occupied by a methane molecule. Periodic boundary conditions were employed. The initial coordinates of the oxygen atoms in the water molecules in the unit cell were those determined by X-ray crystallography [34]. The positions of hydrogen atoms were determined from calculations that minimized the energy in a zero net dipole moment configuration, which is consistent with the ice rule. The unit cell dimension was 11.83 Å (from experimental measurements [35]). The simulation time-step was 0.096755 fs and the fictitious electron mass was 400 a.u. for the Car-Parrinello method. The total simulation time was 35 ps, with the initial 5 ps used for the equilibration and the remaining 30 ps used to average the autocorrelation functions. In the initial 5 ps of equilibration, the velocity scaling method was used to control the temperature to 113.0 K. The other 30 ps to calculate the autocorrelation functions were performed in the constant number of particles Volume, and Energy ( $NVE$ ) ensemble. To prevent temperature drift, the temperature was scaled to 113 K when the temperature fluctuated above 133 K and under 93 K. However, over the 30 ps, there were only two instances when the scaling was applied (at 4.237 ps and 4.272 ps) caused by fluctuations in the temperature. Therefore, there is little effect to the molecular vibrations by the scaling. The actual average temperature of the 30 ps calculation was 112.4 K. The length of an autocorrelation function was 16.0 ps; a total of 1400 autocorrelation functions were calculated every 10.1 fs and then averaged. The resolution of the vibrational spectra was  $2.08 \text{ cm}^{-1}$ . The Hann window function was employed for the Fourier transforms.

It should be noted that in our chosen computational method with CPMD, two issues must be clearly stated to understand the limitations of the presented results:

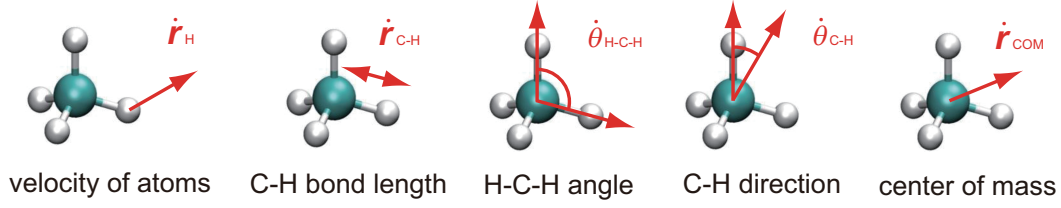


Fig.3.2 The five modes of molecular motions for the autocorrelation functions: velocity of hydrogen atoms, change in the C–H bond length, change in the H–C–H angle, change in the C–H direction, and center of mass velocity. In the calculations, the  $\cos(\theta_{C-H})$  was used for  $\theta_{C-H}$  and the  $\cos(\theta_{H-C-H})$  for  $\theta_{H-C-H}$ .

van der Waals correction in the DFT method and treatment of the fictitious electron mass in the Car-Parrinello method. It is known that the estimation of the van der Waals force in DFT is insufficient [36] and several van der Waals corrections are advocated [37, 38] to solve this issue. We do not consider the van der Waals correction here and the effect of the correction in the vibrational spectra of clathrate hydrates should be considered in a future study. It is also reported that the fictitious electron mass used in the Car-Parrinello method changes vibrational spectra, [39–43] such as the redshift shown in this study. Therefore, the calculated vibrational spectra should be compared with that calculated from Born-Oppenheimer molecular dynamics simulation to estimate the influence of the fictitious electron mass in clathrate hydrate system.

### 3.2.1 Calculation of autocorrelation functions

The vibrational spectra of molecules are computed by the Fourier transform of autocorrelation functions [44]. The autocorrelation function shows the relation between the physical value at time  $t'$   $\mathbf{A}(t')$  and the value at the time  $t''$ ,  $\mathbf{A}(t'')$ . The autocorrelation function  $C(t'', t')$  is defined as

$$C_{AA}(t'', t') = \langle \mathbf{A}(t'') \cdot \mathbf{A}(t') \rangle. \quad (3.1)$$

If the time is replaced to  $t = t'' - t'$ , equation (3.1) is

$$\begin{aligned} C_{AA}(t'', t') &= \langle \mathbf{A}(t'' - t' + t') \cdot \mathbf{A}(t') \rangle \\ &= \langle \mathbf{A}(t + t') \cdot \mathbf{A}(t') \rangle. \end{aligned} \quad (3.2)$$

When the system is in equilibrium,  $C(t'', t')$  is not depending on the time  $t'$ . Therefore, the  $C(t'', t')$  is function of the difference of the time  $t = t'' - t'$ . If  $t' = 0$ ,

$$C_{AA}(t) = \langle \mathbf{A}(t) \cdot \mathbf{A}(0) \rangle. \quad (3.3)$$

In equilibrium state, time-correlation function has symmetric time development, i.e.,

$$C_{AA}(t) = C_{AA}(-t). \quad (3.4)$$

The autocorrelation function in MD simulation is calculated by averaging the functions,

$$C_{AA}(t) = \frac{\sum_{k=1}^M \mathbf{A}(t + t_k) \cdot \mathbf{A}(t_k)}{M}, \quad (3.5)$$

where  $M$  is the number of averages of the correlation functions that is sampled every  $t_k$ .

Velocity autocorrelation function of atoms or molecules,  $C_{\mathbf{v}}$ , is commonly used in MD simulation to characterize the dynamics of particles, i.e.,

$$C_{\mathbf{v}}(t) = \frac{\langle \mathbf{v}(t) \cdot \mathbf{v}(0) \rangle}{\langle \mathbf{v}(0) \cdot \mathbf{v}(0) \rangle}. \quad (3.6)$$

Relaxation of autocorrelation functions are closely linked with the environment of the molecules, especially for the phase. The velocity autocorrelation function of molecules in solid phase vibrate and decay slowly to 0. That in the liquid phase also show the vibration, but the decay is much faster than that in the solid. The decay of the autocorrelation function of mono atomic molecules in gas phase is quite slow but not vibrating. Similarly, the autocorrelation function of molecular axis or direction of bond reflect the dynamics of the molecular rotation and intramolecular angle changing. In this study, we calculated five types of autocorrelation functions as shown in figure 3.2. The mathematical definition of the each autocorrelation functions are explained in the followings.

- Velocity of atom

$$\mathbf{A}(t) = \mathbf{v}_A(t) = \frac{d}{dt} \mathbf{r}_A(t) \quad (3.7)$$

- Change of the intramolecular bond length A–B

$$A(t) = \frac{d}{dt} r_{\text{AB}_{\text{bond}}}(t) = \frac{d}{dt} |\mathbf{r}_A(t) - \mathbf{r}_B(t)| \quad (3.8)$$

- Angle of bonds A–B–C

$$A(t) = \frac{d}{dt} \cos\theta_{\text{A–B–C}}(t) = \frac{d}{dt} \frac{\mathbf{r}_{\text{AB}}(t) \cdot \mathbf{r}_{\text{BC}}(t)}{|\mathbf{r}_{\text{AB}}(t)| |\mathbf{r}_{\text{BC}}(t)|} \quad (3.9)$$

- Direction of intramolecular bond A–B

$$A(t) = \frac{d}{dt} \cos\theta_{\text{AB}}(t) = \frac{d}{dt} \frac{\mathbf{r}_{\text{AB}}(0) \cdot \mathbf{r}_{\text{AB}}(t)}{|\mathbf{r}_{\text{AB}}(0)| |\mathbf{r}_{\text{AB}}(t)|} \quad (3.10)$$

- Velocity of the center of the center of mass of the molecules

$$\mathbf{A}(t) = \frac{d}{dt} \mathbf{r}_{\text{Molecule}}(t) = \frac{d}{dt} \frac{\sum_{i=1}^N m_i \mathbf{r}_i}{\sum_{i=1}^N m_i} \quad (3.11)$$

### 3.3 Results and Discussions

#### 3.3.1 Autocorrelation function of methane molecules

The autocorrelation functions of methane molecules in clathrate hydrates are shown in Figure 3.3. The red solid lines and dashed green lines indicates that in the  $5^{12}$  and  $5^{12}6^2$  cages, respectively. The autocorrelation function computed from velocity of hydrogen atom has information of all of the motion of the methane molecules, translation, rotation, and intramolecular vibrations. So the decay of this autocorrelation function is faster than that of velocity of carbon atoms mainly representing translational motion of molecules as shown in Figures 3.3 and 3.4. The autocorrelation functions related with the intramolecular vibrations, C–H bond length and H–C–H angle shown in Figures 3.5 and 3.6, respectively, vibrated and the decay of the altitude of the function is slower than the autocorrelation function of velocity of hydrogen atoms. On the other hand, the decay of the autocorrelation function from C–H vector that related with the rotation of molecules are slow and very similar to the velocity autocorrelation function of hydrogen atoms. Therefore, the rapid decay of the velocity autocorrelation function of hydrogen atoms are originated from the rotation of the molecules in the cages. The velocity autocorrelation function of carbon atoms are similar to the velocity autocorrelation function of the center of mass of the methane molecules that corresponds translational motion of the molecules as shown in Figure 3.8.

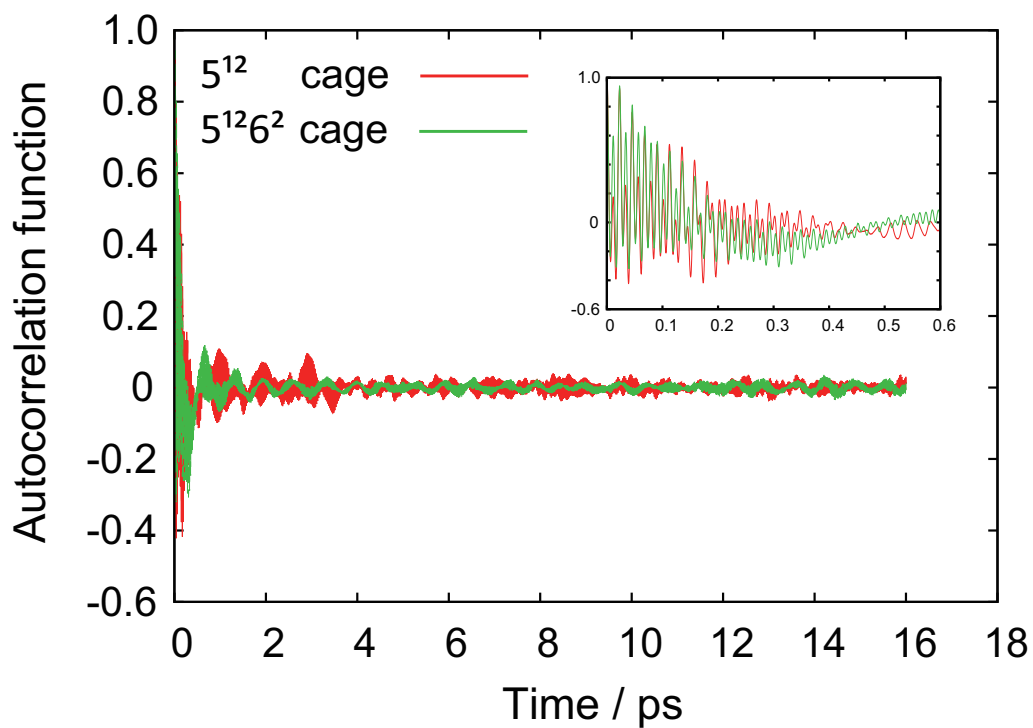


Fig.3.3 Autocorrelation function from velocity of hydrogen atoms in methane molecules

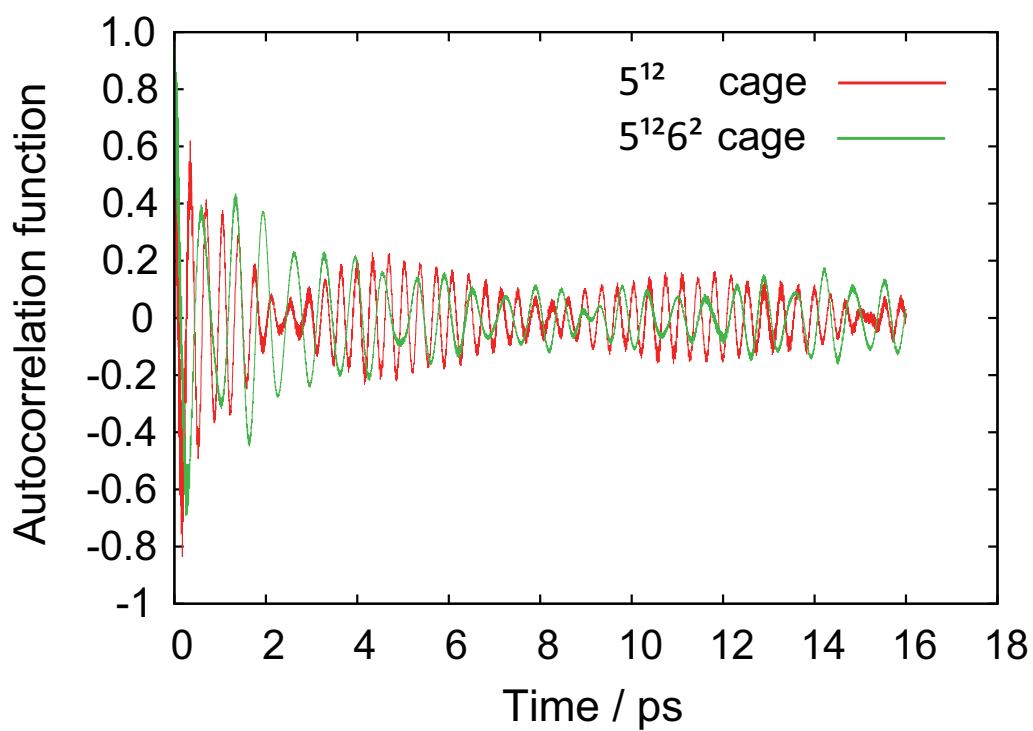


Fig.3.4 Autocorrelation function from velocity of carbon atoms in methane molecules

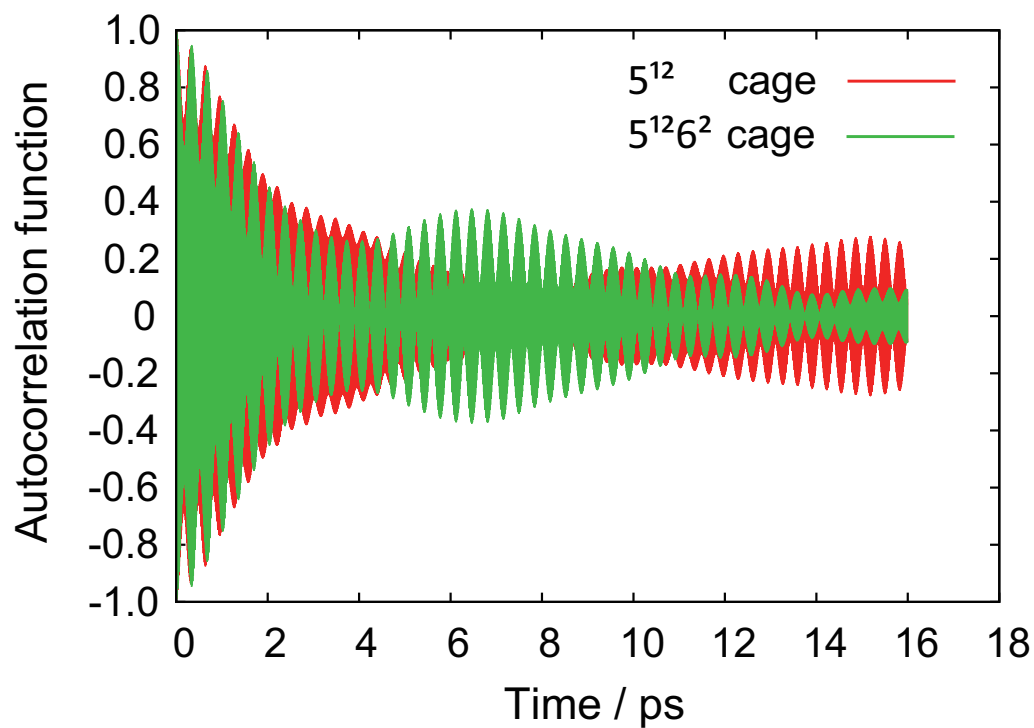


Fig.3.5 Autocorrelation function from C–H bond length in methane molecules

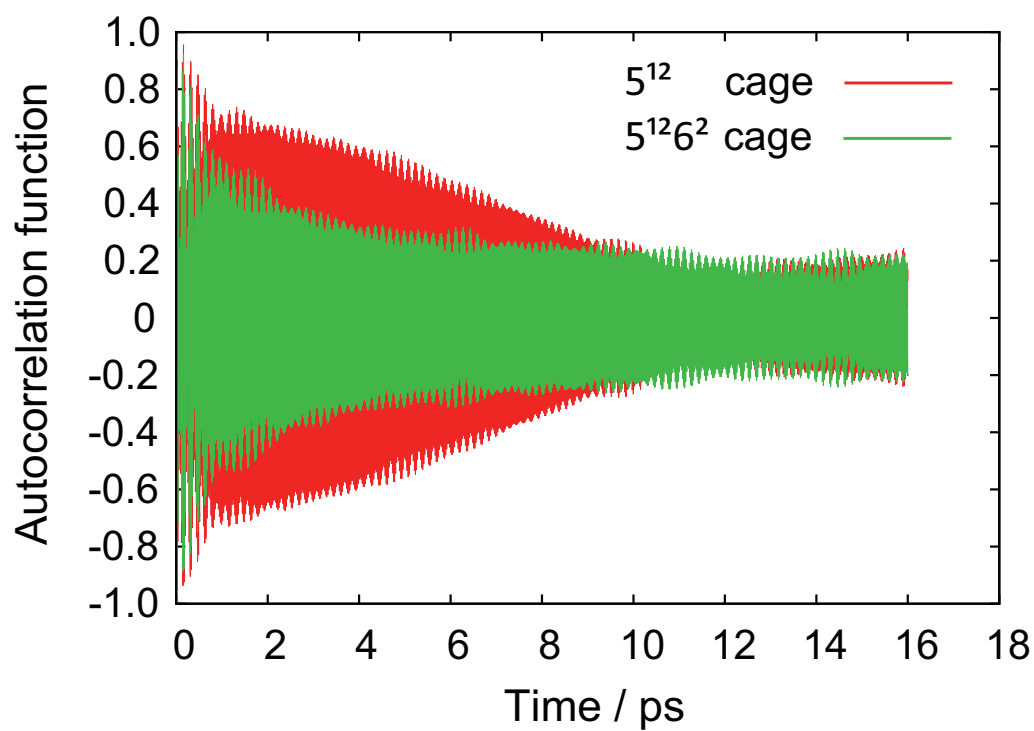


Fig.3.6 Autocorrelation function from H–C–H angle in methane molecules

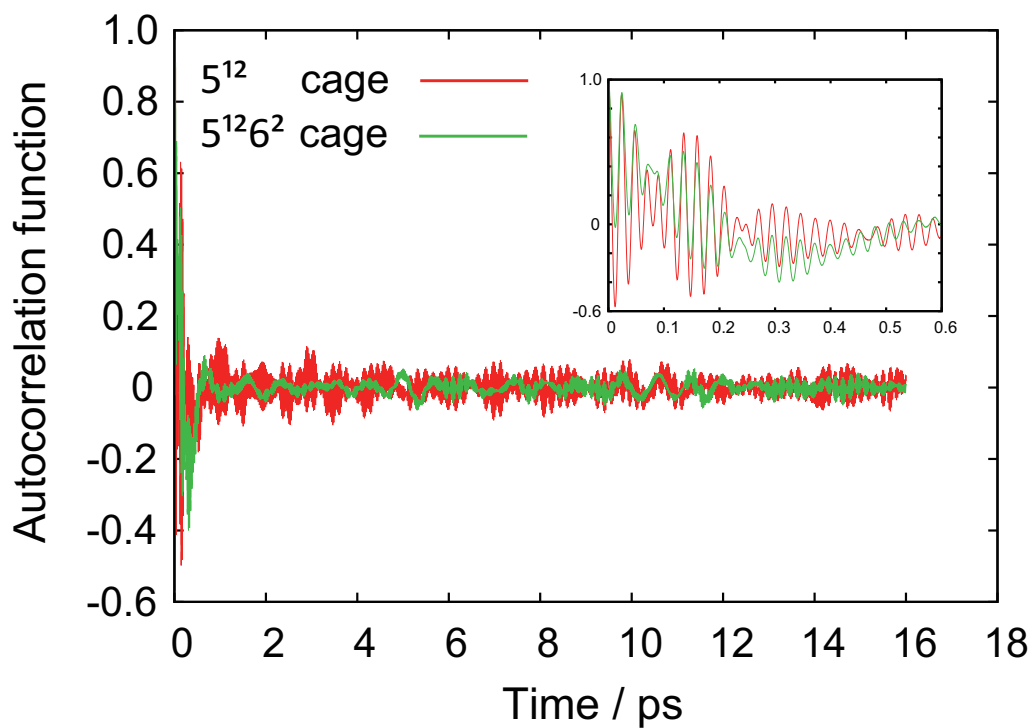


Fig.3.7 Autocorrelation function from C–H vector in methane molecules

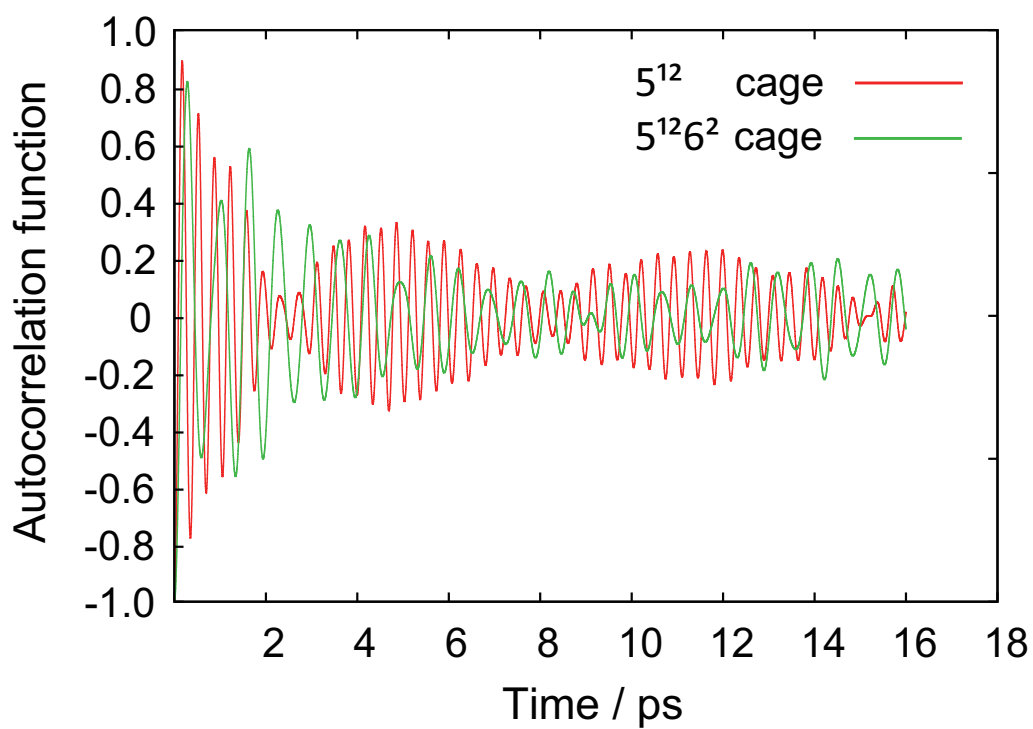


Fig.3.8 Autocorrelation function from center of mass of methane molecules

### 3.3.2 Vibrational spectra

#### Stretching vibrations

The vibrational spectra are computed by the Fourier transform of the autocorrelation functions, i.e.,

$$\begin{aligned} I(\omega) &= \frac{1}{2} \int_{-\infty}^{\infty} \langle \mathbf{A}(t) \cdot \mathbf{A}(0) \rangle \exp(i\omega t) dt \\ &= \frac{1}{2\pi} \int_{-\infty}^{\infty} C_{AA}(t) \exp(i\omega t) dt. \end{aligned} \quad (3.12)$$

Wavenumber  $\tilde{\nu}$  ( $\text{cm}^{-1}$ ) is frequently used in the discussion of the vibrational spectra of the molecular vibrations. Wavenumber, spatial frequency of a wave, is defined as

$$\tilde{\nu} = \frac{1}{\lambda}, \quad (3.13)$$

where  $\lambda$  is wavelength. The wavenumber can be converted to frequency  $\nu$  by,

$$c = \nu\lambda, \quad (3.14)$$

$$\tilde{\nu} = \frac{f}{c}, \quad (3.15)$$

where  $c$  is velocity of the wave in the medium. In Raman spectroscopic measurement, the velocity  $c$  is velocity of light in  $\text{cm}^{-1}$ . For example,  $33 \text{ cm}^{-1} \sim 1 \text{ THz}$ .

Figure 3.9 shows the calculated spectra of the symmetric and asymmetric C–H stretching vibrations of methane in the hydrate cages based on the autocorrelation function for the velocity of hydrogen atoms and C–H bond length. In both of the calculated spectra, the vibrational frequencies for methane in the large cages are lower than those in the small cages, in agreement with experimental Raman spectroscopic measurements [25, 43] and previous simulations [10] (see Table 3.1). Due to the effect of the Car-Parrinello method, the calculated vibrational frequencies were smaller about  $200 \text{ cm}^{-1}$  than the previous *ab initio* MD simulation that was performed under the Born-Oppenheimer MD simulation with SIESTA. The fluctuations of the spectra calculated from the velocity of hydrogen atoms are larger than those from the C–H bond length. This result from the larger deviation in the motion of the hydrogen atoms compared to the changes in the C–H bond length. The comparison of the two spectra in Figure 3.9 indicates that the spectra from the C–H bond length autocorrelation function provides a clearer signature of the

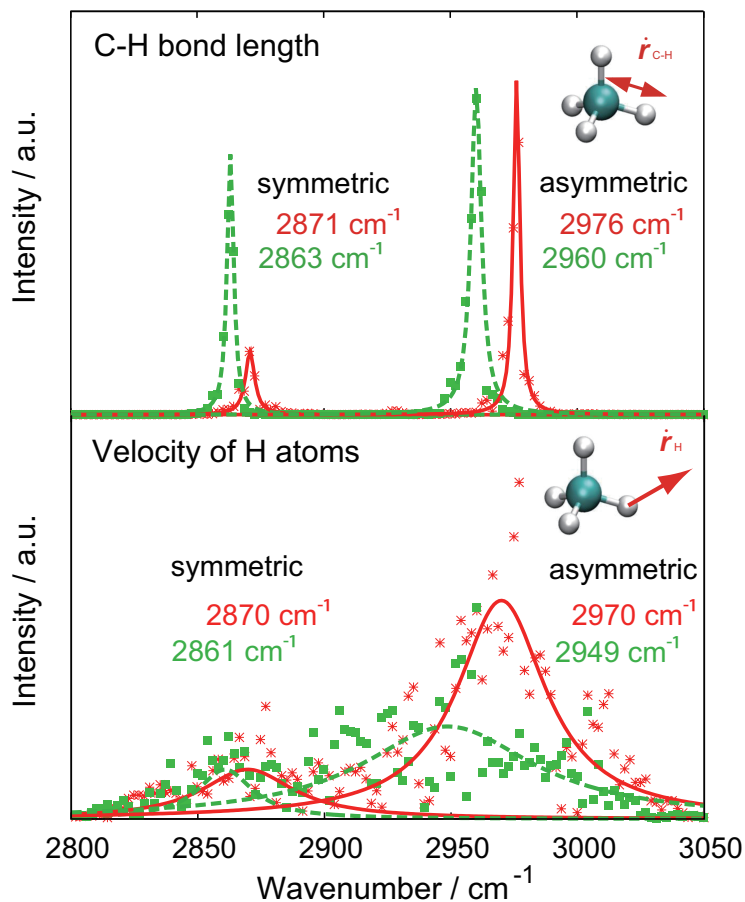


Fig.3.9 Vibrational spectra of symmetric and asymmetric stretching vibrations calculated from C–H bond length and velocity of hydrogen atoms autocorrelation functions. The vibrational frequencies in the large cages are lower than those in the small cages. The vibrational frequencies at the higher wavenumbers correspond to the asymmetric stretching mode. The red and green symbols/lines correspond to the small ( $5^{12}$ ) and large ( $5^{12}6^2$ ) cages, respectively. Vibrational spectra from simulations (symbols) were fitted with Lorentzian-type distributions.

symmetric and asymmetric stretching vibrational modes for methane in the hydrate cages. The difference in the symmetric C–H stretching frequencies is calculated to be  $16 \text{ cm}^{-1}$  and  $8 \text{ cm}^{-1}$  from the velocity of hydrogen atoms and C–H bond length, respectively, which is in reasonable agreement with the experimental value obtained with Raman spectroscopy of  $10 \text{ cm}^{-1}$  [25].

Figures 3.10 and 3.11 shows the effect of the averaged time of the autocorrelation functions. The convergence of the absolute values of the fitted vibrational frequencies of the symmetric stretching vibrations are slow in the case of the velocity autocorrelation functions because of the large fluctuation of the spectra as

Table 3.1 Comparison of the stretching vibrational frequencies and average C–H bond lengths.

|  | Cage type | This work | Tse [10] | Experimental         |
|--|-----------|-----------|----------|----------------------|
| Symmetric stretch<br>/ $\text{cm}^{-1}$  | Small     | 2871      | 3014     | 2915 [25], 2914 [10] |
|  | Large     | 2863      | 2967     | 2905 [25], 2901 [10] |
| Asymmetric stretch<br>/ $\text{cm}^{-1}$ | Small     | 2976      | 3167     | -                    |
|  | Large     | 2960      | 3152     | -                    |
| C–H bond length<br>/ $\text{\AA}$        | Small     | 1.0970    | 1.1107   | 1.098 [10]           |
|  | Large     | 1.0980    | 1.1122   | 1.148 [10]           |

shown in Figure 3.10. On the other hand, the frequencies from C-H bond length are converged more quickly than velocity autocorrelation functions. The frequency differences of the symmetric and asymmetric stretching vibrational modes are also quickly converged in the C-H length autocorrelation functions. The calculation of the vibrational frequencies of stretching vibrations from C-H bond length is useful. Figure 3.12 shows the effect of the length of the autocorrelation functions. The length of the autocorrelation functions determine the resolution of the calculated vibrational spectra. (about  $2 \text{ cm}^{-1}$  for 16 ps,  $4 \text{ cm}^{-1}$  for 8 ps,  $8 \text{ cm}^{-1}$  for 4 ps, respectively.) The effect of the length of the autocorrelation functions are about  $2 \text{ cm}^{-1}$  in this range.

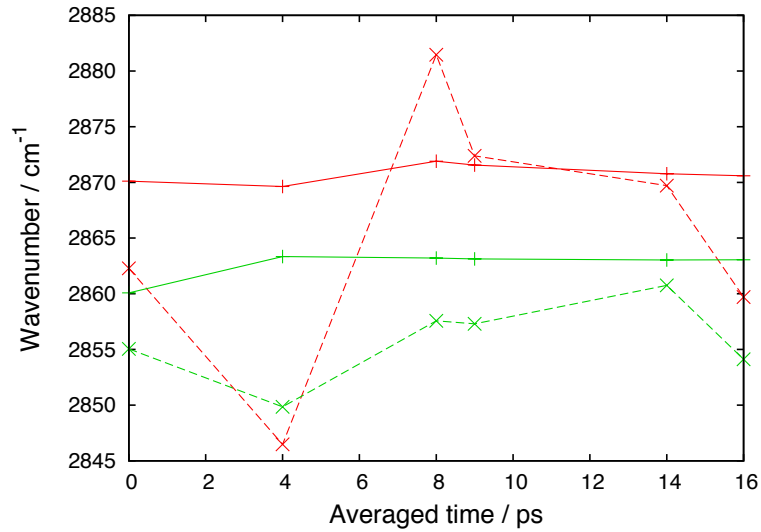


Fig.3.10 Dependence of the vibrational frequency of C-H symmetric stretching vibrations of methane on averaged time. The red and green solid lines are frequencies from autocorrelation of C–H bond length in  $5^{12}$  and  $5^{12}6^2$  cages, respectively. The red and green dashed lines are from velocity autocorrelation of H atoms in  $5^{12}$  and  $5^{12}6^2$  cages, respectively. Autocorrelation functions (16 ps each) are averaged in 0 ps, 4 ps, 8 ps, 9 ps, 14 ps, and 16 ps

Table 3.2 Comparison of the vibrational frequencies of isolated methane molecules.

|                             | Symmetric stretching | Asymmetric stretching |
|-----------------------------|----------------------|-----------------------|
| Frozen phonon               | 2963.94              | 3082.93               |
| Born-Oppenheimer MD         | 2950.82              | 3064.28               |
| Car-Parrinello MD           | 2863.30              | 2960.63               |
| Experiment (gas phase) [28] | 2917.0               | 3019.5                |

To understand the cause of the differences between the experimentally observed and calculated results, the vibrational frequency of the isolated methane molecules are calculated in frozen phonon method, Born-Oppenheimer molecular dynamics method, and Car-Parrinello molecular dynamics method. The results are shown in Table 3.2. The calculated frequencies from frozen phonon method based on perturbation theory were about  $50 \text{ cm}^{-1}$  larger than the experimental values. The frequencies from Born-Oppenheimer MD were a little smaller than the frozen phonon method. The Car-Parrinello MD showed  $100 \text{ cm}^{-1}$  red-shift due to the fictitious electron mass.

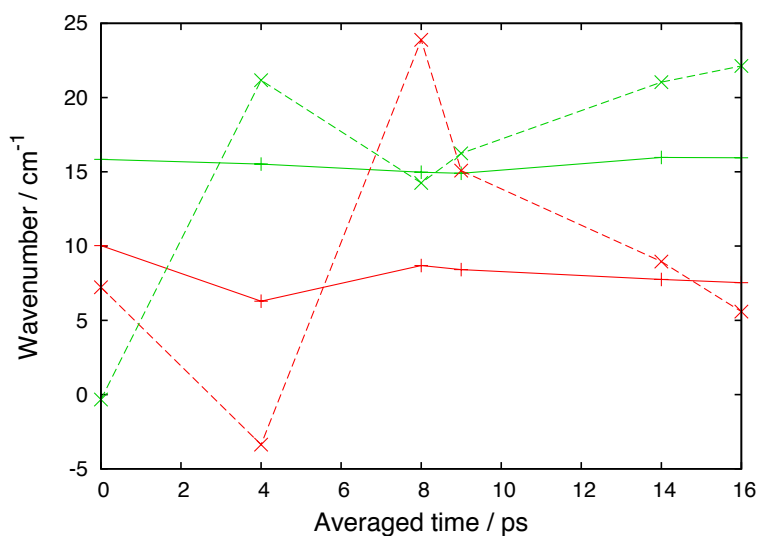


Fig.3.11 Dependence of the vibrational frequency of C-H symmetric stretching vibrations of methane between cages on averaged time. The red and green solid lines are frequencies from autocorrelation of C-H bond length in  $5^{12}$  and  $5^{12}6^2$  cages, respectively. The red and green dashed lines are from velocity autocorrelation of H atoms in  $5^{12}$  and  $5^{12}6^2$  cages, respectively. Autocorrelation functions (16 ps each) are averaged in 0 ps, 4 ps, 8 ps, 9 ps, 14 ps, and 16 ps

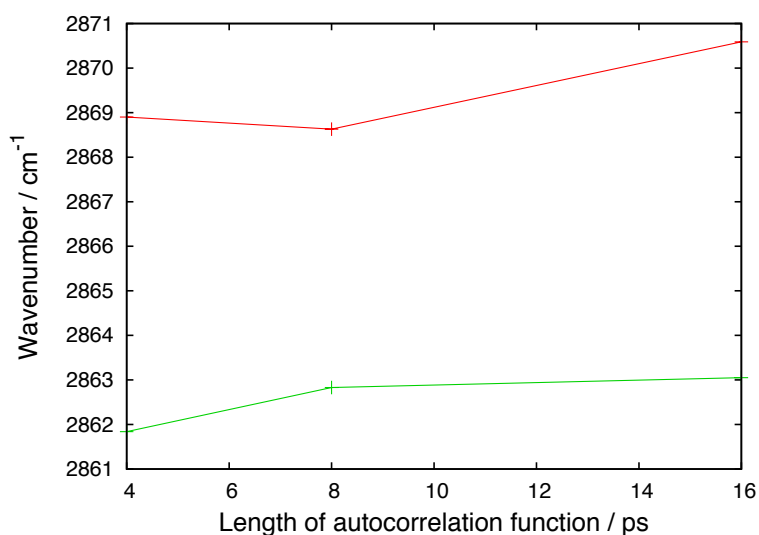


Fig.3.12 Dependence of the vibrational frequency of C-H symmetric stretching vibrations of methane on the length of the autocorrelation functions. The red and green solid lines are frequencies from autocorrelation of C-H bond length in  $5^{12}$  and  $5^{12}6^2$  cages, respectively. Length of the autocorrelation functions are 4 ps, 8 ps, and 16 ps, that are averaged in 16 ps.

### Bending and rocking modes

Figure 3.13 shows the spectra for the bending and rocking vibrations of methane molecules in the hydrate cages calculated from the velocity of hydrogen atoms, H–C–H angle, and C–H direction autocorrelation functions. In all three spectra, the vibrational frequencies of the bending and rocking modes nearly overlap for methane in the small and large cages. Well defined spectra are obtained for the rocking vibration from the H–C–H angle as expected from the nature of the rocking motion. On the other hand, the spectra of bending vibration are quite scattered, possibly resulting from the three complex types of degenerated motions.

### Vibrational spectra of translation and rotation modes

Figure 3.14 shows the spectra for molecular rotation and translation of the methane molecules computed from the velocity of hydrogen atoms, C–H vector direction, and center of mass of the methane molecule. The vibrational spectra calculated from velocity of hydrogen atoms are quite scattered; however, the spectra from the C–H direction and center of mass are better defined for the molecular rotation and translation. The higher frequency of molecular translation in the small cages reflects the higher gradient of the cell potential. The splitting of the molecular translation in the large cages into three peaks may reflect the anisotropic environment of methane in these cages. Since the large cages are oblate spheroids, methane molecules in the large cages will have different potential fields in the two of the Cartesian directions than in the third. Furthermore, the proton arrangements in the water molecules may be different in the six different large cages of the unit cell. The low-frequency vibrational modes such as translations are known as the rattling modes. The results on the rattling modes obtained in the present study are in reasonable agreement with those obtained in the previous classical molecular dynamics simulations [45].

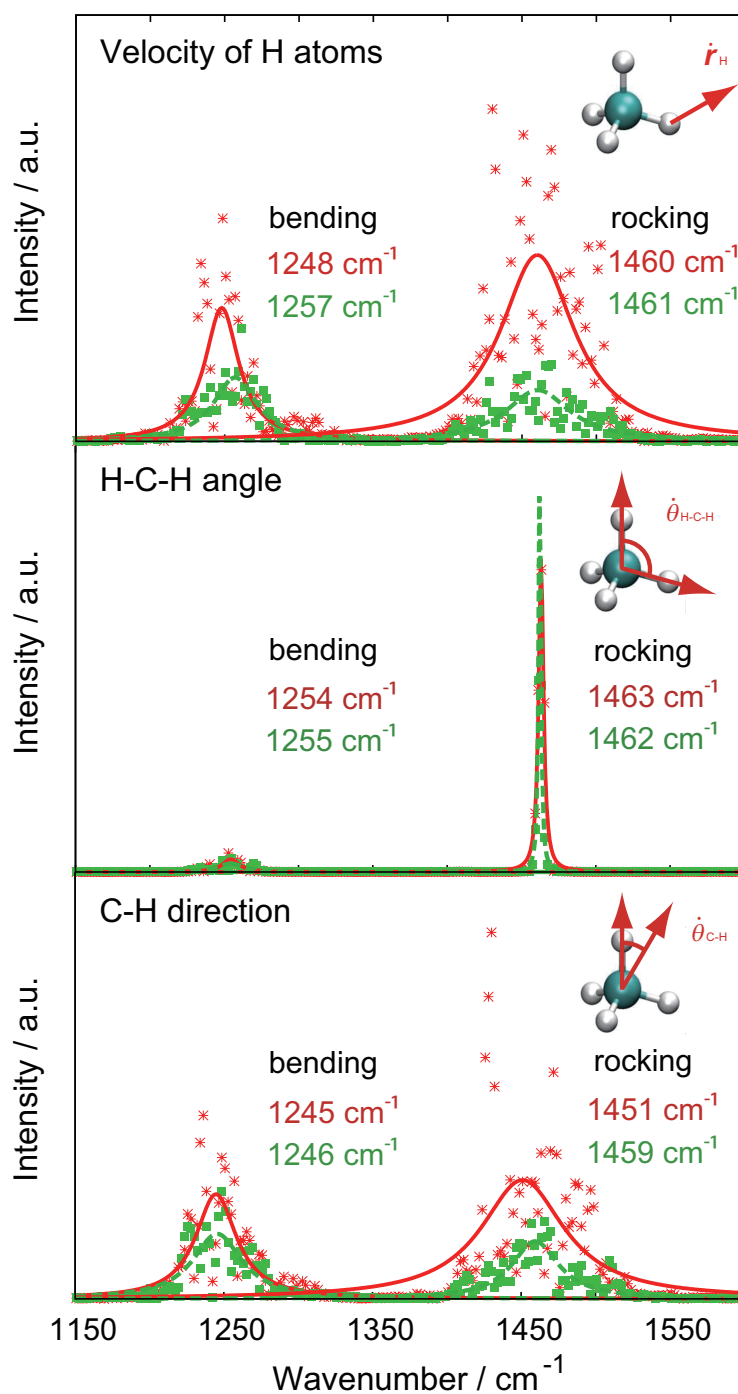


Fig.3.13 Vibrational spectra for the bending and rocking vibrational modes calculated from velocity of hydrogen atoms, H-C-H angle, and C-H direction autocorrelation functions. The vibrational spectra in the rocking mode from the H-C-H angle are sharp and well defined; the vibrational frequencies for the bending and rocking modes are nearly identical in the small and large cages. The red and green symbols/lines correspond to the small ( $5^{12}$ ) and large ( $5^{12}6^2$ ) cages, respectively. Vibrational spectra from simulations (symbols) were fitted with Lorentzian-type distributions.

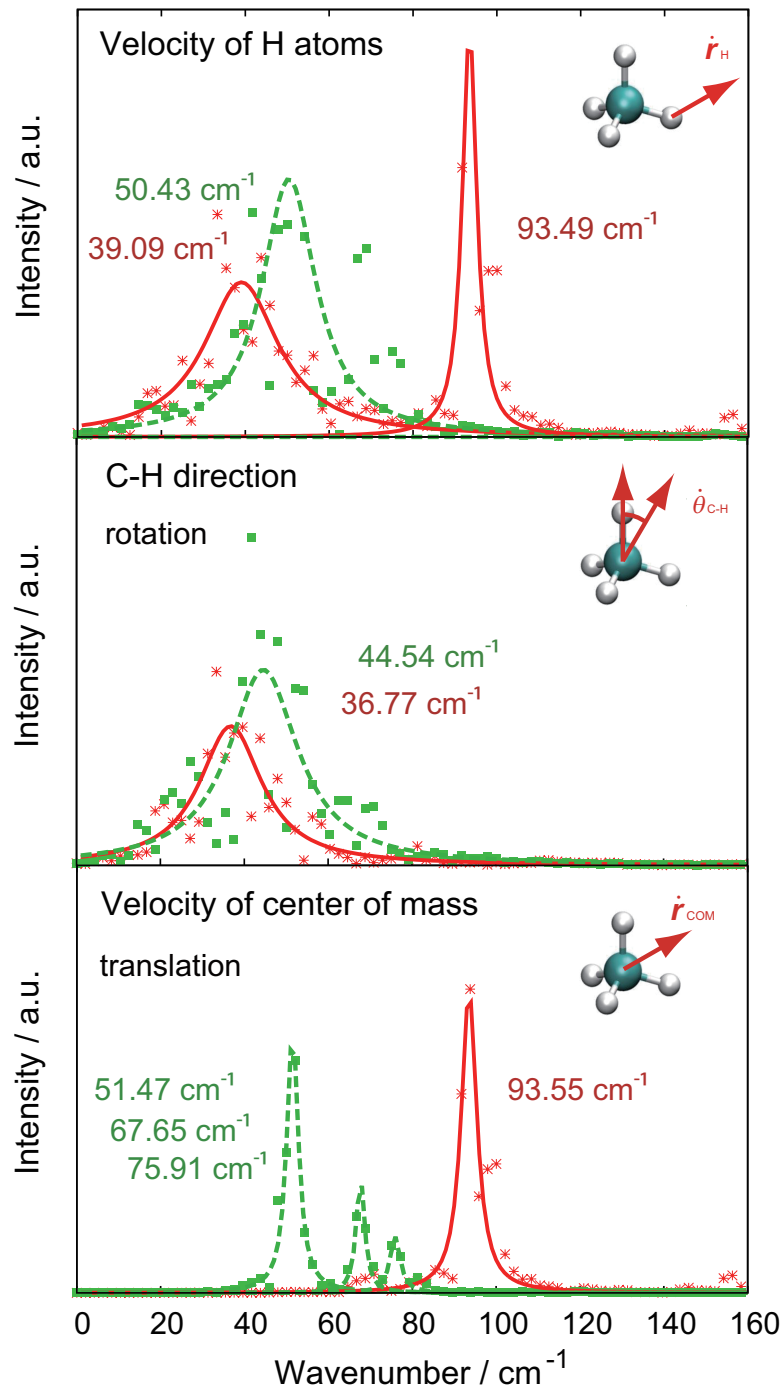


Fig.3.14 Vibrational spectra for the molecular rotation and translation calculated from velocity of hydrogen atoms, C-H direction, and velocity of center of mass autocorrelation functions. The higher frequency of molecular translation in small cages reflects the higher gradient of the cell potential. The red and green symbols/lines correspond to the small ( $5^{12}$ ) and large ( $5^{12}6^2$ ) cages, respectively. Vibrational spectra from simulations (symbols) were fitted with Lorentzian-type distributions.

### 3.3.3 Distribution of guest molecule in the cages

From the resulting vibrational spectra shown in Figures 3.9 and 3.13, the C–H bond length (stretching vibration) and the H–C–H angle (rocking vibration) provide the clearest intramolecular modes distinguishing the occupancy of methane in the small and large cages of sI hydrates. The autocorrelation functions for these two vibrational modes couple the motion of the carbon and hydrogen atoms, whereas for the others, the autocorrelation function for the motion of the hydrogen atoms alone determine the vibrational mode. As such, the C–H bond length and H–C–H angle are more reliable and suitable to determine the vibrational changes resulting from the interactions of methane in the cages of sI hydrates.

A key characteristic differentiating methane in the small and large cages of a hydrate structure is the frequency of the C–H vibrational frequency. In agreement with experimental measurement [25, 43] and the previous *ab initio* MD study [10], the frequency for the C–H bond stretch in the large cage is lower than that in the small cage. The reason for this pronounced intensity of the asymmetric C–H stretch can be understood from the position of the methane molecule in the cages. As shown in Figure 3.15, the methane molecules are slightly off-center in the cage, thus exposing their hydrogen atoms closer to water molecules forming the cages. This uneven proximity of the hydrogen atoms results in more frequent asymmetric interactions. Additionally, this higher intensity for the asymmetric stretching vibration can be also attributed to the larger number of degenerate modes (three) compared a single one for the symmetric stretching.

On average, the C–H bond length for methane in the small cage (1.0970 Å) is slightly shorter than in the large cage (1.0980 Å). While small, this difference may explain the lower frequency for the C–H stretching mode of methane in the large cages than in the small cages. The C–H bond length reflects the changes in the molecular interactions between methane and the water molecules of the cages. The C–H bonds of methane in the large cages are slightly longer because the large cage is elongated (water molecules in the hexagonal faces are relatively closer to the center of the cage than the water along the elongated direction—see distribution for water in Figure 3.15). The average distance between methane and water molecules is 3.843 Å and 4.257 Å in the small and large cages, respectively. Moreover, the elongation of the large cages causes the methane molecules to be located even more off-center,

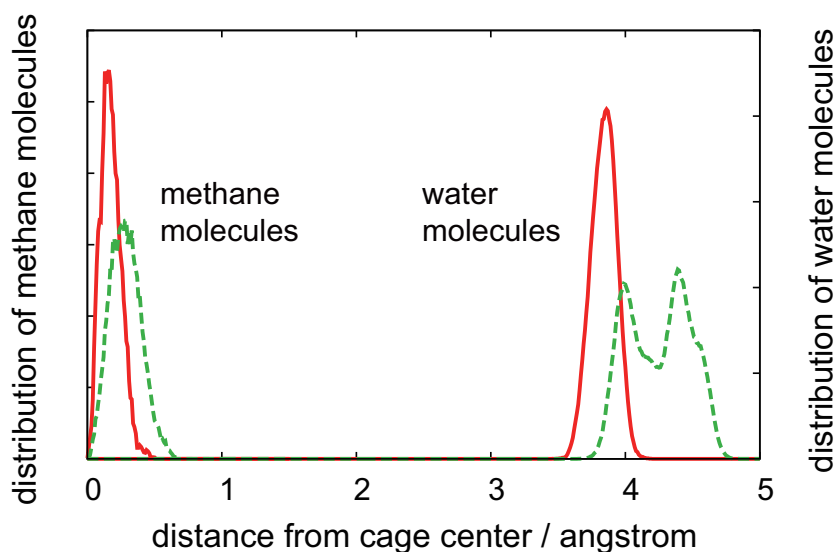


Fig.3.15 Distribution of methane and water molecules from the center of each cage type. The distribution shown is simply the probability of the distance between the molecules and the cage center (not accounted for the volume as in a radial distribution function). For the water molecules, the oxygen atoms were used in the calculation. The distributions of oxygen atoms show the size of the cages. The center of the cages is defined as the average position of the oxygen atoms in each cage. The red and green lines correspond to the small ( $5^{12}$ ) and large ( $5^{12}6^2$ ) cages, respectively.

contributing to the anisotropic interaction of methane with the water molecules. In consequence, the asymmetric C–H stretching interactions are more frequent and show with greater intensity in the vibrational spectrum. One important insight from these results is that if one can measure the asymmetric stretching of methane in the hydrate cages, one can potentially obtain significantly better resolution and information of the molecular interactions of methane and water molecules.

The discussions given above are based on the direct observations using molecular dynamics simulations. The trend of the frequency shifts of stretching vibrational modes agreed with the predictions of the loose cage-tight cage model. In the loose cage-tight cage modes, the vibrational frequency shift are affected by the gradient of the cell potential in the cages. Further analysis of the anisotropic interaction potential between methane and cage water molecules is required to understand molecular vibrations in the clathrate hydrates in terms of the loose cage-tight cage model, and is in progress.

Another important observation from the results shown in Figures 3.9 and 3.13 is that the vibrational differences of methane in the small and large cages are clearly

distinguishable in the stretching mode, but not so discernable in either the rocking or bending modes. In the rocking and bending modes, the methane molecule in the cages remains relatively stationary (motion is done by small orientational changes of hydrogen atoms with carbon atom in place). These motions arise from internal degrees of freedom that are less influenced by the interactions with the surrounding water molecules, whereas in the stretching vibration the water molecules attenuate the differences in molecular environment (orientation and position) in the small and large cages. As discussed above, changes in the C–H bond length lead to the observed vibrational frequencies of methane in the small and large cages. However, the rocking and bending vibrational modes are largely unaffected by the changes on the C–H bond length, as the motions for these modes result from the change in direction of the C–H vectors, not in the magnitude.

### 3.4 Conclusions

Clear vibrational spectra of methane molecules in a structure I clathrate hydrate were calculated from *ab initio* MD simulations using autocorrelation functions from five different modes, including the C–H bond length and H–C–H angle. The results reveal a distinct separation in the vibrational frequency of the symmetric and asymmetric C–H stretching modes for methane in the small and large cages. The observed stretching vibrational frequencies are closely linked with the position of methane in the cages and the changes in the C–H bond length distribution resulting from the interactions with the water molecules. The rocking and bending vibrational modes for methane are undistinguishable in the small and large cages.

## Chapter 4

# Structure H methane hydrate

### 4.1 Introduction

The sH unit cell is composed of three  $5^{12}$  cages, two  $4^35^66^3$  cages, and one  $5^{12}6^8$  cage with 34 water molecules. Although the crystal structure of the simple methane hydrate is sI, when a large molecule guest substance such as 2,2-dimethylbutane coexists with methane, a sH hydrate is formed. Methane molecules occupy  $5^{12}$  and  $4^35^66^3$  cages, and large molecule guest substances (LMGSs) occupy the  $5^{12}6^8$  cages. In case of the sI clathrate hydrate, the vibrational frequencies of C–H symmetric stretching of methane molecules in  $5^{12}$  and  $5^{12}6^2$  cages are clearly distinguished by Raman spectroscopy [25,43]. For the methane molecules in the  $5^{12}$  and  $4^35^66^3$  cages for sH, it is unclear whether different vibrational frequencies of C–H stretching modes are expected in these environments. Uchida et al. [46] reported that the C–H stretching vibrational frequencies for methane are  $2913\text{ cm}^{-1}$  and  $2901\text{ cm}^{-1}$  in the  $5^{12}$  and  $4^35^66^3$  cages, respectively, for a structure H hydrate formed with methane and neohexane. More recently, Ohno et al. [43] reported the vibrational frequencies of  $2912\text{ cm}^{-1}$  and  $2910\text{ cm}^{-1}$  in the  $5^{12}$  and  $4^35^66^3$  cages, respectively, for the structure H hydrate formed with methane and methylcyclohexane. However, other previous studies by Raman spectroscopy [6,25] observed only one peak at  $2913\text{ cm}^{-1}$  for sH hydrates. The goal of this study is to perform computational studies to obtain further insight into the vibrational frequencies of methane in sH and provide a better understanding on the possible discrepancy among these conflicting experimental studies. In this study, we calculated the vibrational frequencies of methane molecules in sH hydrate with neohexane as LMGS.

## 4.2 Computational method

The computational method used was very similar to the study in Chapter 3. The vibrational spectra were calculated by Fourier transform of autocorrelation functions that were computed from trajectories generated by *ab initio* MD simulations. The Car-Parrinello method was employed as the *ab initio* MD simulation for sufficiently long time to ensure resolution of the vibrational spectra. The pseudopotentials used in this study are provided by CPMD [30]. The preparation of these pseudopotentials were different from that used in the previous study for sI clathrate hydrate. The pseudopotentials used in the previous sI study were constructed in our group with the fhi98PP package [47]. However, in this study we used the pseudopotentials from CPMD for convenience. In order to compare the vibrational spectra in sH clathrate hydrate with the sI clathrate hydrate in the same condition, both calculations of the sH and sI clathrate hydrate were newly performed using same pseudopotential provided by CPMD package [30]. The result of the sI hydrates was nearly identical as in previous calculations. The unit cell of sH was composed of 34 water molecules consisting of three  $5^{12}$ , two  $4^35^66^3$ , and one  $5^{12}6^8$  cages. All  $5^{12}$  and  $4^35^66^3$  cages were occupied by a methane molecule and the  $5^{12}6^8$  cage are occupied by 2,2-dimethylbutane (neohexane). The configuration measured by x-ray crystallography [48] was employed for the initial coordinates of oxygen atoms in the water molecules for the computation. The positions of hydrogen atoms in the unit cell of sH were determined to minimize the energy in a zero net dipole moment configuration consistent with the ice rule [49]. The lattice constants of the hexagonal unit cell were  $a = 12.19 \text{ \AA}$  and  $c = 10.01 \text{ \AA}$  (based on experimental values [50]). The fictitious electron mass was 400 a.u. for the Car-Parrinello method. The simulation time-step was 0.096756 fs and the total simulation time was 35.0 ps, with the initial 5.0 ps used for the equilibration and the remaining 30.0 ps used to average the autocorrelation functions. The velocity scaling method was used to control the temperature to 113.0 K for the initial equilibration.

## 4.3 Results and Discussions

### 4.3.1 Vibrational spectra

#### Stretching vibration

Figure 4.1 shows the calculated vibrational spectra of the symmetric and asymmetric C–H stretching vibrations of methane molecule in the sH clathrate hydrate. For the vibrational spectra from velocity autocorrelation function, large fluctuations were observed and determination of the frequencies of each vibrational mode was difficult. In the previous study, it is reported that the autocorrelation functions from C–H bond length is suitable to compute clear vibrational spectra of symmetric and asymmetric stretching modes. Therefore, we fitted the vibrational spectra from the C–H bond length with Lorentzian curves to determine the vibrational frequencies of the symmetric and asymmetric vibrational modes. The determined vibrational frequencies from autocorrelation functions of C–H bond length are shown in Table 4.1. Although the redshifts of the frequencies are observed due to the fictitious mass of Car-Parrinello method, the vibrational frequencies of symmetric stretching mode for methane molecules in the  $4^35^66^3$  cages are lower than those in the  $5^{12}$  cages and followed the same trend as observed from Raman spectroscopic measurements [43, 46]. We also see that the asymmetric stretching vibrational mode shows lower frequency in the  $4^35^66^3$  cage than that in the  $5^{12}$  cage. The difference in the calculated symmetric stretching frequencies of methane in  $5^{12}$  and  $4^35^66^3$  cages are considered to be significant because the calculated frequency difference,  $3.8 \text{ cm}^{-1}$  and  $6.5 \text{ cm}^{-1}$ , are sufficiently greater than the computational resolution  $2.08 \text{ cm}^{-1}$  determined by the length of the autocorrelation functions, 16.0 ps, used for the Fourier transform. This result agrees well with the prediction of the “loose cagetight cage model” [26, 27] that explains the trend of the vibrational frequencies in the matrix using perturbation theory. The gradient of the cell potential ascribe higher frequencies in smaller cages (tight cage) and lower frequencies in large cages (loose cage) in this model. The difference of the frequencies between  $5^{12}$  and  $4^35^66^3$  cages in sH hydrate were smaller than those between  $5^{12}$  and  $5^{12}6^2$  cages in sI hydrate,  $11.0 \text{ cm}^{-1}$  ( $2865.0 \text{ cm}^{-1}$  in  $5^{12}$  and  $2876.0 \text{ cm}^{-1}$  in  $5^{12}6^2$ ) for symmetric stretching and  $16.9 \text{ cm}^{-1}$  ( $2962.5 \text{ cm}^{-1}$  in  $5^{12}$  and  $2979.4 \text{ cm}^{-1}$  in  $5^{12}6^2$ ) for asymmetric stretching modes. The average C–H bond length of methane molecules in the  $5^{12}$  cages ( $1.0959 \text{ \AA}$ ) is slightly shorter than that in the  $4^35^66^3$  cages ( $1.0968$

Å). This trend of larger bond length of lower stretching frequencies is in agreement with previous *ab initio* calculations for sI hydrate [10]. The C–H bond length for methane in  $5^{12}$  and  $5^{12}6^2$  cages in sI were 1.0966 Å and 1.0976 Å in this study, respectively. The differences of the C–H bond length were almost same or a little bit shorter in sH (0.0009 Å) than in sI clathrate hydrate (0.0010 Å). Here, we should mention that the vibrational frequencies of the methane molecules may depend on the LMGS in the  $5^{12}6^8$  cages. The dependence of the lattice parameters, occupancies, and kinetics of crystal growth on LMGSs is reported by experimental measurements for sH hydrate [51, 52] and the vibrational frequencies are closely linked with the size of the cages. In addition, the interactions between methane and LMGS may affect each others' vibrational frequencies. The effect of the LMGS on the molecular vibration of methane is an interesting and important issue and a topic for future studies to understand guest-guest and guest-host interactions in hydrates.

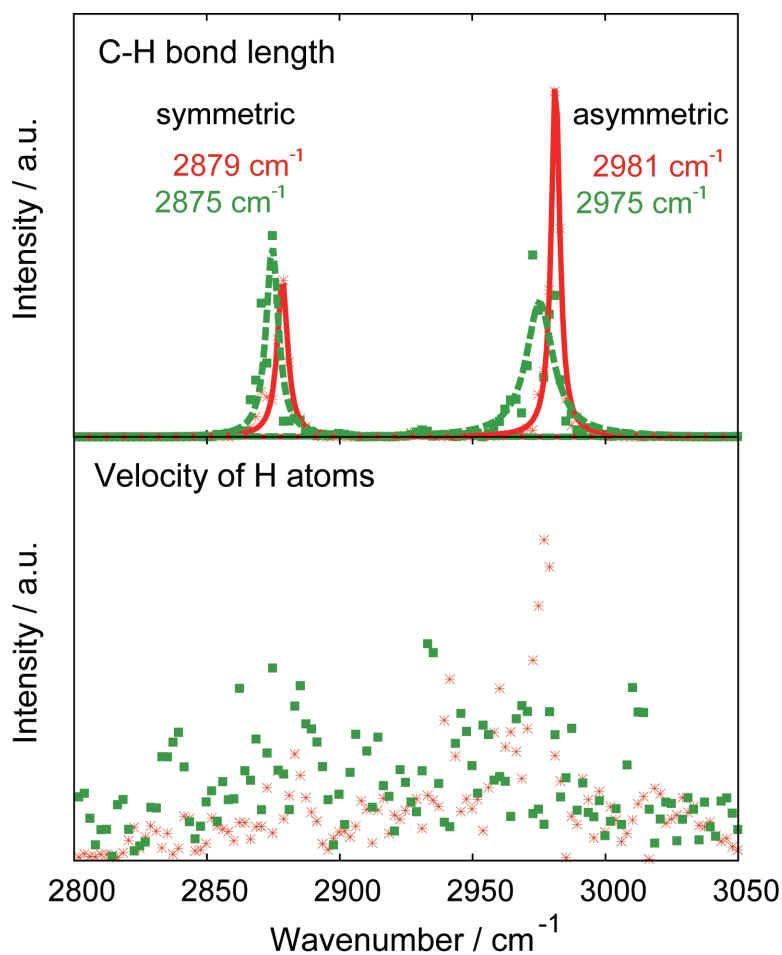


Fig.4.1 Vibrational spectra of symmetric and asymmetric stretching vibrations of methane molecules in sH calculated from C–H bond length and velocity of hydrogen atoms autocorrelation functions. The red symbols/solid lines and green symbols/dashed lines correspond to the  $5^{12}$  and medium  $4^3 5^6 6^3$  cages, respectively. Vibrational spectra of C–H bond length from simulations (symbols) were fitted with Lorentzian-type distributions. The vibrational spectra from velocity of hydrogen atoms are very scattered. The vibrational frequencies in the  $4^3 5^6 6^3$  cages are lower than those in the  $5^{12}$  cages.

Table 4.1 Comparison of the stretching vibrational frequencies and average C–H bond lengths.

|                                       | Structure H   |           |             | Structure I |              |           |           |
|---------------------------------------|---------------|-----------|-------------|-------------|--------------|-----------|-----------|
|                                       | Cage type     | This work | Uchida [46] | Ohno [43]   | Cage type    | This work | Ohno [43] |
| Symmetric stretch / $\text{cm}^{-1}$  | $5^{12}$      | 2878.5    | 2911.0      | 2911.9      | $5^{12}$     | 2876.0    | 2913.6    |
|                                       | $4^3 5^6 6^3$ | 2874.7    | 2901.5      | 2910.1      | $5^{12} 6^2$ | 2865.0    | 2901.2    |
| Asymmetric stretch / $\text{cm}^{-1}$ | $5^{12}$      | 2981.3    | ...         | ...         | $5^{12}$     | 2979.4    | ...       |
|                                       | $4^3 5^6 6^3$ | 2975.3    | ...         | ...         | $5^{12} 6^2$ | 2962.5    | ...       |
| C-H bond length / Å                   | $5^{12}$      | 1.0959    | ...         | ...         | $5^{12}$     | 1.0966    | ...       |
|                                       | $4^3 5^6 6^3$ | 1.0968    | ...         | ...         | $5^{12} 6^2$ | 1.0976    | ...       |

### Bending and rocking vibration

The vibrational spectra for the bending and rocking vibrations of methane molecules in the sH hydrate cages calculated from the velocity of hydrogen atoms, and H–C–H angle autocorrelation functions are shown as Figure 4.2. From the autocorrelation function of the H–C–H angle, sharp vibrational peaks are observed in the rocking vibrational mode. However, the bands for the bending mode were scattered and low intensity due to the complex motion of that mode. The vibrational frequencies of the bending mode from the velocity of hydrogen atoms nearly overlap for methane in the 5<sup>12</sup> and 4<sup>3</sup>5<sup>6</sup>6<sup>3</sup> cages. The differences of the vibrational frequencies for rocking vibrations were 2.4 cm<sup>-1</sup> from the velocity of hydrogen atoms and 2.2 cm<sup>-1</sup> from the H–C–H bond length. This overlap and small difference of the vibrational spectra in bending and rocking modes were also observed in the sI hydrate. The effect of the cages on the changes in the vibrational frequencies of guest molecules is larger in the symmetric stretching vibrational modes than those in the bending and rocking modes. The motions of the hydrogen atoms of methane molecules in the symmetric and asymmetric stretching vibrational modes are mainly normal in direction to the water molecules of the cages. Therefore, the stretching vibrational frequencies are strongly affected by the gradient of the cell potential as described in the loose cagetight cage model. On the other hand, the bending and rocking modes are less influenced by the water molecules as it is mainly determined by vibrations in the H–C–H angle.

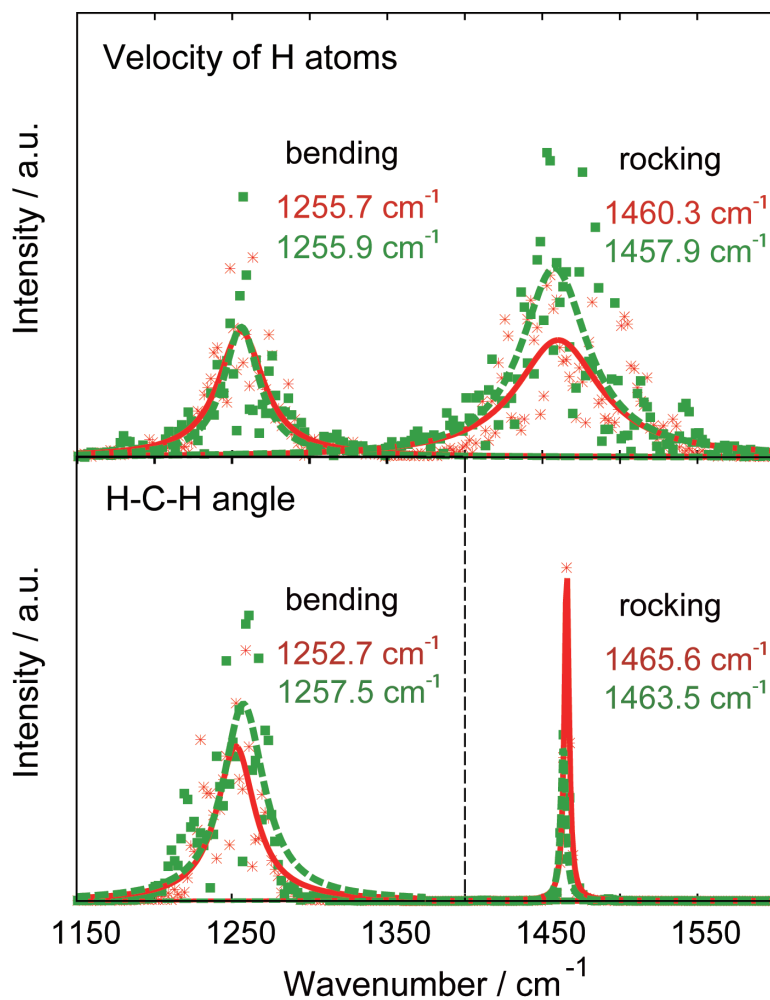


Fig.4.2 Vibrational spectra for the bending and rocking vibrational modes of methane molecules in sH hydrate calculated from velocity of hydrogen atoms and H–C–H angle. The vibrational spectra in the rocking mode from the H–C–H angle are sharp and well defined for rocking vibration. The red symbols/solid lines and green symbols/dashed lines correspond to the  $5^{12}$  and  $4^35^66^3$  cages, respectively. Vibrational spectra from simulations (symbols) were fitted with Lorentzian-type distributions.

### Translation and rotation

Figure 4.3 shows the spectra for the molecular rotation and translation of the methane molecules in sH computed from the velocity of hydrogen atoms, C–H vector direction, and center of mass of the methane molecules. These low-frequency vibrational modes corresponding to translations are known as rattling modes [45]. The C–H vector direction and center of mass are defined as the molecular rotation and translation of methane molecules in the cages. The vibrational spectra calculated from velocity of hydrogen atoms include both of them and their deconvolution is difficult due to the overlap of the spectra. The translational mode of methane in the  $5^{12}$  cages has only one peak, whereas there are two or three peaks in the  $4^35^66^3$  cages. The vibrational frequencies for methane translation in the  $5^{12}$  cages ( $89.108\text{ cm}^{-1}$ ) fall in between those in the  $4^35^66^3$  cage ( $72.390\text{ cm}^{-1}$ ,  $97.317\text{ cm}^{-1}$ , and  $113.63\text{ cm}^{-1}$ ). The only one peak of molecular translation in the  $5^{12}$  cages is from the higher and isotropic gradient of the cell potential. On the other hand, the splitting of the molecular translation in the  $4^35^66^3$  cages into three peaks may reflect the anisotropic environment of methane in these cages. Although both  $5^{12}$  and  $4^35^66^3$  cages are constructed of 12 faces of water molecules, the  $4^35^66^3$  cage is distorted by the combination of the square faces as shown in Figure 4.4. The effective major and minor axes are 4.87 and 4.53 Å in the  $5^{12}$  cage and 4.96 and 4.26 Å in the  $4^35^66^3$  cage [53]. The larger distortion in the  $4^35^66^3$  cage is closely related with the splitting of peaks. Figure 4.4 shows the calculated distribution of distances between the cage center and water molecules in the  $4^35^66^3$  cages and the wide spread in the distances compared to the nearly symmetrical  $5^{12}$  cages. This distort to the cage cause a biased distribution, which can result in the splitting of peaks of the translation and lower frequencies of largest peaks in  $4^35^66^3$  cages. Figure 4.4 also shows that several water molecules are closer to the cage center in the  $4^35^66^3$  than those in the  $5^{12}$  cages. The two higher frequencies peaks in the  $4^35^66^3$  cages are ascribed from these closer water molecules. The similar splitting of the translational frequencies was observed in the previous structure I clathrate hydrate simulation in the  $5^{12}6^2$  cages that are known as oblate spheroids having anisotropic cell potential. The splitting of the energy levels of the translation along the major and minor axes in the  $5^{12}6^2$  in sI is also reported by quantum dynamics calculations [54].

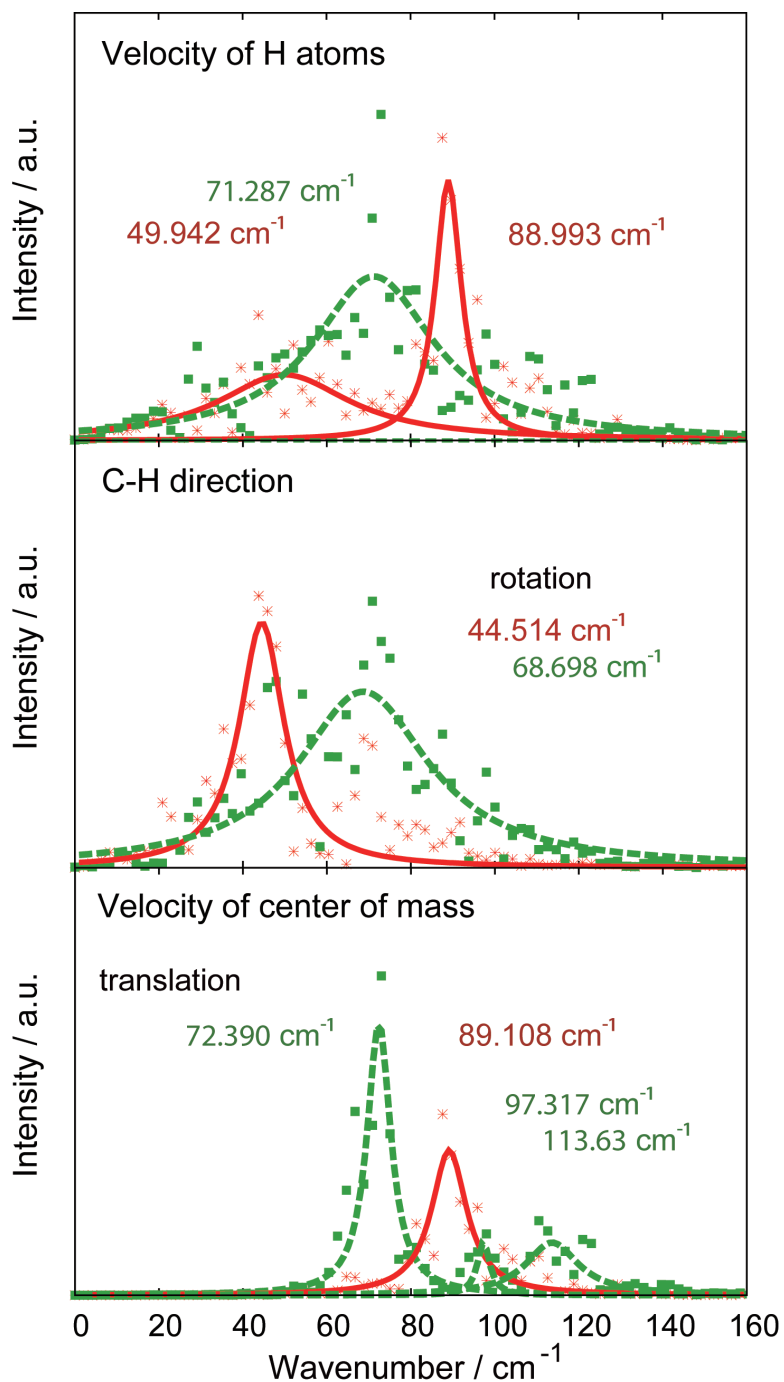


Fig.4.3 Vibrational spectra for the molecular rotation and translation of methane molecules in sH hydrate calculated from velocity of hydrogen atoms, C–H direction, and velocity of center of mass autocorrelation functions. The red symbols/solid lines and green symbols/dashed lines correspond to the  $5^{12}$  and  $4^35^66^3$  cages, respectively. Vibrational spectra from simulations (symbols) were fitted with Lorentzian-type distributions.

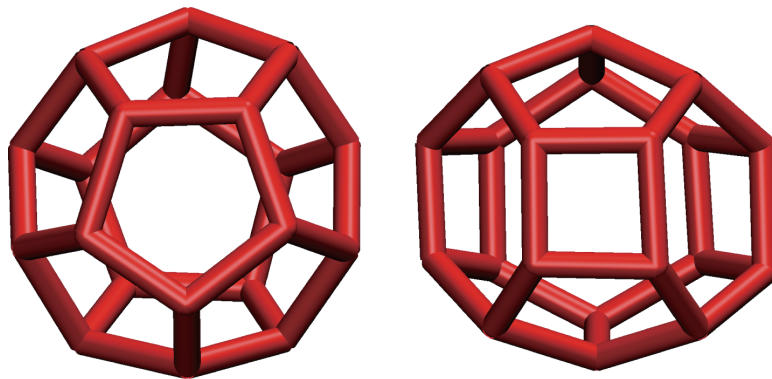


Fig.4.4 Image of the  $5^{12}$  (left) and  $4^3 5^6 6^3$  (right) cages in structure H clathrate hydrates. Each vertex shows oxygen atoms of water molecules and hydrogen atoms are located between the oxygen atoms. The effective major and minor axes are 4.87 and 4.53 Å in the  $5^{12}$  cage and 4.96 and 4.26 Å in the  $4^3 5^6 6^3$  cage.<sup>32</sup>

In the rotational motion, broad and fluctuating spectra were observed. The previous quantum dynamics calculation for the  $5^{12}$  and  $5^{12}6^2$  cages in sI hydrate [54] observed the broad splitting of energy levels in the rotational motion caused by the angular anisotropy environment in the cages. This trend may agree with the case of the  $5^{12}$  and  $4^3 5^6 6^3$  cages in sH hydrate and cause the broad and fluctuated rotational spectra. Also the higher frequency was observed in the  $4^3 5^6 6^3$  cages than that in the  $5^{12}$  cages. This lower frequency in the  $5^{12}$  cages for the rotational modes was observed in the previous sI clathrate hydrate study. The high frequency of the rotational motion in the larger cages may be attenuated by the non-spherical shape and motion of the cage. The water molecules in the cage are locally fluctuating and thus affecting the rotation of methane in the cage. As such, the non-spherical shape and fluctuation of water in the  $4^3 5^6 6^3$  cage could cause a higher frequency in the rotational motion of methane than that in the symmetrical and spherical  $5^{12}$  cage. In addition, a quantum dynamics study [54] with rigid water molecules did not observe clear differences of rotational energy levels between  $5^{12}$  and  $5^{12}6^2$  cages in sI hydrate. Therefore, the dynamics of the water molecules in the cage may enhance the effect on the molecular motion of guest molecules in the hydrate cages.

### Distribution of guest molecules in the cages of sH hydrate

Figure 4.5 shows the distributions of the distances between the methane and cage-water molecules (oxygen atoms) in sI and sH hydrates. The distributions nearly overlap in the  $5^{12}$  and  $4^35^66^3$  cages for sH, which is different from sI hydrates. For the sI clathrate hydrate, the  $5^{12}$  cages are dodecahedra consisting of 12 hexagonal faces and the  $5^{12}6^2$  cages are tetrakaidecahedra consisting of 12 hexagonal faces and 2 pentagonal faces. On the other hand, both  $5^{12}$  and  $4^35^66^3$  cages are dodecahedra for sH clathrate hydrate. The  $4^35^66^3$  cages are constructed with 3 square faces, 6 pentagonal faces, and 3 hexagonal faces. Thus, the forms of the cages ( $5^{12}$  and  $4^35^66^3$ ) in sH hydrate are much more similar than those in the sI clathrate hydrates,  $5^{12}$  and  $5^{12}6^2$  cages. This difference between the sI and sH explains the smaller deviation in the frequency of stretching vibrational modes in the sH than those in the sI clathrate hydrate. In addition, methane molecules are moving in the cages as shown in Figure 4.5 and that makes the distributions closer between the cages. This overlap of the distribution between methane and water molecule makes the environment around the methane molecules in the  $5^{12}$  and  $4^35^66^3$  cages closer than those of the  $5^{12}$  and  $5^{12}6^2$  cages of sI hydrate. The average distances between methane and water molecules are 3.872 Å in the  $5^{12}$  and 3.930 Å in the  $4^35^66^3$  cages for sH, and 3.845 Å in the  $5^{12}$  and 4.258 Å in the  $5^{12}6^2$  for sI. The differences in this average distance are 0.058 Å for sH and 0.413 Å for sI. Thus, the small differences in the stretching vibrational frequencies of methane molecules in sH clathrate hydrates are directly linked with the small difference in the distance between methane and water molecules in the cages.

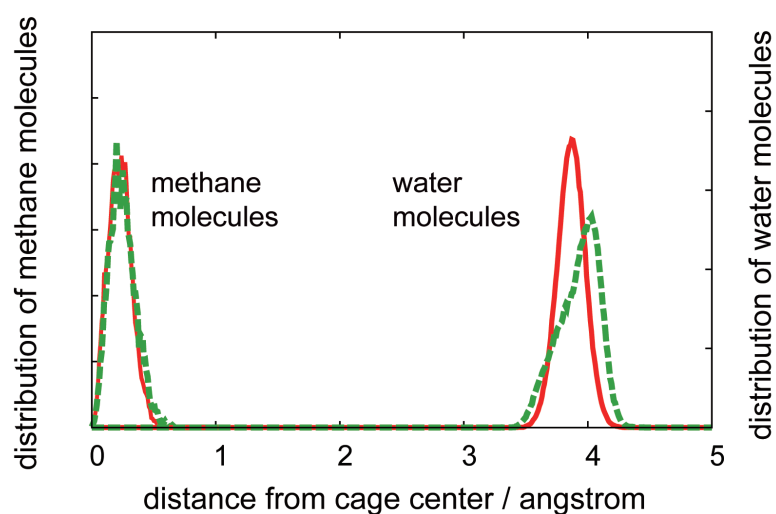


Fig.4.5 Distribution of methane and water molecules from the center of each cage type in sH hydrates. The distribution shown is simply the probability of the distance between the molecules and the cage center (not accounted for the volume as in a radial distribution function). The oxygen atoms were used in the calculation for the water molecules. The distributions of oxygen atoms show the size of the cages. The center of the cages is defined as the average position of the oxygen atoms in each cage. The red solid lines and green dashed lines correspond to the  $5^{12}$  and  $4^3 5^6 6^3$  cages, respectively.

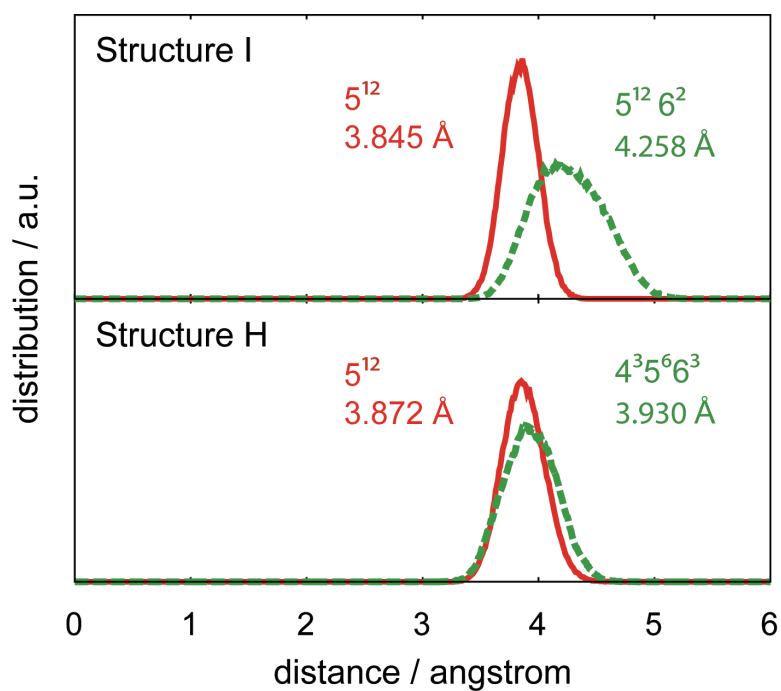


Fig.4.6 Distributions of distance for methane and water molecules in the computation for each cage type. The distribution shown is simply the probability of the distance between the molecules and the cage center (not accounted for the volume as in a radial distribution function). For the water molecules, the oxygen atoms were used in the calculation. The red solid lines and green dashed lines correspond to the  $5^{12}$  and  $5^{12}6^2$  cages in sI hydrate, and  $5^{12}$  and  $4^35^66^3$  cages in sH hydrate, respectively. The distributions of  $5^{12}$  and  $4^35^66^3$  cages in sH nearly overlap.

## 4.4 Conclusions

Vibrational frequencies of methane molecules in a structure H clathrate hydrate are calculated from *ab initio* MD simulations. The vibrational spectra are calculated using autocorrelations from C–H bond length and H–C–H angle for the stretching and rocking vibrational modes. The observed stretching vibrational frequencies of methane in the  $4^35^66^3$  cages are lower than  $5^{12}$  cages. The differences of symmetric stretching frequencies in sH hydrate are smaller than those in a sI hydrates and it reflects the average distance between methane and cage water molecules. The C–H bond length of methane molecules in the  $4^35^66^3$  cages was longer than that in the  $5^{12}$  cages. These results help to explain the observed shifts in the vibrational frequencies for methane as measured experimentally by Raman spectroscopy.

## Chapter 5

# Structure I deuterated methane hydrate

### 5.1 Introduction

Due to the guest-host intermolecular interaction in the hydrates cages, the vibrational frequencies of the guest molecules are unique, resulting in vibrational spectra that characterize the properties of the clathrate hydrate. To clearly obtain the vibrational spectra of guest molecules in the clathrate hydrate structure, it is often common practice to deuterate the hydrogen atoms so that the vibrational peaks are shifted and deconvoluted from other peaks in the vibrational spectrum [17, 55–58]. However, the effect of deuteration on the vibrational spectra of the clathrate hydrates is still unclear.

Previous Raman spectroscopy measurements showed the effect of deuteration on the vibrational frequency and width of the spectrum for sI methane hydrate [56, 57]. The stretching vibrational frequency of  $\text{CH}_4$  molecules in the hydrate with  $\text{H}_2\text{O}$  in the lattice is observed at  $2915.42\text{ cm}^{-1}$  in  $5^{12}$  cages and  $2904.03\text{ cm}^{-1}$  in  $5^{12}6^2$  cages at 271 K, while with  $\text{D}_2\text{O}$  in the lattice the corresponding frequencies are at  $2913.06\text{ cm}^{-1}$  and  $2901.35\text{ cm}^{-1}$  at 273 K [56]. In another more recent study [57], the vibrational frequency of C-H stretching was observed at  $2913.0\text{ cm}^{-1}$  in  $5^{12}$  cages and  $2901.3\text{ cm}^{-1}$  in  $5^{12}6^2$  cages with a  $\text{H}_2\text{O}$  lattice and at  $2913.4\text{ cm}^{-1}$  and  $2901.6\text{ cm}^{-1}$  with a  $\text{D}_2\text{O}$  lattice at 113 K. The frequencies were very similar but not identical. The full-width at half maximum (FWHM) of the vibrational peaks was also measured as well as the differences due to the lattice molecules.

Although the understanding of guest-host coupling was studied with neutron scattering and molecular dynamics (MD) simulation of guest molecules [56, 59–63], the

mechanism from the deuteration effect on the intramolecular vibrational frequencies and shape of the spectra in the clathrate hydrates are poorly understood. To obtain insight into the mechanism due to deuteration, MD simulation is a useful method. The changes on the C-H vibrational frequencies for undeuterated systems have been reported by classical and *ab initio* MD simulations [6–8,10,59]. Although the results from classical MD simulations show good agreement of the vibrational shift in clathrate hydrates, quantum mechanics is required for describing the covalent bond in order to avoid the uncertainty from empirical models used for the intramolecular vibrations in classical simulations. Therefore, in this study, we performed *ab initio* MD simulations to quantify the changes to the vibrational spectra of methane hydrate with deuterated water ( $\text{CH}_4\text{-D}_2\text{O}$ ) and the vibrational spectra of deuterated methane with protonated water ( $\text{CD}_4\text{-H}_2\text{O}$ ).

## 5.2 Computational method

Vibrational spectra of clathrate hydrates were computed by Fourier transform of the velocity autocorrelation functions computed from the trajectories generated by Car-Parrinello MD [29] simulations using the CPMD package [30]. The main procedure of the computations is similar to our previous study on the calculation of the vibrational spectra of sI methane hydrate. The calculation was based on density functional theory using PBE [31] for the approximation of the exchange correlation function. The basis set was plane wave functions with an energy cutoff of 80 Ry. The Brillouin zone of the supercell was sampled at the  $\Gamma$  point. The Troullier-Martines [32] norm-conserving pseudopotential using Kleinman-Bylander [33] separation scheme was employed for the valence-core interaction for carbon, hydrogen and oxygen. Deuterium atoms were described by the changing the atomic mass of hydrogen to 2.0158 from 1.0079. The fictitious mass of the electrons used in the Car-Parrinello MD was 400 a.u. The simulations used a time-step of 0.0968 fs. The total calculation time was 30 ps, with the initial 1 ps used for temperature control (velocity scaling) and another 4 ps for equilibration. The 90 autocorrelation functions were computed every 0.1 ps and averaged during the last 25 ps. The length of each autocorrelation function was 16 ps. The calculations were performed on a unit cell of sI clathrate hydrate enclosing methane ( $\text{CH}_4$ ) or deuterated methane ( $\text{CD}_4$ ) molecules. The initial coordinates of oxygen atoms were determined by X-ray crystallography [34] and the position of hydrogen atoms were decided to minimize the

energy in a zero net dipole moment configuration consistent with the ice rule. The lattice constant of the unit cell was 11.83 Å, as determined from experiments [35] for methane hydrate (CH<sub>4</sub>-H<sub>2</sub>O) and used in our previous study. We performed the calculation for two types of the methane hydrates: methane with deuterated water (CH<sub>4</sub>-D<sub>2</sub>O) and deuterated methane with protonated water (CD<sub>4</sub>-H<sub>2</sub>O). Although the vibrational modes of methane in water hydrate (CH<sub>4</sub>-H<sub>2</sub>O) were discussed in our previous study, the results are also shown for comparison of the methane-water coupling.

## 5.3 Results and Discussions

### 5.3.1 Vibrational spectra

#### Stretching vibrational modes

The calculated vibrational spectra of hydrogen and deuterium atoms for methane and water in sI clathrate hydrates are shown in Figures 5.1 to 5.3. The translation and roto-vibrations of H<sub>2</sub>O and D<sub>2</sub>O molecules appear at  $\sim 400$  cm<sup>-1</sup> and  $\sim 1000$  cm<sup>-1</sup>, respectively. The bending modes are near 1550 cm<sup>-1</sup> for H<sub>2</sub>O and 1200 cm<sup>-1</sup> for D<sub>2</sub>O. The symmetric and asymmetric stretching vibrations are broad peaks at 2800-3200 cm<sup>-1</sup> for H<sub>2</sub>O and 2000-2400 cm<sup>-1</sup> for D<sub>2</sub>O. As shown in the simulations for sI clathrate hydrate, the spectra are red-shifted due to the fictitious electron mass used in the Car-Parrinello MD method ( $200$  cm<sup>-1</sup> smaller than previous computational values from Born-Oppenheimer MD [10] at stretching vibrational modes of water. The amount of the red-shift is smaller in lower frequency region), the broad shape of the spectra (which is difficult to reproduce by classical MD [64,65]), and the trend of the frequencies in the cages are in agreement with the experimental observations [66]. The rattling motions (translation and rotations) of CH<sub>4</sub> and CD<sub>4</sub> molecules are distributed  $\sim 150$  cm<sup>-1</sup>. The CH<sub>4</sub> and CD<sub>4</sub> molecules have four intramolecular vibrational modes: bending, rocking, stretching and asymmetric stretching. The symmetric stretching vibrational mode is Raman active and it is the main mode used experimentally to determine the structure and occupancy of clathrate hydrates. The vibrational frequencies of the symmetric and asymmetric stretching modes are determined by curve fitting the bands with Lorentzian-type distributions. The vibrational spectra computed by the Fourier transform of trajectories of the C-H and C-D modes are listed in Table 5.1. Both the C-H and C-D stretching vibrational frequency in the 5<sup>12</sup>6<sup>2</sup> cages are lower than that in the 5<sup>12</sup>

cages. The differences of the frequencies and the trend of the averaged bond length in the symmetric stretching between the  $5^{12}$  and  $5^{12}6^2$  cages are in good agreement with the experimental results for  $\text{CH}_4\text{-H}_2\text{O}$  and  $\text{CH}_4\text{-D}_2\text{O}$  hydrates [10, 57].

The trend that the larger C-H and C-D bond length have lower frequency agrees with previous *ab initio* calculations of clathrate hydrates [10]. The difference of the symmetric C-D stretching frequency between cages in the  $\text{H}_2\text{O}$  lattice is  $9.7\text{ cm}^{-1}$  and is similar to the C-H vibrations in the  $\text{H}_2\text{O}$  lattice ( $8\text{ cm}^{-1}$ ) and in the  $\text{D}_2\text{O}$  lattice ( $11.3\text{ cm}^{-1}$ ). In the loose-cage tight cage model [26, 27], the vibrational shift of the guest molecules in the clathrate hydrate is described by guest-host interactions; as such, the reduced mass of the atoms affects the frequency shift in the cages. Since the reduced mass of the C-D and C-H vibrations are nearly identical, the frequency differences between the cages should be close to the C-H vibrations. The vibrational frequencies of the C-H symmetric stretching vibrations for  $\text{CH}_4$  molecules in the  $\text{D}_2\text{O}$  lattice was a little higher than that in the  $\text{H}_2\text{O}$  lattice, that is,  $4.5\text{ cm}^{-1}$  in the  $5^{12}$  cages and  $1.2\text{ cm}^{-1}$  in the  $5^{12}6^2$  cages. These values compare to experimental values of  $0.4\text{ cm}^{-1}$  ( $5^{12}$  cage) and  $0.3\text{ cm}^{-1}$  ( $5^{12}6^2$  cage) higher in  $\text{D}_2\text{O}$  lattice than in the  $\text{H}_2\text{O}$  lattice at 113 K [57], and correspondingly  $1.6\text{ cm}^{-1}$  and  $2.7\text{ cm}^{-1}$  lower at 273 K [56]. Although the changes of the frequency from the simulations were much larger than the experimental values, the trend of the frequency is consistent among the simulations and experimental results in 113 K.

The statistical error of the calculated vibrational frequencies is significant because the differences of the vibrational spectra is quite small. Figure 5.4 shows the effect of the averaged time of the autocorrelation functions on the vibrational frequencies of the methane molecules. The vibrational frequencies of the symmetric stretching vibration in the  $\text{D}_2\text{O}$  lattice are larger than that in the  $\text{H}_2\text{O}$  lattice in all of the averaged time. The calculated frequencies are within  $2\text{ cm}^{-1}$  for  $\text{D}_2\text{O}$  lattice.

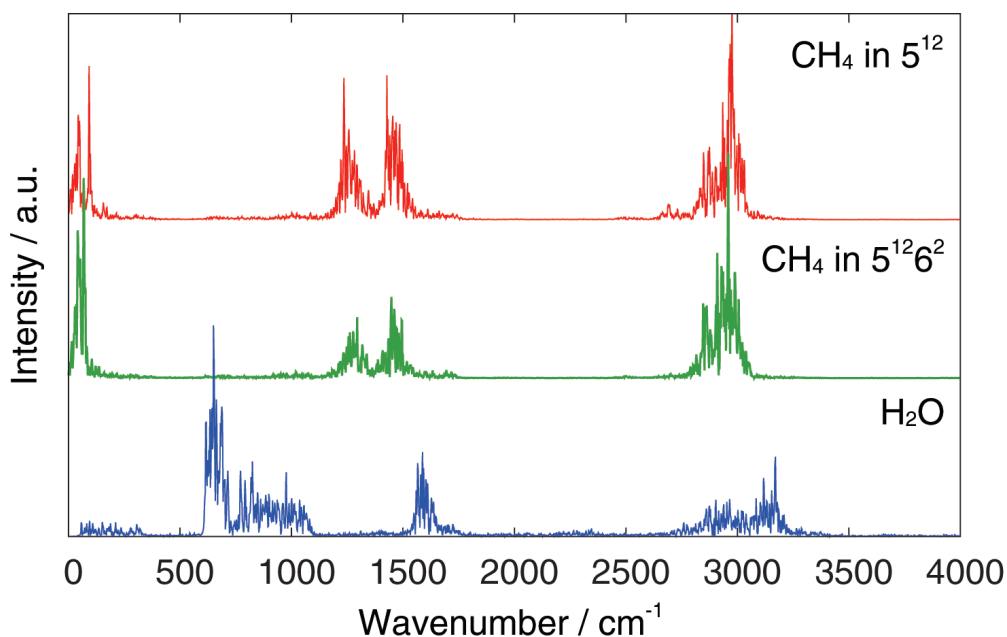


Fig.5.1 Vibrational spectra of CH<sub>4</sub> and H<sub>2</sub>O molecules computed from velocity autocorrelation functions of the hydrogen atoms. The vibrational frequencies of C-H stretching modes in 5<sup>12</sup> cages were lower than that in the 5<sup>12</sup>6<sup>2</sup> cages. The spectra of methane around 600-1000 cm<sup>-1</sup> were slightly affected by the hydrogen bonding motion of water.

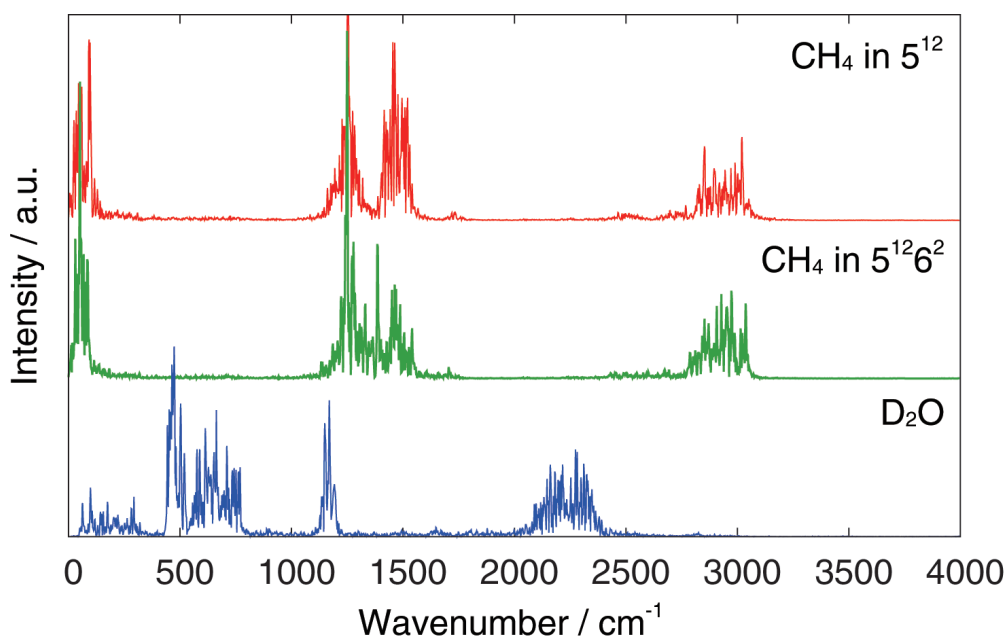


Fig.5.2 Vibrational spectra of CH<sub>4</sub> and D<sub>2</sub>O molecules computed from velocity autocorrelation functions of the hydrogen atoms. The vibrational frequencies of D<sub>2</sub>O molecules are lower than the H<sub>2</sub>O molecules. There are no drastic differences on the vibrational spectra of CH<sub>4</sub> from the CH<sub>4</sub> in H<sub>2</sub>O lattice.

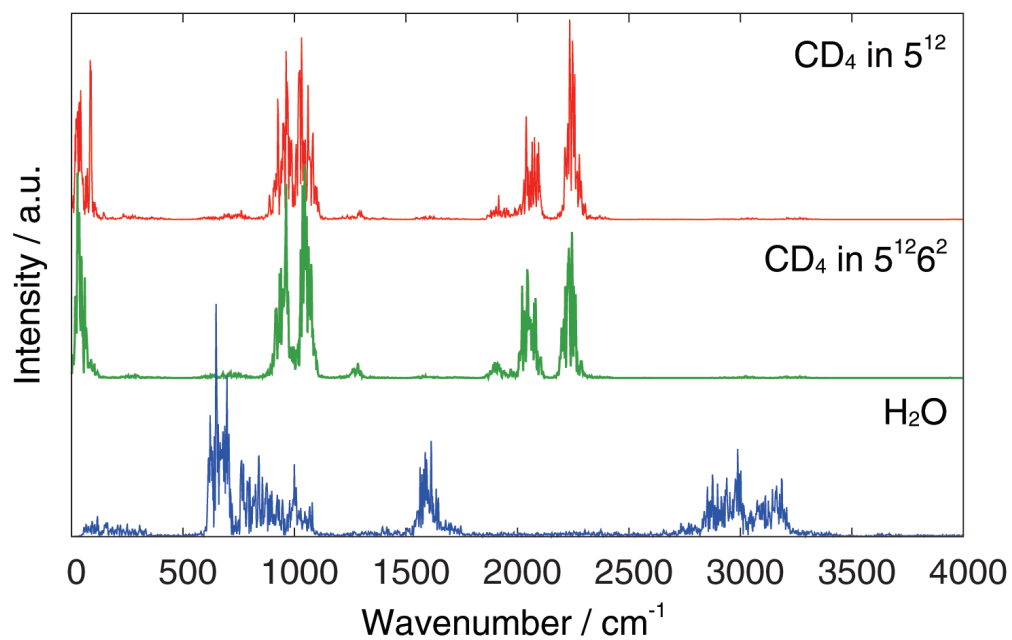


Fig.5.3 Vibrational spectra of CD<sub>4</sub> and H<sub>2</sub>O molecules computed from velocity autocorrelation functions of the hydrogen atoms. The vibrational frequencies are shifted lower compared to those of CH<sub>4</sub> molecules.

Table 5.1 Frequencies of the calculated C-H and C-D stretching vibrations in  $H_2O$  and  $D_2O$  lattices of sI hydrates. The frequency of the C-H stretch in the  $5^{12}6^2$  cages is higher than that in the  $5^{12}6^2$  cages in all cases, with similar values for the frequency shift.

|                                | Cage type   | $CH_4-H_2O$ |          | $CH_4-D_2O$  |           | $CD_4-H_2O$ |              |           |
|--------------------------------|-------------|-------------|----------|--------------|-----------|-------------|--------------|-----------|
|                                |             | This work   | Qin [57] | Schober [56] | This work | Qin [57]    | Schober [56] | This work |
| Symmetric stretch / $cm^{-1}$  | $5^{12}$    | 2871        | 2913.0   | 2915.42      | 2875.5    | 2913.4      | 2913.06      | 2070.6    |
| Asymmetric stretch / $cm^{-1}$ | $5^{12}6^2$ | 2863        | 2901.3   | 2904.03      | 2864.2    | 2901.6      | 2901.35      | 2060.9    |
|                                | $5^{12}$    | 2976        |          |              | 2982.2    |             |              | 2246.1    |
|                                | $5^{12}6^2$ | 2960        |          |              | 2957.7    |             |              | 2230.9    |
| C-H bond length / Å            | $5^{12}$    | 1.0970      |          |              | 1.0962    |             |              | 1.0964    |
|                                | $5^{12}6^2$ | 1.0980      |          |              | 1.0976    |             |              | 1.0980    |

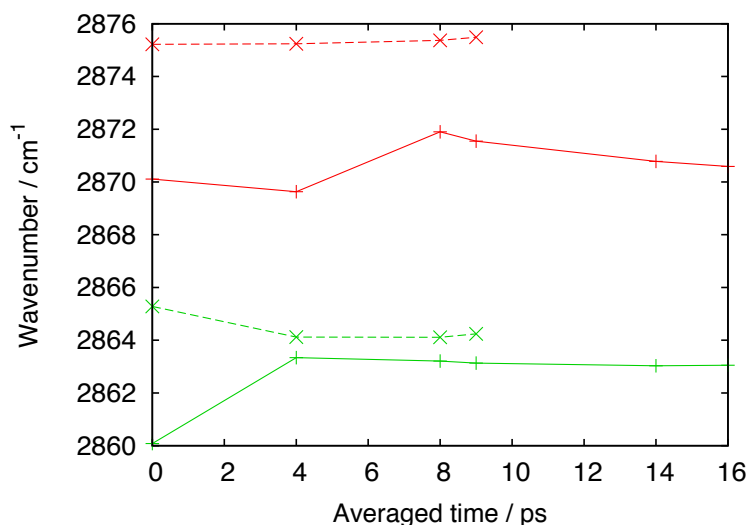


Fig.5.4 Dependence of the vibrational frequency of C-H symmetric stretching vibrations of methane in H<sub>2</sub>O and D<sub>2</sub>O lattice on averaged time. The red and green solid lines are frequencies from methane in the H<sub>2</sub>O lattice 5<sup>12</sup> and 5<sup>12</sup>6<sup>2</sup> cages, respectively. The red and green dashed lines are from methane in the D<sub>2</sub>O lattice 5<sup>12</sup> and 5<sup>12</sup>6<sup>2</sup> cages, respectively.

Vibrational spectra of H<sub>2</sub>O and D<sub>2</sub>O molecules are computed from velocity autocorrelation functions of the hydrogen atoms. The vibrational frequencies of D<sub>2</sub>O molecules are lower than the H<sub>2</sub>O molecules. There are no drastic differences on the vibrational spectra of CH<sub>4</sub> from the CH<sub>4</sub> in H<sub>2</sub>O lattice. The higher frequencies of the CH<sub>4</sub> molecules in the D<sub>2</sub>O lattice in our simulation is caused by the slower motion of the D<sub>2</sub>O molecules induced by its larger mass. The CH<sub>4</sub> molecules are slightly off-centered as they move in the cages. The motion of the methane molecules pushes the H<sub>2</sub>O molecules forming the cages. Since the D<sub>2</sub>O molecules have a slightly larger mass than H<sub>2</sub>O, their response is slower. As a result, the distance between the guest and D<sub>2</sub>O lattice may be shorter and tighter than that in a H<sub>2</sub>O lattice. Figure 5.5 shows radial distribution function of the guest-host molecules. As shown in Table 5.2, the averaged guest-host distance between CH<sub>4</sub> in D<sub>2</sub>O lattice is slightly smaller than that between CH<sub>4</sub> in H<sub>2</sub>O lattice. It should be noted that these results are based on relatively short simulations (only 30 ps due to the large computational cost for the CPMD simulations). The differences of the distances are very slightly and convergence of the value is slow as Figure 5.6. Also the deficiency in describing the van der Waals interactions with the DFT method is important in the calculation of the clathrate hydrates. While we recognize this

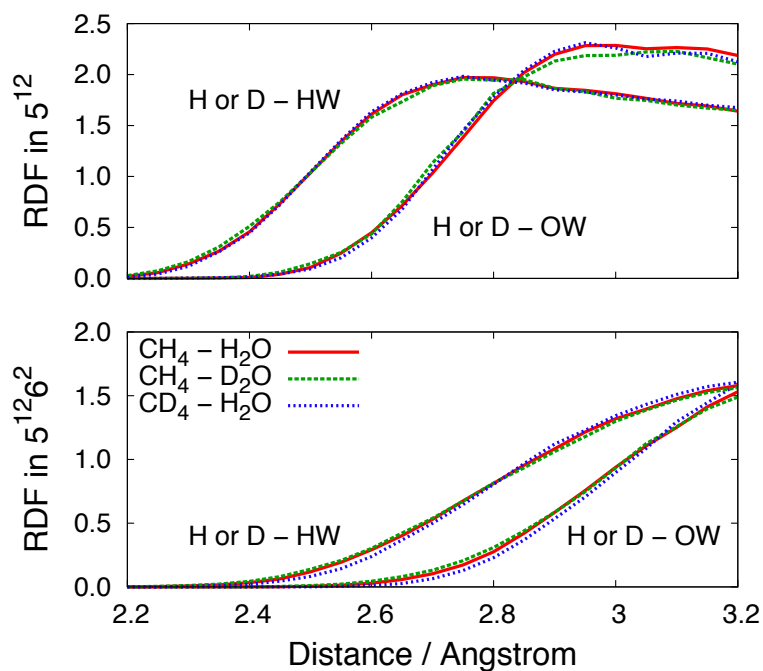


Fig.5.5 Radial distribution functions between H or D atoms in methane and  $\text{H}_2\text{O}$  or  $\text{D}_2\text{O}$  molecules. The guest-host distance between  $\text{CH}_4$  in  $\text{D}_2\text{O}$  lattice is slightly smaller than that between  $\text{CH}_4$  in  $\text{H}_2\text{O}$  lattice.

Table 5.2 Averaged guest-host distances in 25 ps

|  | $5^{12}$ | $5^{12}6^2$ |
|--|----------|-------------|
| H in $\text{CH}_4$ ... O in $\text{H}_2\text{O}$ | 3.9298   | 4.1298      |
| H in $\text{CH}_4$ ... O in $\text{D}_2\text{O}$ | 3.9284   | 4.1292      |
| D in $\text{CD}_4$ ... O in $\text{H}_2\text{O}$ | 3.9309   | 4.1330      |

deficiency, the effect of the corrections of the van der Waals interaction on the vibrational spectra from *ab initio* MD simulations will be addressed in future studies.

#### Bending and Rocking vibration modes

Table 5.3 shows the vibrational frequencies of the bending and rocking vibrational modes, and overtones of the bending vibration in each system. Although the intensity of the peaks of the overtone was much smaller than the fundamental ones, the peaks are large enough to be fitted with Lorentzian functions, except the peak for  $\text{CH}_4$  in the  $5^{12}6^2$  cage in the  $\text{D}_2\text{O}$  lattice. The vibrational spectrum of the overtone for the rocking vibrations is covered by the symmetric and asymmetric stretching

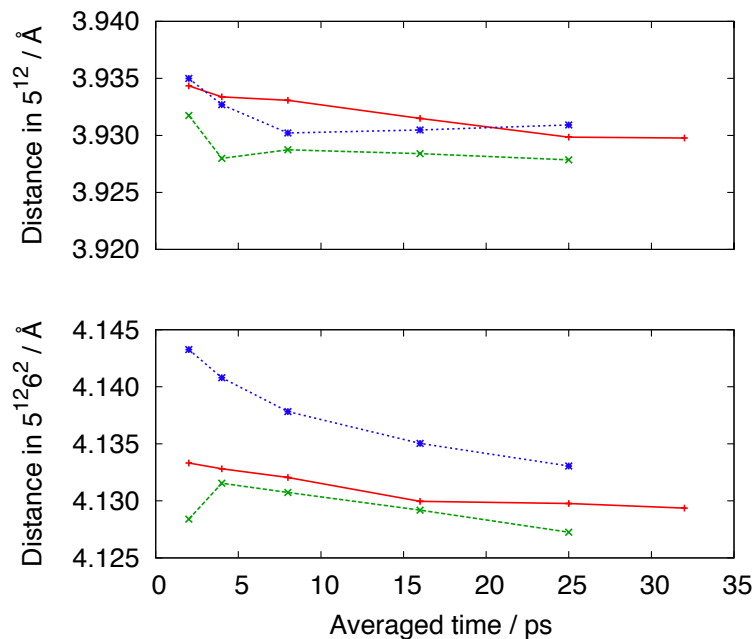


Fig.5.6 Dependence of the averaged guest-host distance on averaged time. The red solid lines are averaged distance between H atoms of  $\text{CH}_4$  and O atoms of  $\text{H}_2\text{O}$  lattice ( $\text{CH}_4\cdots\text{H}_2\text{O}$ ). The green dashed lines are averaged distance between D atoms of  $\text{CD}_4$  and O atoms of  $\text{H}_2\text{O}$  lattice ( $\text{CD}_4\cdots\text{D}_2\text{O}$ ). The blue dashed lines are averaged distance between H atoms of  $\text{CH}_4$  and O atoms of  $\text{D}_2\text{O}$  lattice ( $\text{CH}_4\cdots\text{H}_2\text{O}$ ).

modes, and as such the frequencies are difficult to determine. The difference of the computed vibrational frequencies of bending and rocking, and overtone of the bending modes of the  $5^{12}$  and  $5^{12}6^2$  cages are smaller than that of the stretching vibrations. This trend agrees with experimental observations as measured by Raman spectroscopy.

Table 5.3 Frequencies of the bending, rocking and overtones the bending vibrations for  $\text{CH}_4$  and  $\text{CD}_4$  in  $\text{H}_2\text{O}$  and  $\text{D}_2\text{O}$  lattice of sI hydrates. The differences of the frequencies are smaller than those of the stretching vibrations.

| Cage type                              | $\text{CH}_4\text{-H}_2\text{O}$ |          | $\text{CH}_4\text{-D}_2\text{O}$ |                | $\text{CD}_4\text{-H}_2\text{O}$ |           |
|--|----------------------------------|----------|----------------------------------|----------------|----------------------------------|-----------|
|  | This work                        | Qin [57] | This work                        | Chazallon [55] | Qin [57]                         | This work |
| Bending<br>/ $\text{cm}^{-1}$          | 1248                             | -        | 1252.7                           | -              | -                                | 959.56    |
|  | 1257                             | -        | 1249.4                           | -              | -                                | 955.86    |
| Rocking<br>/ $\text{cm}^{-1}$          | 1460                             | -        | 1467.2                           | -              | -                                | 1032.6    |
|  | 1461                             | -        | 1465.2                           | -              | -                                | 1048.9    |
| Overtone<br>bending / $\text{cm}^{-1}$ | 2504.6                           | 2569.8   | 2570.2                           | 2570.2         | 2570.3                           | 1910.7    |
|  | 2503.9                           | -        | -                                | -              | -                                | 1906.0    |

Also of interest is the coupling of the guest-host molecules in rattling motions. As shown in the Figure 5.1, there is no drastic change on the trend of the spectra between  $\text{CH}_4$  in  $\text{H}_2\text{O}$  and  $\text{CH}_4$  in  $\text{D}_2\text{O}$ , as well as for  $\text{CH}_4$  in  $\text{H}_2\text{O}$  and  $\text{CD}_4$  in  $\text{D}_2\text{O}$  in the four types of intramolecular vibrational modes (bending, rocking, symmetric stretch and asymmetric stretching). However, coupling of the vibrational spectra at the rattling motions is observed. Figure 5.7 shows the vibrations of the methane and water at the rattling vibrational region for  $\text{CH}_4$  in the  $\text{H}_2\text{O}$  and  $\text{D}_2\text{O}$  lattices. The vibrational spectra of the rattling motions of water (changes in the dipole direction without large motion of oxygen) spreads between  $600\text{-}1200\text{ cm}^{-1}$  for  $\text{H}_2\text{O}$  lattice and  $450\text{-}800\text{ cm}^{-1}$  for  $\text{D}_2\text{O}$  lattice. The vibrational spectra of the  $\text{CH}_4$  also have weak peaks in the regions of the rattling motions of water, caused by the coupling of the above  $\text{H}_2\text{O}$  or  $\text{D}_2\text{O}$  motions with van der Waals interaction. On the other hand, the lower frequency region of methane ( $\sim 300\text{ cm}^{-1}$ ) is affected by the motion of oxygen atoms in the  $\text{H}_2\text{O}$  and  $\text{D}_2\text{O}$  molecules that would describe the fluctuation of the cage size and shape. This means that the fluctuation of the cages with the rattling and translational motion of water can affect or be affected by the motion of the guest molecules in the clathrate hydrate. Since the motions of the guest molecules are linked with the guest-host interaction, the rattling motions may affect the intramolecular vibration of methane molecules, such as the frequency and the width of the peaks. In this study, the clear coupling of the intramolecular vibrations is not observed, however, the coupling of the rattling motions may indirectly affect the intramolecular vibrational spectra.

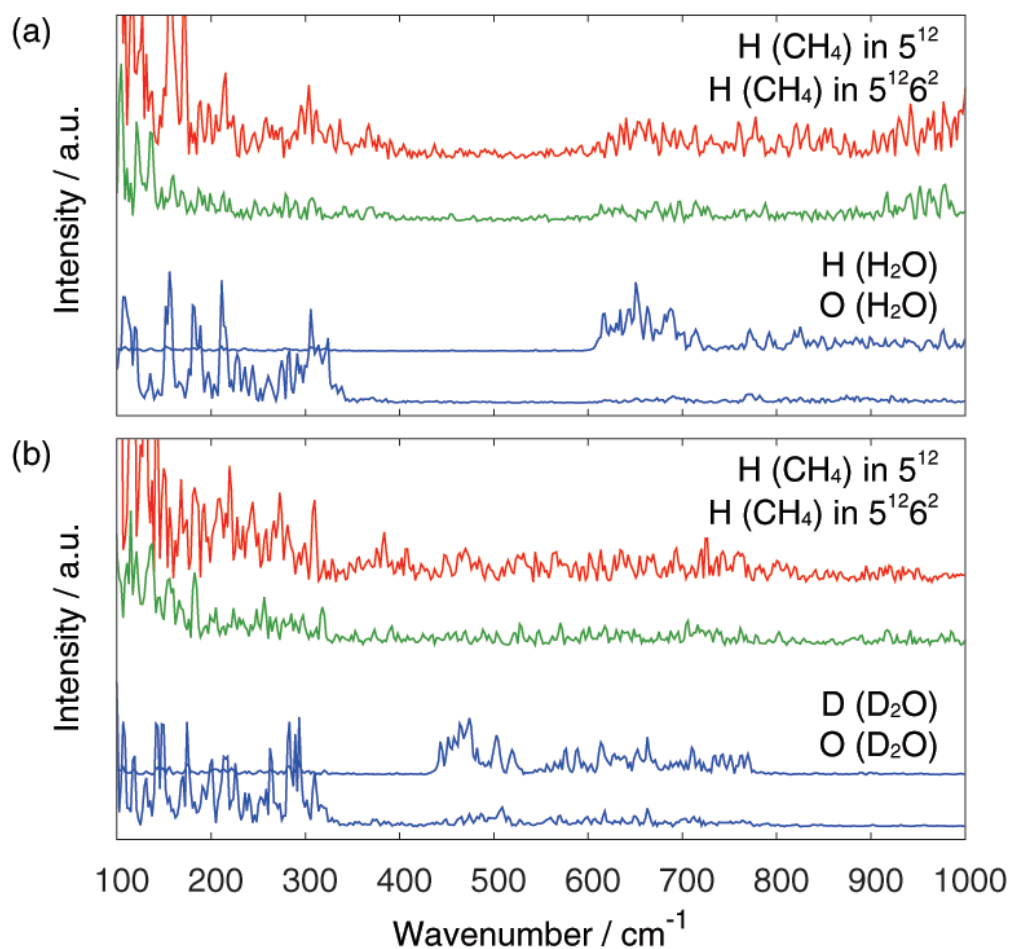


Fig.5.7 Low frequency vibrational spectra of the hydrogen atoms in CH<sub>4</sub> molecules in the H<sub>2</sub>O and D<sub>2</sub>O lattice of sI hydrates. The rattling motion of CH<sub>4</sub> between 600 to 1000 cm<sup>-1</sup> is slightly coupled with the motion of water molecules in the H<sub>2</sub>O hydrate lattice. On the other hand, the CH<sub>4</sub> molecules in the D<sub>2</sub>O hydrate lattice are coupled between 450 to 800 cm<sup>-1</sup>. The translation of CH<sub>4</sub> molecules is also coupled with the translation of oxygen in the H<sub>2</sub>O molecules.

## 5.4 Conclusions

The vibrational spectra of clathrate hydrate containing  $\text{CH}_4$  molecules in a  $\text{D}_2\text{O}$  lattice and  $\text{CD}_4$  molecules in a  $\text{H}_2\text{O}$  lattice were calculated by Car-Parrinello MD simulations. The vibrational frequencies of the C-H stretching and C-D stretching vibrations in the  $5^{12}6^2$  cages were found to be lower than that in the  $5^{12}$  cages. On the other hand, the differences of the vibrational frequency of the bending, rocking, and overtone of the bending vibrations between cages were smaller than the stretching vibrations. The stretching vibrational spectra of  $\text{CH}_4$  molecules in the  $\text{D}_2\text{O}$  lattice were larger than that in the  $\text{H}_2\text{O}$  lattice. Although the intramolecular coupling of guest-water was not clearly revealed from the calculations, the coupling of the vibrational spectra in the rattling motions was observed. These results indicated that the deuteration of the lattice changes the character of the rattling motion of the guest molecule and indirectly affect the intramolecular vibrational spectra with the guest-host intermolecular interaction.

## Chapter 6

# Structure II and Structure H amyl-alcohol hydrate

### 6.1 Introduction

Clathrate hydrates are usually stabilized by suitably sized and hydrophobic guest molecules. The van der Waals-Platteeuw theory [67], which mainly considers guest-host van der Waals interactions as the driving force for hydrate formation, is commonly used to estimate the phase equilibrium conditions of clathrate hydrates [1]. Hydrophilic molecules like methanol, ethanol, and ammonia that form hydrogen bonds with water were historically applied as thermodynamic inhibitors of hydrate formation [12, 13]. However, recent experimental observation reported the formation of clathrate hydrates with these hydrophilic guest molecules without inhibition, and indeed even with promoting effects [14–20]. In clathrate hydrates enclosing hydrophilic molecules, formation of guest-host hydrogen bond is experimentally observed by powder and single X-ray diffraction [68–70], FTIR and Raman observations [17, 71]. Molecular dynamics (MD) simulations show that guest-host hydrogen bonds generate Bjerrum defects in the water lattice hydrogen bond network and affect the motion of guest molecules [16, 72–75]. In these experimental and computational studies, the disorder of the water lattice induced by the guest-host hydrogen bond and dynamics of the guest molecules in the cages are revealed. This type of strong Coulombic interaction also exists in clathrate hydrates containing ionic species [18, 76–78] and halogen molecules [79] as guests and is reported to induce changes on the structures of the water lattice and occupancies of guest substance. To use the effect of the hydrophilic molecules for controlling the thermodynamics of the clathrate, understanding the microscopic structures and effect

on the occupation of guest substance is significant.

In this study, we focus on amyl-alcohol isomers ( $C_5H_{11}OH$ ) as guests in clathrate hydrate phases. One of the amyl-alcohol isomers, 3-methyl-1-butanol, is enclosed in the  $5^{12}6^8$  cages in sH hydrate with the Xe helpgas in  $5^{12}$  and  $4^35^66^3$  cages [80]. A more recent X-ray observation [15] reported this molecule can also be enclosed in  $5^{12}6^4$  cages in sII hydrate with methane helpgas in  $5^{12}$  cages. However, the length of the longest dimension of the 3-methyl-1-butanol in the vacuum determined by DFT calculations using B3LYP with 6-311++G(d,p) is 9.04 Å [17]. This length is considered to be too long for the molecule to fit into the sII  $5^{12}6^4$  cage, where the length of the major axis is 6.29 Å. In comparison, the major axis of the  $5^{12}6^8$  cage in sH hydrates is 8.44 Å [53]. To understand this anomalous enclathration of a large molecule in the sII hydrate, Cha *et al.* synthesized and clathrate hydrates containing eight amyl-alcohol isomers with methane molecules and determined their structures. They found that amyl-alcohol isomers 3-methyl-1-butanol (9.04 Å in end-to-end length in vacuum) and 2-2-dimethyl-1-propanol (7.76 Å end-to-end length) form sII hydrates, while amyl-alcohol isomers, 2-methyl-2-butanol (7.76 Å end-to-end length) and 3-methyl-2-butanol (8.01 Å end-to-end length) form sH clathrate hydrates [17]. They measured the Raman spectra of the hydrate phases and observed that the free 3-methyl-1-butanol O–H stretching vibration observed in sH hydrates was not detected in the sII hydrate. They concluded that the O–H groups of the amyl-alcohols are incorporated into the host cages to fit the relatively small  $5^{12}6^4$  of sII hydrate. These results showed the significant effect of guest-host hydrogen bonding on the structure of clathrate hydrate formed. To provide more detailed and direct insight of guest-host hydrogen bond in clathrate hydrate, we performed MD simulation of amyl-alcohol molecules in sII (3-methyl-1-butanol + methane) and sH (2-methyl-2-butanol + methane) clathrate hydrates. For the characterization of the hydrogen bond and accurate computation of the shift of the intramolecular vibrational frequencies, quantum mechanical computations of the hydrate phase were performed. Since the observation of the dynamics of guest-host hydrogen bonding is difficult in the time scale of *ab initio* MD simulations, we also performed classical MD simulations and analyzed the formation and lifetime of guest-host hydrogen bonds in clathrate hydrates.

## 6.2 Computational method

### 6.2.1 *ab initio* MD simulations

To analyze the guest-host hydrogen bonding and vibrational spectra of the O–H group in the clathrate hydrate, *ab initio* MD simulations were performed on a single unit cell of the binary (3-methyl-1-butanol + methane) sII hydrate and two unit cells of the binary (2-methyl-2-butanol + methane) sH hydrate. To perform sufficiently long simulations to ensure resolution of the vibrational spectra, the Car - Parrinello MD [29] simulation using density functional theory (DFT) in the CPMD package [81] was employed as the *ab initio* MD method. The empirical Grimme correction [38] for the dispersion force in DFT was also applied. The sII clathrate hydrate is cubic and composed of sixteen  $5^{12}$  cages and eight  $5^{12}6^4$  cages formed by 136 water molecules. In this calculation, 3-methyl-1-butanol and methane molecules occupied all  $5^{12}6^4$  and  $5^{12}$  cages, respectively. The unit cell of sH clathrate hydrates is hexagonal and composed of three  $5^{12}$ , two  $4^35^66^3$ , and one  $5^{12}6^8$  cages with 34 water molecules. The 2-methyl-2-butanol guest occupies the  $5^{12}6^8$  cages and methane the  $5^{12}$  and  $4^35^66^3$  cages of the sH hydrate in this study. Initial positions of oxygen atoms in unit cell of clathrate hydrates are determined by X-ray diffractions [34] and proton configurations are decided to satisfy ice rule, zero net-dipole moment and low potential energy. The vibrational spectra of the guests were computed by the Fourier transform of the velocity autocorrelation function of the hydrogen atom in the O–H group of the alcohol molecules computed from the trajectories of MD simulation. The total simulation time was 8 ps. The initial 2 ps was used for the equilibration and remaining 6 ps were used to average the physical values. The velocity autocorrelation function was calculated over 4 ps with a total of 200 autocorrelation functions calculated every 10 fs and then averaged. The resolution of the vibrational spectra was  $8.64 \text{ cm}^{-1}$ . The Hann window function was employed for the Fourier transforms. In the initial 1 ps of equilibration, the velocity scaling method was employed to control the temperature to 113.0 K. The other 6 ps used to calculate the autocorrelation functions were performed in the constant Number of particles, Volume, and Energy (*NVE*) ensemble.

### 6.2.2 Classical MD simulation

The classical MD simulations were performed on the  $2 \times 2 \times 2$  replicas of the unit cells of sII hydrate with 1088 water molecules, and  $3 \times 4 \times 4$  replicas of unit cells of sH with 1632 water molecules to calculate the probability and dynamical properties of hydrogen bonds in the amyl-alcohol clathrate hydrates. The GROMACS [82,83] computational package was used to generate trajectories of clathrate hydrates at the respective temperatures. The TIP4P/ice [84] water model, which is known to reproduce phase diagrams of clathrate hydrates accurately, was used in the simulations. The flexible general AMBER force field [85] (GAFF) was for the 3-methyl-1-butanol, 2-methyl-2-butanol, and methane molecules. The partial charge distribution of the amyl-alcohols and methane molecules were determined by the ChelpG method at the MP2/aug-cc-pVTZ level of theory with Gaussian 03 [86] on the optimized structure with MP2/6-311++G(d,p). The 10 ns MD simulations with a small time step of 0.2 fs were performed by *NPT* with Nosé-Hoover and Parrinello-Rahman algorithm. The computational conditions were set as 113 K, 200 K, 270 K in temperature and 6 MPa in pressure, which correspond to the experimental conditions of hydrate formation. The initial 1 ns was used for the equilibration and remaining 9 ns of simulation time were used for the calculation of the statistical averages. The cut-off of the Lennard-Jones potentials was 14 Å and the calculation of the Coulomb potential was performed with the particle mesh Ewald (PME) method.

## 6.3 Results and Discussions

### 6.3.1 Effect of charges in hydrate cages

With the coordinates of the water molecules of the lowest energy configuration, it is obvious that the guest molecules occupying the cages will experience slightly different proton environments in the different cages of the same type. To estimate the effect of the charges in alcohol molecules, the Coulomb potential for charges in the hydrate cages are calculated. Table 6.1 lists the Coulomb potential energy from the water molecules to a test point charge of  $1.0e$  at the center of the different cages in the sI unit cell. In the TIP4P model of water, Lennard-Jones parameters are only assigned to oxygen atoms in water and as a result, the centers of all similar cages have identical van der Waals potential energies. The Coulomb potential energies

Table 6.1 Coulomb potential energies for a point charge placed at center of the each cage for sI hydrates

| Cage    | Coulomb potential kJ/mol <sup>-1</sup> |
|---------|--|
| Small 1 | -15.7312                               |
| Small 2 | -15.7104                               |
| Large 1 | -50.6478                               |
| Large 2 | -50.6478                               |
| Large 3 | -51.1132                               |
| Large 4 | -51.1132                               |
| Large 5 | -51.1022                               |
| Large 6 | -51.1022                               |

were calculated by the cutoff method. The cutoff length was 500 Å and the oxygen atoms were used for screening of the cutoff. The energies of the guests in the different cages vary by 0.021 kJ mol<sup>-1</sup> and 0.465 kJ mol<sup>-1</sup> for the small and large cages, respectively.

Table 6.2 lists the Coulomb potential energies from the water molecules to a test point charge of 1.0e at the center of the different cages calculated for the sII unit cell. The energies of the guests in the different cages vary by large amounts ranging from 14.80 kJ mol<sup>-1</sup> for small cages and 13.70 kJ mol<sup>-1</sup> for large cages. These energy differences are much greater than those between the cages in the sI unit cell. These energy differences are significant and will affect the local environments of the guests in the different small and large cages of the hydrate phase. The energy differences in the cages are considerable, but the cage shapes in the sII unit cell are quasi-spherical and so the NMR line shape anisotropy is unavailable as a method for gauging the different environments of different cages in the sII hydrate.

The energy differences in the small cages in sH are larger than that in sI but smaller than that in sII hydrate. The guest environment inside the small cages can be different among these three types of structures (Table6.3).

Table 6.2 Coulomb potential energies for a point charge placed at center of the each cage for sII hydrates

| Cage     | Coulomb potential kJ/mol <sup>-1</sup> |
|----------|--|
| Small 1  | -30.6274                               |
| Small 2  | -27.6689                               |
| Small 3  | -20.8737                               |
| Small 4  | -30.2331                               |
| Small 5  | -25.2360                               |
| Small 6  | -21.0696                               |
| Small 7  | -32.3738                               |
| Small 8  | -25.3936                               |
| Small 9  | -25.7720                               |
| Small 10 | -28.1847                               |
| Small 11 | -27.4084                               |
| Small 12 | -28.3898                               |
| Small 13 | -17.5738                               |
| Small 14 | -24.2486                               |
| Small 15 | -22.2669                               |
| Small 16 | -25.8379                               |
| Large 1  | -60.0211                               |
| Large 2  | -48.2347                               |
| Large 3  | -57.4767                               |
| Large 4  | -61.9297                               |
| Large 5  | -53.4989                               |
| Large 6  | -48.8333                               |
| Large 7  | -56.8615                               |
| Large 8  | -54.9082                               |

Table 6.3 Coulomb potential energies for a point charge placed at center of the each cage for sH hydrates

| Cage     | Coulomb potential kJ/mol <sup>-1</sup> |
|----------|--|
| Small 1  | -24.5292                               |
| Small 2  | -22.3840                               |
| Small 3  | -28.3748                               |
| Medium 1 | -35.9031                               |
| Medium 2 | -17.5265                               |
| Large 1  | -67.2454                               |

### 6.3.2 Probability of guest-host hydrogen bonding

Figure 6.1 shows typical structures of the 3-methyl-1-butanol and 2-methyl-2-butanol molecules enclosed in the large cages of sII and sH hydrates, respectively, from the *ab initio* MD simulations. In the  $5^{12}6^4$  cages of sII, strong guest-host hydrogen bonds are formed between 3-methyl-1-butanol and water molecules in both *ab initio* and classical MD simulations. In many of the  $5^{12}6^4$  cages, the O–H groups of the alcohol molecules were inserted between two or three water molecules in the hydrogen bonding network of the cages as shown in the snapshot in Figure 6.1(a) and (b), respectively. The O–H group of 3-methyl-1-butanol in the  $5^{12}6^4$  cages pushes open the wall of the cages. This structural feature has been previously observed in other alcohol guest molecules in hydrate phases [73,87]. On the other hand, the O–H group of the alcohol molecule forming guest-host in the  $5^{12}6^8$  in sH are more centered than that in the sII hydrate as shown in Figure 6.1(c). Furthermore, H atom of the guest molecules ( $H_g$ ) in the  $5^{12}6^8$  in sH were often free from the guest-host hydrogen bonding as shown in Figure 6.1(d).

The probability of the guest-host hydrogen bonding computed from 10 ns of the classical MD simulation is shown in Table 6.4. The probability of the formation of hydrogen bonds with  $i$  molecules  $P_i$  ( $i = 1, 2$  or none 0) is defined as

$$P_i = \frac{N_i}{N_{\text{tot}}}, \quad (6.1)$$

where  $N_i$  is the number of guest molecules forming hydrogen bonds with  $i$  molecules.  $N_{\text{tot}}$  is simply total number of guest molecules.

The  $\text{OH}_g \dots \text{O}_w$  (water O atoms) guest-host hydrogen bond in the sII hydrate of 3-methyl-1-butanol was formed in 98% and 85% of the trajectory time at 113 K and 270 K, respectively. These probabilities are higher than other alcohol molecules such as ethanol, 1-propanol and 2-propanol in the sII clathrate hydrates calculated in previous classical MD simulations, which formed with about 83% and 48% probability at 100 K and 250 K, respectively [73]. In the *ab initio* MD simulation at 113 K, all eight 3-methyl-1-butanol molecules in the unit cell formed hydrogen bonds with water molecules during the 6 ps simulation time. This high probability of guest-host hydrogen bonding shows the contribution of guest-water hydrogen bonding in stabilizing the hydrate structure, which is suggested in previous studies [17]. The guest-host hydrogen bond allows the O–H group of 3-methyl-1-butanol to be incor-

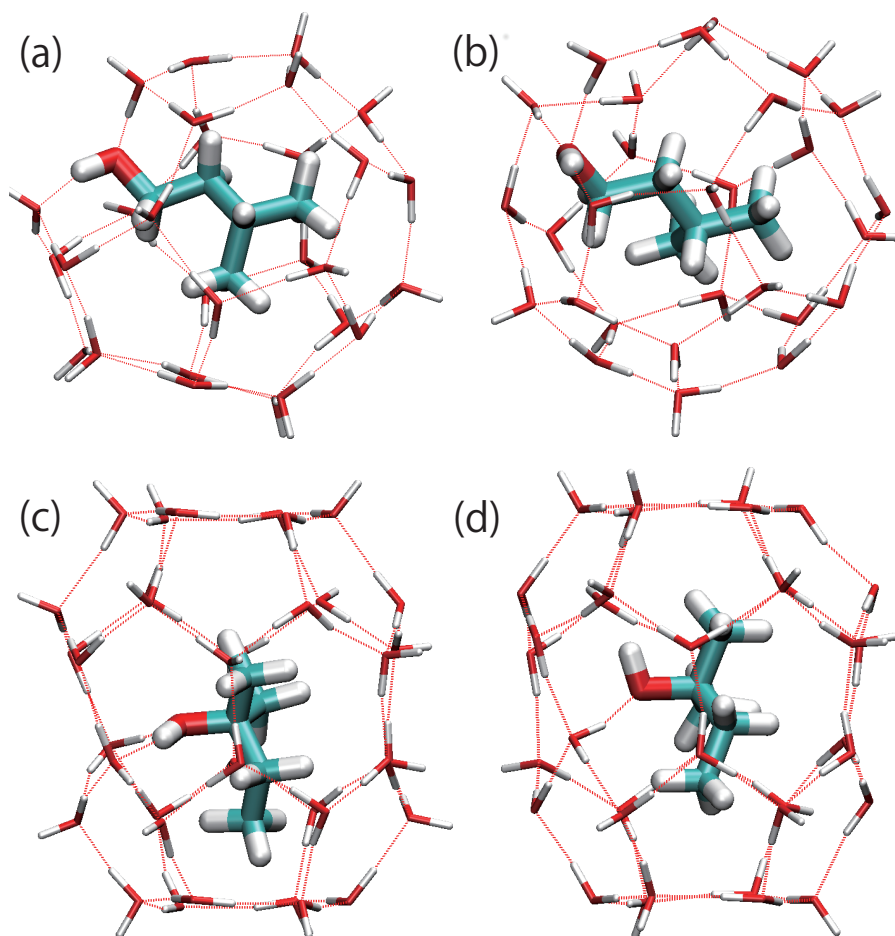


Fig.6.1 Snapshots of the  $5^{12}6^4$  cages in sII and  $5^{12}6^8$  cage in sH clathrate hydrates from the *ab initio* MD simulations.

porated into the cages and the hydrophobic part to fit into the  $5^{12}6^4$  cage. Without this particular form of hydrogen bonding, the amyl-alcohol guest molecule would be too large to fit into the  $5^{12}6^4$  sII hydrate cage. The oxygen atoms of the alcohol molecules act as one or two hydrogen bond proton acceptors from the cage water molecules. The alcohol O–H groups inserted into both five- and six-member water rings in the cages. Configurations where the guest alcohol O atom ( $O_g$ ) hydrogen bonds with the H atoms ( $H_w$ ) of two water molecules were most important in the lower temperature simulations, as shown in Table 6.4.

This high probability of guest-host hydrogen bond shows the contribution of guest-water hydrogen bonding in stabilizing the hydrate structure, which is also indicated in previous studies [17]. The guest-host hydrogen bond allows the O–H group of 3-methyl-1-butanol to be incorporated into the cages and the remaining hydrophobic part fits into the  $5^{12}6^4$  cage. Without this particular form of hydrogen

Table 6.4 Averaged probability of hydrogen bond.

| T / K | $N_{\text{H-bond}}$ | 3-methyl-1-butanol<br>in sII $5^{12}6^4$ |                               | 2-methyl-2-butanol<br>in sH $5^{12}6^8$ |                               |
|-------|---------------------|--|-------------------------------|---|-------------------------------|
|       |                     | $\text{H}_g \dots \text{O}_w$            | $\text{O}_g \dots \text{H}_w$ | $\text{H}_g \dots \text{O}_w$           | $\text{O}_g \dots \text{H}_w$ |
| 113   | 0                   | 0.017                                    | 0.004                         | 0.147                                   | 0.022                         |
|       | 1                   | 0.983                                    | 0.597                         | 0.853                                   | 0.958                         |
|       | 2                   | -  | 0.399                         | -                                       | 0.020                         |
| 200   | 0                   | 0.054                                    | 0.018                         | 0.291                                   | 0.052                         |
|       | 1                   | 0.946                                    | 0.680                         | 0.709                                   | 0.932                         |
|       | 2                   | -  | 0.302                         | -                                       | 0.016                         |
| 270   | 0                   | 0.152                                    | 0.057                         | 0.430                                   | 0.114                         |
|       | 1                   | 0.848                                    | 0.691                         | 0.570                                   | 0.882                         |
|       | 2                   | -  | 0.252                         | -                                       | 0.005                         |

bonding, the amyl-alcohol guest molecule would be too large to fit into the  $5^{12}6^4$  sII hydrate cage. The oxygen atoms of the alcohol molecules act as one or two hydrogen bonds acceptors from the cage water molecules. The alcohol O–H groups inserted into both five- and six-member water rings in the cages. Configurations where the guest alcohol O atom ( $\text{O}_g$ ) hydrogen bonds with the H atoms ( $\text{H}_w$ ) of two water molecules were most important in the lower temperature simulations, as shown in Table 6.4.

In the sH 2-methyl-2-butanol hydrate, the probability of the hydrogen bond was smaller than that in the sII hydrate enclosing 3-methyl-1-butanol (Table 6.4). In this case, about 15% of H atom in the O–H group of the 2-methyl-2-butanol molecules did not form any guest-host hydrogen bonds in the cages of sH hydrate even at 113 K as shown in the snapshot in Figure 6.1(d).

### 6.3.3 Vibrational spectra

Figure 6.2(a) shows the calculated vibrational spectra of the hydrogen atoms in the O–H groups of 3-methyl-1-butanol molecules in the  $5^{12}6^4$  of sII hydrate calculated by *ab initio* MD. The calculated vibrational spectrum of the isolated alcohol molecule in vacuum is also shown for comparison. The vibrational peak of the stretching vibrational mode of the free O–H for an isolated molecule is located at  $3500 \text{ cm}^{-1}$ . In comparison, the vibrational peak of the hydrogen bonded O–H in the cages is shifted to lower frequency, in the range between  $2800 - 3400 \text{ cm}^{-1}$ , along with a broadening in the peak shape. This result supports the interpretation of the

previous experimental Raman observation of amyl-alcohols in the sII hydrate, [17] in that the undetected peak of the free O–H stretching vibration in the sII hydrate is caused by the guest-host hydrogen bond and red shift of the O–H stretching frequency. The amyl-alcohol molecules in sII hydrates form hydrogen bonds with water molecules forming the cages with high probability and as a consequence, the vibrational modes of the amyl-alcohol molecules are drastically altered.

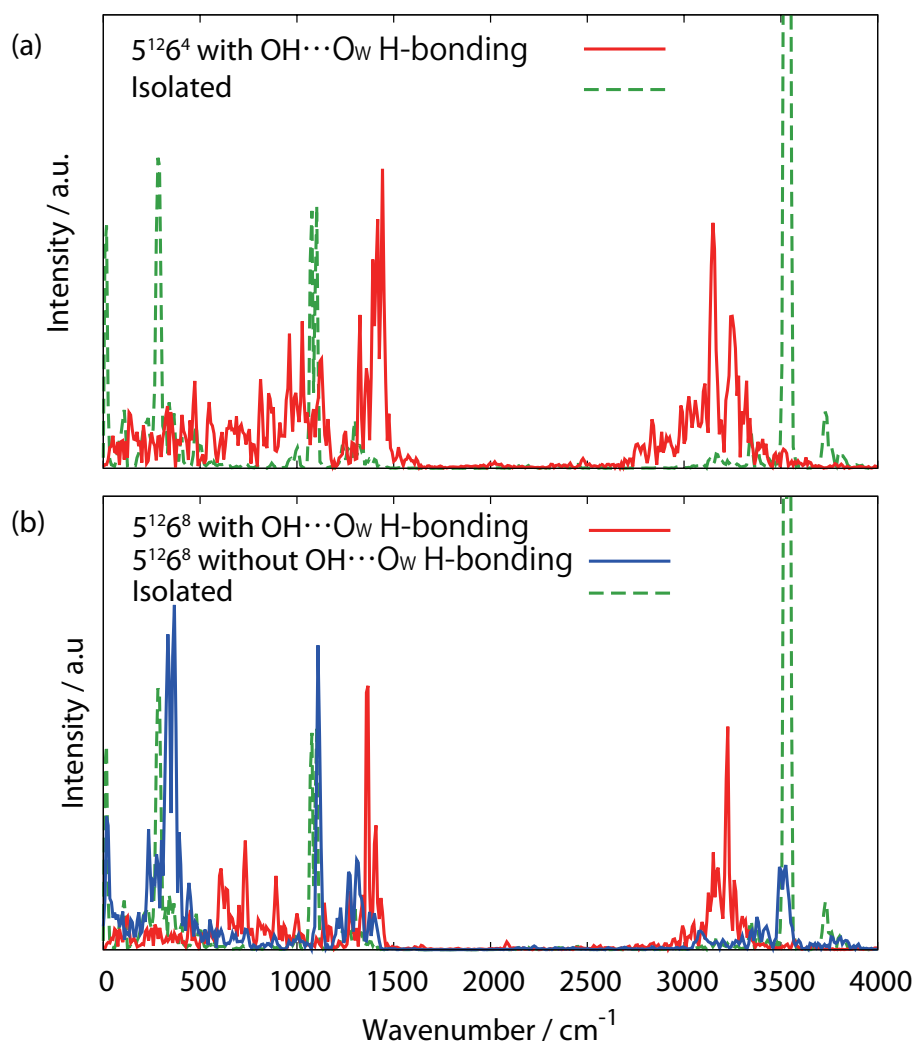


Fig.6.2 (a) Vibrational spectra of 3-methyl-1-butanol molecules in the vacuum (green dashed lines) and in the sII clathrate hydrates computed by the Fourier transform of the velocity autocorrelation function of H atom in the O–H group from *ab initio* MD simulation (red line). The O–H stretching vibrational peak located at the  $3500 \text{ cm}^{-1}$  in vacuum shifted to lower and broad peak around  $3000 \text{ cm}^{-1}$  due to the hydrogen bond between guest and water molecules. In the 8 ps of the *ab initio* MD simulation, all 3-methyl-1-butanol molecules formed hydrogen bond with water molecules in the lattice. (b) Vibrational spectra of 2-methyl-2-butanol molecules in the vacuum and in the sH clathrate hydrate. The red solid line is computed from the guest molecule forming hydrogen bond with water molecules. The blue solid line is from the guest molecule that has no hydrogen bond with host molecules. The frequency shift due to the guest-host hydrogen bond was smaller than that in the sII hydrate.

Figure 6.2(b) shows the vibrational spectra of the hydrogen atoms in O–H groups of 2-methyl-2-butanol molecules in the  $5^{12}6^8$  of sH hydrate calculated from the *ab initio* MD simulations. The red solid line is the vibrational spectrum of selected alcohol molecules in sH hydrate forming guest-host hydrogen bond as shown in Figure 6.1(c). The hydrogen bonded O–H stretching vibrational peak of 2-methyl-2-butanol in the sH hydrates are shifted to lower frequency ( $3000 - 3300 \text{ cm}^{-1}$ ), which is smaller shift than that in the sII hydrate containing 3-methyl-1-butanol. The blue line is the vibrational spectra from a selected 2-methyl-2-butanol molecule in a sH cage that has no  $\text{OH}_g \dots \text{O}_w$  guest-host hydrogen bond as shown in Figure 6.1(d). The frequency of the isolated alcohol molecule and the hydroxyl O–H in 2-methyl-2-butanol molecules with no guest-host hydrogen bond are vibrating with a frequency similar to an uncaged molecule. About 15% of the enclathrated 2-methyl-2-butanol molecules did not form  $\text{OH}_g \dots \text{O}_w$  hydrogen bonds at 113 K and this existence of non-hydrogen bonded, free O–H group of alcohol molecules is consistent with Raman observations [17].

#### 6.3.4 Radial distribution function

Figures 6.3 and 6.4 show the radial distribution function (RDF) of the hydrogen atom in the alcohol O–H group to the oxygen atoms in the cage water molecules calculated from the trajectory of *ab initio* MD and classical MD simulations.

The first peak of the RDF is at  $1.63 \text{ \AA}$  from the *ab initio* MD simulations and at  $1.69 \text{ \AA}$  from the classical MD simulations.

In the sII 3-methyl-1-butanol hydrate, the first peak of the RDF for the hydrogen atom in the alcohol O–H group is at  $1.63 \text{ \AA}$  and  $1.69 \text{ \AA}$  from the *ab initio* and classical MD simulations, respectively. These distances are smaller than the previous observation by classical MD, about  $1.8 \text{ \AA}$  for the ethanol and 2-propanol molecules,  $1.78 \text{ \AA}$  for 1-propanol, [73] and  $2.2 \text{ \AA}$  in tert-butylamine [88] in the  $5^{12}6^4$  cage in sII hydrate. On the other hand, the first peaks of the RDF of oxygen in O–H group to hydrogen atom in water molecules ( $\text{O}_g - \text{H}_w$ ) is  $\sim 1.7 \text{ \AA}$  in all temperatures and structures in classical MD simulations. This value of the ( $\text{O}_g \dots \text{H}_w$ ) hydrogen bond is similar to the corresponding hydrogen bonding length in ethanol, 1-propanol, 2-propanol in [73] and tert-butylamine molecule in the sII hydrate [88] ( $\sim 1.7 \text{ \AA}$ ) in previous computations. The difference of the hydrogen bond length mainly appears in the  $\text{H}_g \dots \text{O}_w$  RDF.

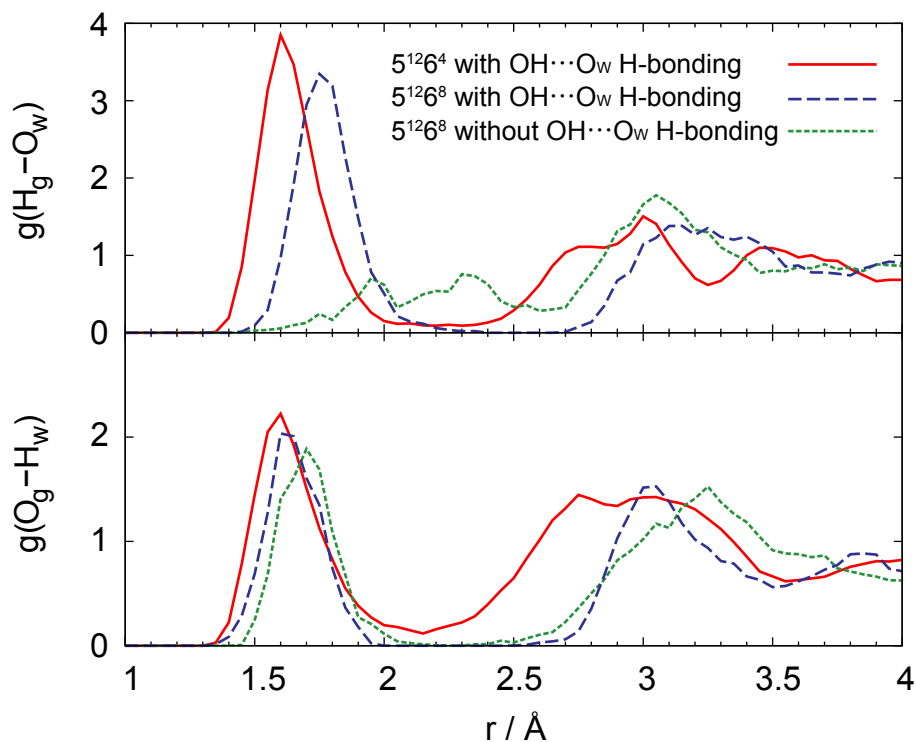


Fig.6.3 Radial distribution function from H atom in the O–H group of guest alcohol to O atom in water molecules ( $H_g \dots O_w$ ; top) and O atom in the O–H group of alcohol to H atom in water ( $O_g \dots H_w$ ; bottom) in cages calculated by ab initio MD simulations. The length of the hydrogen bond in the  $5^{12}6^4$  cages in the sII hydrates are smaller than that in the  $5^{12}6^8$  cages in sH hydrates. The smaller distance reflecting strong hydrogen bond and caused the large frequency shift shown in Figure 6.2(a).

In the sH 2-methyl-2-butanol hydrate, the RDF of RO–H to  $O_w$  was shown in Figures 6.3 and 6.4. The length of the guest-host hydrogen bond in sH was larger than sII and the peak shift of the O–H stretching vibration was less than that in the sII hydrate. This result means that the guest-host hydrogen bond can be formed in the  $5^{12}6^8$  cage but is weaker than that in sII hydrate enclosing 3-methyl-1-butanol. This weaker degree of hydrogen bonding in the sH hydrate is consistent with the observations of the hydrogen bonding strength of pinacolone and tert-butylmethylether in the sH clathrate hydrate [88].

Here we consider structural reasons why different sII and sH structures are obtained for the different amyl-alcohol isomers. Even though the longest large atom distance in the 2-methyl-2-butanol, 7.76 Å, is smaller than that in the 3-methyl-1-butanol, 9.01 Å, only the enclathration of later molecule in the  $5^{12}6^4$  in sII was

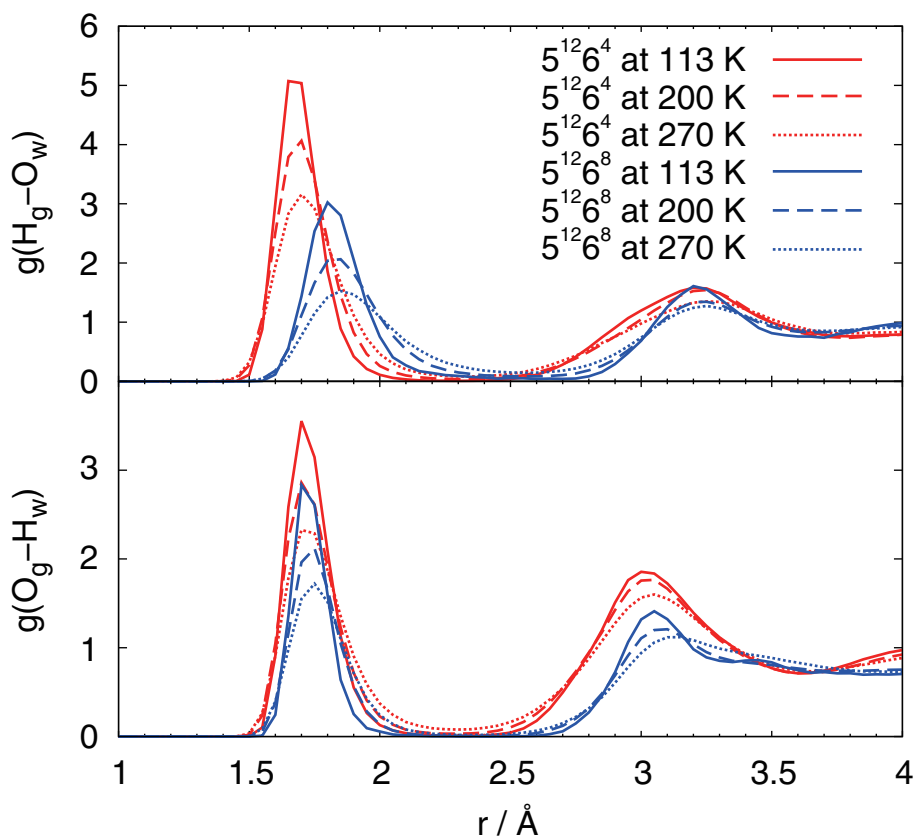


Fig.6.4 Radial distribution function from H atom in the O–H group of guest alcohol to O atom in water molecules ( $H_g \dots O_w$ ; top) and O atom in the O–H group of alcohol to H atom in water ( $O_g \dots H_w$ ; bottom) calculated by classical MD simulations. The length of the  $H_g \dots O_w$  hydrogen bond in the  $5^{12}6^4$  cages in the sII hydrates are smaller than that in the  $5^{12}6^8$  cages in sH hydrates. On the other hand, the length of the  $O_g \dots H_w$  hydrogen bond is identical in all system. The tail of the first peak in  $5^{12}6^8$  cages (blue lines) shows the non-hydrogen bonded amyl-alcohol molecules in sH hydrate, origin of the free O–H vibrational spectra.

observed [17]. The difference in hydrate structures primarily arises from the difference of the location of O–H group in the amyl-alcohol guest molecules. To enclose the 3-methyl-1-butanol molecule into the relatively small  $5^{12}6^4$  cage, the incorporation of the O–H group by the guest-host hydrogen bond is required. The O–H group of the 3-methyl-1-butanol is located at the end of the molecules and is not encumbered by nearby methyl groups. As a result, the O–H group can easily hydrogen bond with water molecules in the cages and even be inserted among the water molecules. As a result, the 3-methyl-1-butanol can be incorporated in the relatively smaller  $5^{12}6^4$  cages in the sII hydrate. The O–H group of 2-methyl-2-

butanol is located close to two methyl groups which cause steric repulsions with cage waters when the O–H hydrogen bonds with the cage waters. The O–H group of 2-methyl-2-butanol cannot be as easily incorporated in the hydrogen bonding of cage water molecules. A similar trend is also observed in other amyl-alcohol molecules discussed in the previous experimental work, [17] namely, 2-2-dimethyl-1-propanol forms sII and 3-methyl-2-butanol forms sH hydrate. As shown here, the structure of the clathrate hydrates forming guest-host hydrogen bonds would be strongly affected by the microscopic structure of the guest substance, including the position of the O–H groups and not only the size of the molecules from van der Waals interactions.

### 6.3.5 Rotation of guest molecules

The guest-host hydrogen bondings affect the rotation of the guest molecules in the cages [72, 73, 88]. To determine the effect of the guest-host hydrogen bondings on motion of the guest molecules, the rotation of the unit vector in the direction of the alcohol O–H group of guest molecules,  $\boldsymbol{\mu}$ , was calculated from classical MD simulation. The rotational motion of a guest molecule at a time  $t$  after some origin is characterized the rotation of this unit vector,

$$\cos\theta(t) = \boldsymbol{\mu}(0) \cdot \boldsymbol{\mu}(t). \quad (6.2)$$

Figure 6.5 shows the autocorrelation functions for the second Legendre polynomial  $M_2(t)$  for the cosine of the rotation angle of the O–H bond,

$$M_2(t) = \frac{1}{2} \langle 3\cos^2\theta(t) - 1 \rangle, \quad (6.3)$$

for 3-methyl-1-butanol in the sII hydrate and 2-methyl-2-butanol in the sH hydrate. The  $M_2(t)$  autocorrelation function is closely linked with relaxation times in NMR spectroscopy [89]. The  $M_2(t)$  decay faster at higher temperatures as the alcohol guests gain greater rotational freedom in the cages. The relaxation times of intramolecular geometry changes are known to have a relaxation time of  $\sim 1$  ps [72, 73, 88] and molecular rotations have larger relaxation time.

Surprisingly, despite the higher probability of guest-host hydrogen bonding in the  $5^{12}6^4$  cages of sII as shown in Table 6.4, the relaxation of the  $M_2(t)$  curves for the 3-methyl-1-butanol in the  $5^{12}6^4$  cages are more quickly than that of the 2-methyl-2-butanol in the larger  $5^{12}6^8$  of the sH cages. To understand this trend, we calculate

the continuous hydrogen bond time correlation function  $S_{\text{HB}}(t)$  [90],

$$S_{\text{HB}}(t) = \frac{\langle H(0)H(t) \rangle}{\langle H(0)^2 \rangle}, \quad (6.4)$$

where  $H(t)$  is hydrogen bonding population valuable defined such that  $H(t) = 1$  if the guest-host hydrogen bond pair remains stable continuously from  $t = 0$  to time  $t$  and it is zero otherwise (i.e., if the guest-host hydrogen bonding is broken or the pair is changed). The brackets represent ensemble averages over all guest molecules in system.  $S_{\text{HB}}(t)$  describes the probability that guest-host hydrogen bond pair remains stable at all times up to  $t$ . Figure 6.6 shows that the hydrogen bond correlation function,  $S_{\text{HB}}(t)$  for 3-methyl-1-butanol in the sII  $5^{12}6^4$  cages decays faster than that for 2-methyl-2-butanol in the sH  $5^{12}6^8$  cages. Despite having greater hydrogen bonding probability, the guest-host hydrogen bond pairs for 3-methyl-1-butanol in the sII  $5^{12}6^4$  cages break and reform more frequently than those for the 2-methyl-2-butanol in the sH  $5^{12}6^8$ . This more frequent transition of the guest-host hydrogen bonding pair indicates the lower potential barrier of the transition and results in the faster decay of  $M_2(t)$  for 3-methyl-1-butanol in the sII  $5^{12}6^4$  cages.

The relaxation times of the rotation are computed by fitting  $M_2(t)$  to a sum of exponential functions corresponding to different intramolecular geometry changes and rotation of the molecules as

$$M_2(t) = \sum_{k=1}^n A_k \exp(-t/\tau_k). \quad (6.5)$$

Fit parameters for the molecular rotations of the guest molecules in Figure 6.5 at different temperatures in the hydrates are given in Table 6.5. To fit the decay of the  $M_2(t)$  related with molecular rotations, one to four exponential functions were used. The multiple relaxation times in the  $M_2(t)$  decay reflect the complicated motions and environment in the cage due to the guest-host hydrogen bonding, especially for the  $5^{12}6^4$  cages in the sII hydrate.

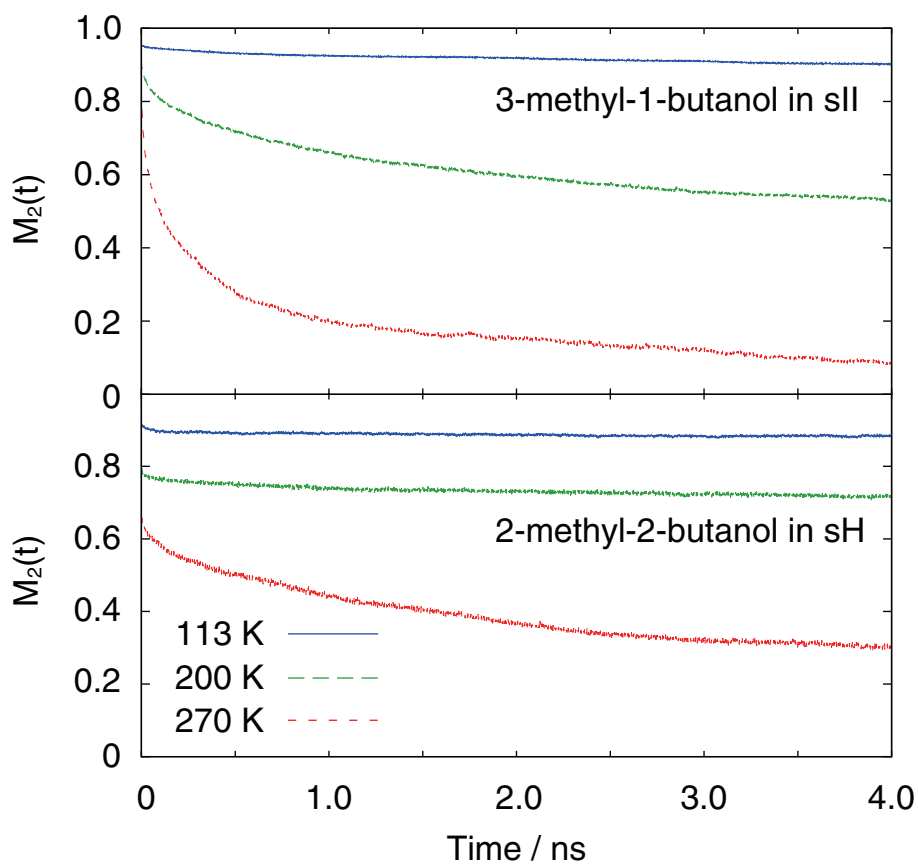


Fig.6.5 Decay of the  $M_2$  autocorrelation functions with time for 3-methyl-1-butanol in the sII (top) and 2-methyl-2-butanol in the sH hydrate (bottom). The relaxation time of  $M_2$  in the sII hydrate is smaller than that in the sH hydrates at all temperatures.

Table 6.5 Fitted relaxation time

| Guest (Temp.)    | $A$   | $\tau_1 / \text{ps}$ | $B$   | $\tau_2 / \text{ps}$ | $C$   | $\tau_3 / \text{ps}$ | $D$   | $\tau_4 / \text{ps}$ |
|------------------|-------|----------------------|-------|----------------------|-------|----------------------|-------|----------------------|
| 3Me1BuOH (113 K) | 0.048 | 0.327                | 0.018 | 244                  | 0.934 | 112567               | -     | -                    |
| 3Me1BuOH (200 K) | 0.120 | 0.923                | 0.080 | 103                  | 0.213 | 1216                 | 0.585 | 35527                |
| 3Me1BuOH (270 K) | 0.209 | 0.600                | 0.185 | 25.1                 | 0.360 | 289                  | 0.245 | 4023                 |
| 2Me2BuOH (113 K) | 0.102 | 0.985                | 0.894 | 256066               | -     | -                    | -     | -                    |
| 2Me2BuOH (200 K) | 0.243 | 0.667                | 0.754 | 69315                | -     | -                    | -     | -                    |
| 2Me2BuOH (270 K) | 0.396 | 0.680                | 0.258 | 1238                 | 0.342 | 23403                | -     | -                    |

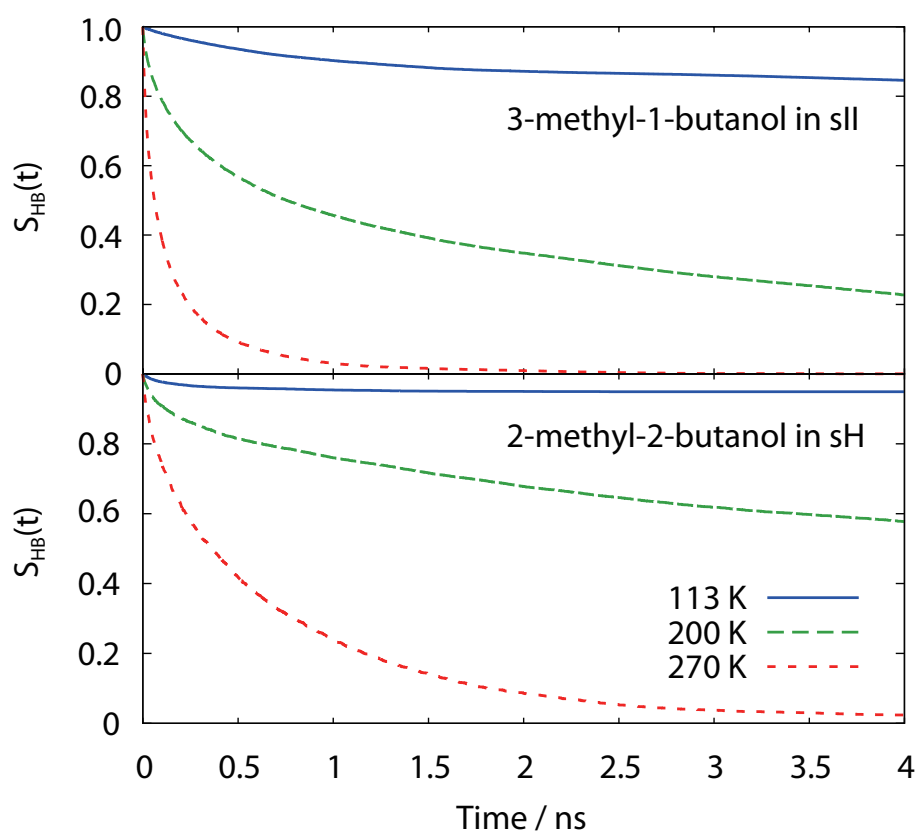


Fig.6.6 Decay of the  $S_{HB}$  with time for 3-methyl-1-butanol in the sII (top) and 2-methyl-2-butanol in the sH hydrate (bottom). The continuous time of the guest-host hydrogen bond pair of the sII 3-methyl-1-butanol hydrate is shorter than that of the sH 2-methyl-2-butanol hydrate.

### 6.3.6 Guest-guest hydrogen bonding

In the 10 ns of the classical MD simulation, we also observed guest-guest host hydrogen bonds in the sII hydrate. Since all  $5^{12}6^4$  cages in sII hydrates share hexagonal faces with other  $5^{12}6^4$  cages, the rotating O–H groups in the cages can be close each other. As shown in Table 6.4, about 4 % of the alcohol molecules formed guest-guest hydrogen bonds through the hexagonal faces at 270 K. The same geometric criteria of O–H...O distance and O–H...O angle with guest-host hydrogen bonds were used to determine the presence of guest-guest hydrogen bonding. A snapshot of a guest-guest hydrogen bond in the cages is shown in the Figure 6.7. In previous studies, the guest-guest interactions are usually not considered when estimating the thermodynamic stability of the hydrate phase. However, as seen in our study, such guest-guest interactions can have important consequences on hydrate stability.

The guest-guest hydrogen bonds can affect the rotation of the guest molecules and microscopic structure of the cages. The rotational autocorrelation function of O–H vector in alcohol molecules from classical MD simulations are shown in Figure 6.5.

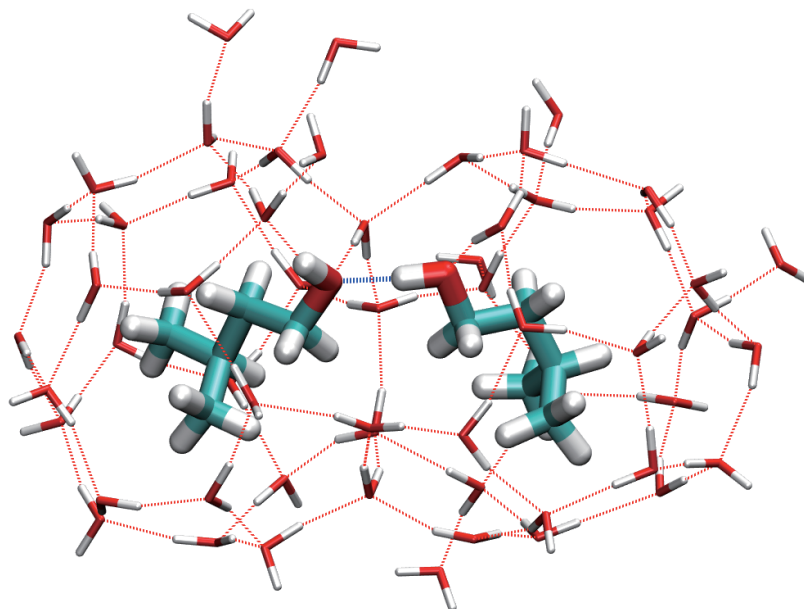


Fig.6.7 Snapshot of the guest-guest hydrogen bond between 3-methyl-1-butanol molecules in sII hydrate observed in the classical MD simulation. The probability of the guest-guest hydrogen bond was about 0.04.

### 6.3.7 Displacement of water molecule by the O–H group of alcohol

Another possibility for the incorporation of 3-methyl-1-butanol molecules in sII hydrate lattice is the displacement of a water molecule by the O–H group of alcohol. The incorporation of the hydroxyl groups of the alcohol molecules into the cages is a possibility and would retain the 28 oxygen vertices of the  $5^{12}6^4$  cage. However, this would introduce Bjerrum L-defects into the hydrogen bonding network, and make the cage structures more disordered.

We artificially removed a water molecule from hydrate lattice and computed vibrational spectra of 3-methyl-1-butanol by *ab initio* MD. Figure 6.8 gives the O–H vibrational spectra and snapshot 3-methyl-1-butanol molecule that replaced water molecule in the  $5^{12}6^4$  cage in the sII hydrate. The structure was stable during the 8 ps of the *ab initio* MD and there are no drastic differences in the vibrational spectra of the 3-methyl-1-butanol incorporated in the cages as compared to the case where the O–H bond is inserted in the hydrogen bonded network. Although it is difficult to detect this configuration using Raman spectroscopy, the incorporation of the alcohol O–H groups as part of the water cages may be possible and retain the 28 oxygen vertices of the  $5^{12}6^4$  cage.

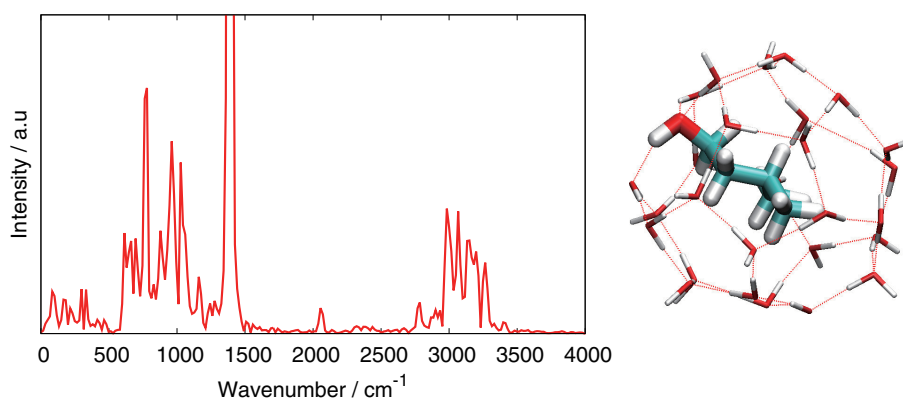


Fig.6.8 Vibrational spectrum and snapshot of a 3-methyl-1-butanol molecule that replaces a water molecule in the  $5^{12}6^4$  cage. The spectrum was computed from H atom in the O–H group of 3-methyl-1-butanol molecule. The initial structure was artificially generated by removing one water molecule from the cage. The form of the vibrational spectrum was very similar to the configuration with O–H bond inserted between the hydrogen bond of water molecules shown in Figure 6.1(a,b).

## 6.4 Conclusions

*Ab initio* and classical molecular dynamics simulation were performed to study the effects of guest-host hydrogen bonding on the structure and stability of two amyl-alcohol clathrate hydrates. The simulations showed the formation of strong guest-host hydrogen bonds and the large frequency shift of the O–H stretching vibration of the 3-methyl-1-butanol molecule in sII clathrate hydrate. The guest-host hydrogen bond was quite stable and the calculated O–H vibrational frequency shift was consistent with previous experimental Raman spectra where the free O–H stretching vibrational peak of amyl-alcohol in sII hydrate was not observed [17]. The O–H group of the 3-methyl-1-butanol molecules were incorporated into the water lattice of  $5^{12}6^4$  cages. As the result of the incorporation, the large alcohol molecule can fit the relatively small  $5^{12}6^4$  cages. Guest-host hydrogen bonding was also observed in sH clathrate hydrate enclosing 2-methyl-2-butanol. The guest-host hydrogen bonding was relatively weaker than in the sII hydrate and a smaller  $100\text{ cm}^{-1}$  frequency shift of the O–H stretching vibration was observed in this case. 15% of the enclathrated 2-methyl-2-butanol molecules did not form hydrogen bonds and this existence of non-hydrogen bonded free O–H group of alcohol molecule is consistent with Raman observations [17]. The differences of the behavior of the guest-host hydrogen bonds were related to the location of the O–H group in the alcohol molecules. The O–H group of the 3-methyl-1-butanol is located at the head of the alcohol and is easily incorporated into the hydrate cage. In contrast, the O–H group of the 2-methyl-2-butanol is located closer to the center of the molecule and the formation of strong hydrogen bonds with the cage water molecules is more difficult due to the steric effects of the methyl groups. Therefore, the 3-methyl-1-butanol molecules are enclosed in the  $5^{12}6^4$  in sII with methane while the 2-methyl-2-butanol is observed in the larger  $5^{12}6^8$  cages in the sH hydrate. The position of the hydrophilic part of guest molecule plays an important role in determining the stability of the cages and the structure of the clathrate hydrate.

We should mention that we used full occupancy of the small cage methane guest molecules in these simulations. The previous MD simulation reported that the relaxation time is affected by the occupancy of clathrate hydrate and combined molecules [88]. More detailed analysis focusing on the occupancy and types of guest substances should be performed in future researches were experimental small

cage guest occupancies are used.

## Chapter 7

# Conclusions

*Ab initio* and classical molecular dynamics simulations on the methane hydrates and alcohol clathrate hydrates are performed to understand the vibrational spectra of clathrate hydrates. The main conclusions from this work are as follow.

Molecular dynamics simulations using five types of autocorrelation functions well determined the intramolecular and intermolecular vibrational spectra of methane molecules in sI clathrate hydrate. The calculated frequency changes of the stretching vibrational modes of sI methane clathrate hydrates agreed with the previous experimental observation. The changes of the stretching vibrational frequencies were closely linked with the C–H bond length. The vibrational frequencies of rocking and bending modes of methane molecules were indistinguishable in this calculation.

In sH methane hydrate, the calculated vibrational frequencies of stretching vibrational modes in the  $5^{12}$  cages were larger than that in the  $4^35^66^3$  cages. The smaller differences of the intramolecular vibrational frequencies than sI hydrate were caused by the similar size of the cages in sH hydrates. However, the unspherical form of the cages clearly affected the molecular motions of the methane molecules.

The effect of the deuteration of the hydrate lattice on the intramolecular and intermolecular vibrational spectra of methane molecules were indicated. The stretching vibrational spectra of  $\text{CH}_4$  molecules in the  $\text{D}_2\text{O}$  lattice were larger than that in the  $\text{H}_2\text{O}$  lattice due to the dynamics of the water lattice.

The vibrational spectra of alcohol O–H bonds were calculated by *ab initio* and classical MD simulations. The simulations showed the formation of strong guest–host hydrogen bonds and the large frequency shift of the O–H stretching vibration of the 3-methyl-1-butanol molecule in sII clathrate hydrate. The O–H group of alcohol molecules are incorporated into the water framework. On the other hand, the frequency shift of 2-methyl-2-butanol molecules in sH clathrate hydrates were

smaller. Furthermore, the incorporation of the O–H group were not observed in the sH hydrate. The position of the hydrophilic part of guest molecule plays an important role in determining the stability of the cages and the structure of the clathrate hydrate.

In this study, the new methodology of the calculation of the vibrational spectra of guest molecules in clathrate hydrates using *ab initio* MD simulation are suggested and the trend of the calculated spectra agreed with the previous experimental observations. For the practical application of clathrate hydrates, controlling of occupancy of guest molecules and stability of clathrate hydrates are important. These properties of the clathrate hydrates are determined by the interactions between guest and host molecules. This study performed the calculation of the vibrational spectra that reflect the guest-host interactions and revealed the relation between the vibrational spectra and microscopic structure of the guest molecules in clathrate hydrates.

As shown in this study, the structure of the clathrate hydrates containing hydrophilic molecules is more complex than the clathrate hydrates stabilized by simple van der Waals interactions. To understand such strong and complex guest-host interactions of inclusion compounds for future use of clathrate hydrates, molecular dynamics and *ab initio* calculations will provide valuable information.



# References

- [1] E. D. Sloan. Fundamental principles and applications of natural gas hydrates. *Nature*, 426(6964):353–363, 2003.
- [2] H. Davy. On a Combination of Oxymuriatic Gas and Oxygene Gas. *Philos. Trans. R. Soc. London*, 101(1811):155–162, 1811.
- [3] M. Faraday. On Hydrate of Chlorine. *Quart. J. Sci.*, 15:71, 1823.
- [4] E. G. Hammerschmidt, T. Natural, and G. Company. Gas Hydrates in Natural Gas Transmission Lines. *Ind. Eng. Chem.*, 26(8):851–855, 1934.
- [5] K. A. Kvenvolden. Potential effects of gas hydrate on human welfare. *Proc. Natl. Acad. Sci. U. S. A.*, 96(7):3420–3426, 1999.
- [6] H. Itoh and K. Kawamura. Molecular Dynamics Simulations of Clathrate Hydrate: Intramolecular Vibrations of Methane. *Ann. N. Y. Acad. Sci.*, 912(1):693–701, 2000.
- [7] J. A. Greathouse, R. T. Cygan, and B. a. Simmons. Vibrational spectra of methane clathrate hydrates from molecular dynamics simulation. *J. Phys. Chem. B*, 110(13):6428–6431, 2006.
- [8] F. Castillo-Borja, R. Vázquez-Román, and U. I. Bravo-Sánchez. Dynamic properties of methane, water and methane hydrates using computational simulations. *Mol. Simul.*, 36(3):229–239, 2010.
- [9] T. Ikeda and K. Terakura. Structural transformation of methane hydrate from cage clathrate to filled ice. *J. Chem. Phys.*, 119(13):6784, 2003.
- [10] J. S. Tse. Vibrations of Methane in Structure I Clathrate Hydrate—an ab initio Density Functional Molecular Dynamics Study. *J. Supramol. Chem.*, 2(4-5):429–433, 2002.
- [11] M. Soler, E. Artacho, J. D. Gale, A. Garc, J. Junquera, P. Ordej, and S.-P. Daniel. The SIESTA method for ab initio order- N materials. *J. Phys. Condens. Matter*, 14:2745–2779, 2002.
- [12] D. Davidson, S. Gough, J. Ripmeester, and H. Nakayama. The effect of

- methanol on the stability of clathrate hydrates. *Can. J. Chem.*, 59:2587–2590, 1981.
- [13] B. Gbaruko, J. Igwe, P. Gbaruko, and R. Nwokeoma. Gas hydrates and clathrates: Flow assurance, environmental and economic perspectives and the Nigerian liquified natural gas project. *J. Pet. Sci. Eng.*, 56(1-3):192–198, 2007.
- [14] K. K. Østergaard, B. Tohidi, R. Anderson, A. C. Todd, and A. Danesh. Can 2-Propanol Form Clathrate Hydrates? *Ind. Eng. Chem. Res.*, 41(8):2064–2068, 2002.
- [15] R. Ohmura, S. Takeya, T. Uchida, I. Y. Ikeda, T. Ebinuma, and H. Narita. Clathrate hydrate formation in the system methane + 3-methyl-1-butanol + water: equilibrium data and crystallographic structures of hydrates. *Fluid Phase Equilib.*, 221(1-2):151–156, 2004.
- [16] V. Buch, J. P. Devlin, I. A. Monreal, B. Jagoda-cwiklik, N. Uras-Aytemiz, and L. Cwiklik. Clathrate hydrates with hydrogen-bonding guests. *Phys. Chem. Chem. Phys.*, 11(44):10245–10265, 2009.
- [17] M. Cha, K. Shin, and H. Lee. Spectroscopic identification of amyl alcohol hydrates through free OH observation. *J. Phys. Chem. B*, 113(31):10562–10565, 2009.
- [18] M. Cha, K. Shin, M. Kwon, D.-Y. Koh, B. Sung, and H. Lee. Superoxide ions entrapped in water cages of ionic clathrate hydrates. *J. Am. Chem. Soc.*, 132(11):3694–3696, 2010.
- [19] K. Shin, R. Kumar, K. A. Udachin, S. Alavi, and J. A. Ripmeester. Ammonia clathrate hydrates as new solid phases for Titan, Enceladus, and other planetary systems. *Proc. Natl. Acad. Sci. U. S. A.*, 109(37):14785–14790, 2012.
- [20] K. Shin, K. A. Udachin, I. L. Moudrakovski, D. M. Leek, S. Alavi, C. I. Ratcliffe, and J. A. Ripmeester. Methanol incorporation in clathrate hydrates and the implications for oil and gas pipeline flow assurance and icy planetary bodies. *Proc. Natl. Acad. Sci. U. S. A.*, 110(21):8437–42, 2013.
- [21] L. Verlet. Computer experiments on classical fluids. I. Thermodynamical Properties of Lennard-Jones Molecules. *Phys. Rev.*, 159(1):98–103, 1967.
- [22] W. C. Swope. A computer simulation method for the calculation of equilibrium constants for the formation of physical clusters of molecules: Application to small water clusters. *J. Chem. Phys.*, 76(1):637, 1982.
- [23] J. E. Jones. On the Determination of Molecular Fields. II. From the Equation

- of State of a Gas. *Proc. R. Soc. A Math. Phys. Eng. Sci.*, 106(738):463–477, 1924.
- [24] P. Hohenberg. Inhomogeneous electron gas. *Phys. Rev.*, 136(3B):B864—B871, 1964.
- [25] A. K. Sum, R. C. Burruss, and E. D. Sloan. Measurement of Clathrate Hydrates via Raman Spectroscopy. *J. Phys. Chem. B*, 101(38):7371–7377, 1997.
- [26] G. C. Pimentel and S. W. Charles. *Infrared Spectral Perturbations in Matrix Experiments*, volume 7. 1963.
- [27] S. Subramanian and E. D. Sloan. Trends in Vibrational Frequencies of Guests Trapped in Clathrate Hydrate Cages. *J. Phys. Chem. B*, 106(17):4348–4355, 2002.
- [28] T. Shimanouchi. *Molecular Vibrational Frequencies*, 2012.
- [29] R. Car and M. Parrinello. Unified approach for molecular dynamics and density-functional theory. *Phys. Rev. Lett.*, 55(22):2471–2474, 1985.
- [30] <http://www.cpmd.org>.
- [31] J. Perdew, K. Burke, and M. Ernzerhof. Generalized gradient approximation made simple. *Phys. Rev. Lett.*, 77(18):3865–3868, 1996.
- [32] N. Troullier and J. L. Martins. Efficient pseudopotentials for plane-wave calculations. *Phys. Rev. B*, 43(3):1993–2006, 1991.
- [33] L. Kleinman and D. M. Bylander. Efficacious form for model pseudopotentials. *Phys. Rev. Lett.*, 48(20):1425–1428, 1982.
- [34] R. K. McMullan, G. A. Jeffrey, P. Of, and T. H. E. Crystals. Polyhedral Clathrate Hydrates. IX. Structure of Ethylene Oxide Hydrate. *J. Chem. Phys.*, 42(8):2725, 1965.
- [35] V. P. Shpakov, J. S. Tse, C. A. Tulk, B. Kvamme, and V. R. Belosludov. Elastic moduli calculation and instability in structure I methane clathrate hydrate. *Chem. Phys. Lett.*, 282(2):107–114, 1998.
- [36] G. Román-Pérez, M. Moaied, J. Soler, and F. Yndurain. Stability, Adsorption, and Diffusion of CH<sub>4</sub>, CO<sub>2</sub>, and H<sub>2</sub> in Clathrate Hydrates. *Phys. Rev. Lett.*, 105(14):8–11, 2010.
- [37] R. W. Williams and D. Malhotra. van der Waals corrections to density functional theory calculations: Methane, ethane, ethylene, benzene, formaldehyde, ammonia, water, PBE, and CPMD. *Chem. Phys.*, 327(1):54–62, 2006.
- [38] S. Grimme. Semiempirical GGA - type density functional constructed with a

- long - range dispersion correction. *J. Comput. Chem.*, 16, 2006.
- [39] P. Tangney and S. Scandolo. How well do CarParrinello simulations reproduce the BornOppenheimer surface? Theory and examples. *J. Chem. Phys.*, 116(1):14, 2002.
- [40] P. Tangney. On the theory underlying the Car-Parrinello method and the role of the fictitious mass parameter. *J. Chem. Phys.*, 124(4):44111, 2006.
- [41] I.-F. W. Kuo, C. J. Mundy, M. J. Mcgrath, and J. I. Siepmann. Time-Dependent Properties of Liquid Water : A Comparison of Car-Parrinello and Born-Oppenheimer Molecular Dynamics Simulations. *J. Chem. Theory Comput.*, 2(5):1274–1281, 2006.
- [42] M.-P. Gaigeot. Theoretical spectroscopy of floppy peptides at room temperature. a dftmd perspective: gas and aqueous phase. *Phys. Chem. Chem. Phys.*, 12:3336–3359, 2010.
- [43] H. Ohno, M. Kida, T. Sakurai, Y. Iizuka, T. Hondoh, H. Narita, and J. Nagao. Symmetric stretching vibration of CH<sub>4</sub> in clathrate hydrate structures. *ChemPhysChem*, 11(14):3070–3073, 2010.
- [44] T. D. J. Allen, MP. *Computer simulation of liquids*. Clarendon Press, 1989.
- [45] N. J. English and J. M. D. Macelroy. Structural and dynamical properties of methane clathrate hydrates. *J. Comput. Chem.*, 24(13):1569–1581, 2003.
- [46] T. Uchida, R. Ohmura, I. Y. Ikeda, J. Nagao, S. Takeya, and A. Hori. Phase equilibrium measurements and crystallographic analyses on structure-H type gas hydrate formed from the CH<sub>4</sub>-CO<sub>2</sub>-neohexane-water system. *J. Phys. Chem. B*, 110(10):4583–4588, 2006.
- [47] M. Fuchs and M. Scheffler. Ab initio pseudopotentials for electronic structure calculations of poly-atomic systems using density-functional theory. *Comput. Phys. Commun.*, 119:67–98, 1999.
- [48] K. A. Udachin, C. I. Ratcliffe, G. D. Enright, and J. a. Ripmeester. Structure H Hydrate: A Single Crystal Diffraction Study of 2,2-dimethylpentane<sub>5</sub>(Xe, H<sub>2</sub>S)<sub>34</sub>H<sub>2</sub>O. *Supramol. Chem.*, 8(3):173–176, 1997.
- [49] Y. Okano and K. Yasuoka. Free-energy calculation of structure-H hydrates. *J. Chem. Phys.*, 124(2):24510, 2006.
- [50] S. Takeya, A. Hori, T. Uchida, and R. Ohmura. Crystal lattice size and stability of type H clathrate hydrates with various large-molecule guest substances. *J. Phys. Chem. B*, 110(26):12943–12947, 2006.

- 
- [51] R. Susilo, J. A. Ripmeester, and P. Englezos. Characterization of gas hydrates with PXRD, DSC, NMR, and Raman spectroscopy. *Chem. Eng. Sci.*, 62(15):3930–3939, 2007.
- [52] R. Susilo, J. A. Ripmeester, and P. Englezos. Methane Conversion Rate into Structure H Hydrate Crystals from Ice. *AIChE J.*, 53(9):2451–2460, 2007.
- [53] S. Alavi, K. Udachin, C. I. Ratcliffe, and J. A. Ripmeester. Clathrate Hydrates. In *Supramol. Chem. From Mol. to Nanomater.*, pages 1–16. 2012.
- [54] I. Matanović, M. Xu, J. W. Moskowitz, J. Eckert, Z. Bačić, and Z. Bacić. Methane molecule confined in the small and large cages of structure I clathrate hydrate: Quantum six-dimensional calculations of the coupled translation-rotation eigenstates. *J. Chem. Phys.*, 131(22):224308, 2009.
- [55] B. Chazallon, C. Focsa, J.-L. Charlou, C. Bourry, and J.-P. Donval. A comparative Raman spectroscopic study of natural gas hydrates collected at different geological sites. *Chem. Geol.*, 244(1-2):175–185, 2007.
- [56] H. Schober, H. Itoh, a. Klapproth, V. Chihaiia, and W. F. Kuhs. Guest-host coupling and anharmonicity in clathrate hydrates. *Eur. Phys. J. E*, 12(1):41–49, 2003.
- [57] J. Qin and W. F. Kuhs. Quantitative Analysis of Gas Hydrates Using Raman Spectroscopy. *AIChE J.*, 59(6):2155–2167, 2013.
- [58] M. Celli, A. Powers, D. Colognesi, M. Xu, Z. Bacic, and L. Ulivi. Experimental inelastic neutron scattering spectrum of hydrogen hexagonal clathrate-hydrate compared with rigorous quantum simulations. *J. Chem. Phys.*, 139(16):164507, 2013.
- [59] J. S. Tse, V. P. Shpakov, V. V. Murashov, and V. R. Belosludov. The low frequency vibrations in clathrate hydrates. *J. Chem. Phys.*, 107(21):9271, 1997.
- [60] J. S. Tse, C. I. Ratcliffe, B. M. Powell, V. F. Sears, and Y. P. Handa. Rotational and Translational Motions of Trapped Methane . Incoherent Inelastic Neutron Scattering of Methane Hydrate. *J. Phys. Chem. A*, 101(25):4491–4495, 1997.
- [61] C. Gutt, B. Asmussen, W. Press, M. R. Johnson, and Y. P. Handa. The structure of deuterated methane hydrate. 4713, 2000.
- [62] B. Chazallon, H. Itoh, M. Koza, W. F. Kuhs, and H. Schober. Anharmonicity and guest-host coupling in clathrate hydrates. *Phys. Chem. Chem. Phys.*, 4(19):4809–4816, 2002.
- [63] J. S. Tse, D. D. Klug, J. Y. Zhao, W. Sturhahn, E. E. Alp, J. Baumert,

- C. Gutt, M. R. Johnson, and W. Press. Anharmonic motions of Kr in the clathrate hydrate. *Nat. Mater.*, 4(12):917–921, 2005.
- [64] K. Yoshida, N. Matubayasi, Y. Uosaki, and M. Nakahara. Density effect on infrared spectrum for supercritical water in the low- and medium-density region studied by molecular dynamics simulation. *J. Chem. Phys.*, 137(19):194506, 2012.
- [65] K. Yoshida, N. Matubayasi, Y. Uosaki, and M. Nakahara. Effect of heavy hydrogen isotopes on the vibrational line shape for supercritical water through rotational couplings. *J. Chem. Phys.*, 138(13):134508, 2013.
- [66] J. M. Schicks, J. Erzinger, and M. A. Ziemann. Raman spectra of gas hydrates—differences and analogies to ice 1h and (gas saturated) water. *Spectrochim. Acta. A. Mol. Biomol. Spectrosc.*, 61(10):2399–2403, 2005.
- [67] J. H. van der Waals and J. C. Platteeuw. Clathrate solutions. *Adv. Chem. Phys.*, 2:1, 1959.
- [68] S. Takeya, K. A. Udachin, I. L. Moudrakovski, R. Susilo, and J. a. Ripmeester. Direct space methods for powder X-ray diffraction for guest-host materials: applications to cage occupancies and guest distributions in clathrate hydrates. *J. Am. Chem. Soc.*, 132(2):524–531, 2010.
- [69] K. A. Udachin and J. A. Ripmeester. A complex clathrate hydrate structure showing bimodal guest hydration. *Nature*, 397(6718):420–3, 1999.
- [70] K. Udachin, S. Alavi, and J. a. Ripmeester. Communication: Single crystal x-ray diffraction observation of hydrogen bonding between 1-propanol and water in a structure II clathrate hydrate. *J. Chem. Phys.*, 134(12):121104, 2011.
- [71] I. A. Monreal, L. Cwiklik, B. Jagoda-cwiklik, and J. P. Devlin. Classical to Nonclassical Transition of Ether – HCN Clathrate Hydrates at Low Temperature. *J. Phys. Chem. Lett.*, 1(1):290–294, 2010.
- [72] R. Susilo, S. Alavi, I. L. Moudrakovski, P. Englezos, and J. a. Ripmeester. Guest-host hydrogen bonding in structure H clathrate hydrates. *ChemPhysChem*, 10(5):824–829, 2009.
- [73] S. Alavi, S. Takeya, R. Ohmura, T. K. Woo, and J. A. Ripmeester. Hydrogen-bonding alcohol-water interactions in binary ethanol, 1-propanol, and 2-propanol+methane structure II clathrate hydrates. *J. Chem. Phys.*, 133(7):074505, 2010.
- [74] S. Alavi and J. A. Ripmeester. Effect of small cage guests on hydrogen bonding

- of tetrahydrofuran in binary structure II clathrate hydrates. *J. Chem. Phys.*, 137(5):54712, 2012.
- [75] T. M. Chang, R. J. Cooper, and E. R. Williams. Locating protonated amines in clathrates. *J. Am. Chem. Soc.*, 135(39):14821–30, 2013.
- [76] W. Lee, D. Lim, and H. Lee. Electrochemical stability of ionic clathrate hydrates and their structural consideration. *Electrochim. Acta*, 109:852–858, 2013.
- [77] S. Muromachi, K. A. Udachin, K. Shin, S. Alavi, I. L. Moudrakovski, R. Ohmura, and J. A. Ripmeester. Guest-induced symmetry lowering of an ionic clathrate material for carbon capture. *Chem. Commun.*, 50(78):11476–9, 2014.
- [78] S. Alavi, K. Shin, and J. Ripmeester. Molecular Dynamics Simulations of Hydrogen Bonding in Clathrate Hydrates with Ammonia and Methanol Guest Molecules. *J. Chem. Eng. Data*, in press.
- [79] K. a. Udachin, S. Alavi, and J. a. Ripmeester. WaterHalogen Interactions in Chlorine and Bromine Clathrate Hydrates: An Example of Multidirectional Halogen Bonding. *J. Phys. Chem. C*, 117(27):14176–14182, 2013.
- [80] J. A. Ripmeester and C. I. Ratcliffe.  $^{12}\text{Xe}$  NMR Studies of Clathrate Hydrates: New Guests for Structure I1 and Structure H+. *J. Phys. Chem.*, 94(25):8773–8776, 1990.
- [81] J. Hutter and M. Iannuzzi. CPMD: Car-Parrinello molecular dynamics. *Zeitschrift für Krist.*, 220(5-6-2005):549–551, 2005.
- [82] D. Van Der Spoel, E. Lindahl, B. Hess, G. Groenhof, A. E. Mark, and H. J. C. Berendsen. GROMACS: fast, flexible, and free. *J. Comput. Chem.*, 26(16):1701–18, 2005.
- [83] B. Hess, C. Kutzner, D. van der Spoel, and E. Lindahl. GROMACS 4: Algorithms for Highly Efficient, Load-Balanced, and Scalable Molecular Simulation. *J. Chem. Theory Comput.*, 4(3):435–447, 2008.
- [84] J. L. F. Abascal, E. Sanz, R. García Fernández, C. Vega, and R. García Fernández. A potential model for the study of ices and amorphous water: TIP4P/Ice. *J. Chem. Phys.*, 122(23):234511, 2005.
- [85] W. D. Cornell, P. Cieplak, C. I. Bayly, I. R. Gould, K. M. Merz, D. M. Ferguson, D. C. Spellmeyer, T. Fox, J. W. Caldwell, and P. a. Kollman. A Second Generation Force Field for the Simulation of Proteins, Nucleic Acids, and Organic Molecules. *J. Am. Chem. Soc.*, 117(19):5179–5197, 1995.

- [86] M. J. Frisch, G. W. Trucks, H. B. Schlegel, G. E. Scuseria, M. A. Robb, J. R. Cheeseman, J. A. Montgomery, Jr., T. Vreven, K. N. Kudin, J. C. Burant, J. M. Millam, S. S. Iyengar, J. Tomasi, V. Barone, B. Mennucci, M. Cossi, G. Scalmani, N. Rega, G. A. Petersson, H. Nakatsuji, M. Hada, M. Ehara, K. Toyota, R. Fukuda, J. Hasegawa, M. Ishida, T. Nakajima, Y. Honda, O. Kitao, H. Nakai, M. Klene, X. Li, J. E. Knox, H. P. Hratchian, J. B. Cross, V. Bakken, C. Adamo, J. Jaramillo, R. Gomperts, R. E. Stratmann, O. Yazyev, A. J. Austin, R. Cammi, C. Pomelli, J. W. Ochterski, P. Y. Ayala, K. Morokuma, G. A. Voth, P. Salvador, J. J. Dannenberg, V. G. Zakrzewski, S. Dapprich, A. D. Daniels, M. C. Strain, O. Farkas, D. K. Malick, A. D. Rabuck, K. Raghavachari, J. B. Foresman, J. V. Ortiz, Q. Cui, A. G. Baboul, S. Clifford, J. Cioslowski, B. B. Stefanov, G. Liu, A. Liashenko, P. Piskorz, I. Komaromi, R. L. Martin, D. J. Fox, T. Keith, M. A. Al-Laham, C. Y. Peng, A. Nanayakkara, M. Challacombe, P. M. W. Gill, B. Johnson, W. Chen, M. W. Wong, C. Gonzalez, and J. A. Pople. Gaussian 03, Revision C.02, 2004. Gaussian, Inc., Wallingford, CT, 2004.
- [87] S. Alavi, R. Ohmura, and J. a. Ripmeester. A molecular dynamics study of ethanol-water hydrogen bonding in binary structure I clathrate hydrate with CO<sub>2</sub>. *J. Chem. Phys.*, 134(5):54702, 2011.
- [88] S. Alavi, K. Udachin, and J. A. Ripmeester. Effect of guest-host hydrogen bonding on the structures and properties of clathrate hydrates. *Chemistry*, 16(3):1017–1025, 2010.
- [89] N. Bloembergen, E. Purcell, and R. Pound. Relaxation Effects in Nuclear Magnetic Resonance Absorption. *Phys. Rev.*, 73(7):679–712, 1948.
- [90] J. R. Choudhuri, V. K. Yadav, A. Karmakar, B. S. Mallik, and A. Chandra. A first-principles theoretical study of hydrogen-bond dynamics and vibrational spectral diffusion in aqueous ionic solution : Water in the hydration shell of a fluoride ion. 85(1):27–40, 2013.